NTNU – Trondheim
Norwegian University of
Science and Technology

2-D Finite Difference Modelling and Analysis of Shallow Gas Leakage Scenarios, Using Time-Lapse Refraction

Paola Rodríguez

Petroleum Geosciences
Submission date: June 2013
Supervisor: Martin Landrø, IPT

Norwegian University of Science and Technology
Department of Petroleum Engineering and Applied Geophysics

Norwegian Univesirty of Science and Technology

Department of Petroleum Engineering and Applied Geophysics

2D Finite Difference Modelling and Analysis of Shallow Gas Leakage Scenarios, using Time-Lapse Refraction

Author:

PaolaRodriguez Masiu

Supervisor:

Pr. Martin Landro

June 16, 2013

June 16, 2013

Abstract

Department of Petroleum Engineering and Applied Geophysics
Norwegian University of Science and Technology

2D Finite Difference Modelling and Analysis of Shallow Gas Leakage Scenarios, using Time-Lapse Refraction

By
Paola Rodríguez Masiu

4D seismic is a relatively new technology used aggressively in the oil industry, over the years it has proved its potential. However, there is a need for development of new techniques with high precision that enable the record of subtle changes in seismic properties, where conventional monitoring methods have not succeeded. Experience shows that refraction time-lapse seismic might be a solution. By measuring timeshifts, between base and monitor surveys, on first arrival head-waves, the method aims the estimation of reservoir velocity changes at a much lower cost than conventional 4D seismic monitoring. Preliminary results show timeshifts in the order of $1ms$ to $10ms$, caused by variation in the reservoir P-wave velocity due hydrocarbon flow. Furthermore, the method offers an accurate estimation of lateral extension of the velocity anomalies, even when the extension is smaller than hundred meters. Limitations of this method are related with the existence of positive velocity contrast in the reservoir layer, existence of long offset data and repeatability of the seismic. Further investigation is needed, in order to identify crucial bottlenecks that are likely to meet for a real data case.

Aknowledgement

I wish to express my sincere gratitude to my supervisor Professor Martin Landrø for his guidance, generous contribution of knowledge and experience, valuable comments and encouragement from the start until the end of this study.

I would like to thank to my home university "Universidad Simon Bolivar" for providing me with excellent academic, professional and personal guidance during 4 years.

"Tusen takk" to all the beautiful and funny people that I have met during my stay in Trondheim. I want to say thanks to all my friends: Luis saenz, Luis ugueto, Andre, David, Gabriel and especially to Mari Gaby, my dearest friend. Thanks to Daniel, for remaining always in my side, even in the hardest.

I would like to make a special mention to Arnaud Hoffman for all his invaluable help, for all the fruitful and joyful discussions that we had together, and for helped me get on the road with LaTeX.

Thanks to my Daddy, for supporting me, even during my "nonsenses". To all my brothers and sisters: Carlos, Carolina, Agustin and especially Maria Teresa. Above all to Maria Teresa who more than my sister is my loved mother. To my brother-in-law Norberto for his endless hours helping me with maths, and in everything that he could.

Thanks to the persons who fill-up my heart all the days with their smiles: Rosi, Rosa, Carlitos, Roberto, Rivaldo , Leonardo y Diego. "Pulgas" I loved you so much.

Finally, I wish to dedicate this study to my Mom Rosa Elena. Mommy, you always told me to "reach for the stars." I think I got my first one. Thanks.

Contents

List of Figures

List of Tables

Chapter 1

Introduction

Considerable studies of feasibility has been carry out for several years to find out under which circumstances 4D seismic would provide useful information on reservoir dynamics. Nowadays, conventional 4D seismic is a proven technology in several developed oilfields, this monitoring is particularly effective in high-porosity sandstone reservoirs. However, the 4D response in case of carbonate reservoirs is not encouraging. The main cause for this is that the expected relative velocity and density changes, due to production are more significant in sand reservoirs compared to high velocity reservoirs (carbonate reservoirs). Therefore, there is a need for development of new techniques with high precision to enable the record of such small velocity changes, and experience shows that refraction time-lapse seismic might be a solution. The most successful time-lapse seismic studies are (Landrø et al; 1999, Koster et al; 2000 and Landrø et al; 2001). Another nice feature of refraction time-lapse is that it is a precise tool for estimating velocity changes only (Landrø, 2001, Tura and Lumley, 1999 and Landrø et al; 2001). In order to discriminate between pressure and saturation changes in a producing reservoir, a method that estimates velocity changes only, might be very useful.

Refraction Time-lapse seismic monitoring has potential for accurate estimation of reservoir velocity changes (Landrø et al., 2004). Variations in the reservoir properties can create amplitude anomalies or timeshift. Therefore, such variations in the reservoir properties can be detected by measuring timeshifts on first arrival head-waves from a refracting layer at the top reservoir. Time-lapse refraction aims to detect changes and inverts them to reservoir parameters. This idea is attractive because critical offset (x_c) and travel times for refracted events seem to be very sensitivity to modest variations on the reservoir P-wave velocity. The existence of a critical angle in seismic leading to critical refraction is only possible for a medium (reservoir) that offers a positive contrast in velocity (i.e. the reservoir exhibits higher wave velocity than the overburden).

Chapter 2

Finite-Difference Methods

2.1 Seismic wave equation

The seismic wave equation, which is used to describe how seismic waves propagate through the earth, is a differential equation containing spatial and temporal derivatives. For an elastic and isotropic medium the wave equation can be written as follows:

$$\rho(x)\frac{\partial^2 u_i}{\partial t^2} = \frac{\partial \sigma_{ij}}{\partial x_i} + f_i, \tag{2.1}$$

where $\rho(x)$ is the density, u_i is the particle displacement in the direction i, f_i is an external force (i.e. source), σ_{ij} is the stress tensor, t is time and x refers to the position. A constitutive relation between the stress tensor and the particle displacement, known as the Hooke's law is introduced.

$$\sigma_{ij} = \lambda\delta_{ij}\frac{\partial u_k}{\partial x_k} + \mu(\frac{\partial u_i}{\partial x_j} + \frac{\partial u_j}{\partial x_i}), \tag{2.2}$$

λ and μ are the Lame parameters. For the acoustic case ($\mu = 0$) and denoting the isotropic stress as $p = \lambda\delta_{ij}\frac{\partial u_k}{\partial x_k}$ equation (2.2) yields to:

$$\sigma_{ij} = -p\delta_{ij}. \tag{2.3}$$

Neglecting the force term and assuming constant density, spatial derivation ($\frac{\partial}{\partial x_i}$) is performed on both sides of Equation (2.1). Substituting Equation (2.3) into Equation (2.1) leads to:

$$\frac{\partial^2 p}{\partial t^2} = c^2\nabla^2 p, \tag{2.4}$$

where $p = p(x,t)$ is the wave field and $c = \sqrt{\frac{\lambda}{\rho}}$ is P-wave velocity.

2.2 Finite-difference approximations

The finite-difference methods (FDMs) have been widely used in seismic modelling and migration (Liu et al; 2008 [20]). The explicit FDMs are the most popular in the seismic community for its low computational cost.

The finite-difference approximation give a numerical solution of partial differential equations. The accuracy of this solution is dependent on the order of approximations, namely, the numbers of terms used in the Taylor series representation of the function. Ultimately, all the finite difference methods are based on Taylor Series approximations (Scales, 1997 [7]). Therefore, a discrete version of the wave equation is obtained. Initial conditions or starting point from which the wave field would be propagated, is required.

In the Geophysical world, the constant density acoustic wave equation for a homogeneus medium (Equation 2.4) have been the most popularly used, due to its simplicity. The 1D wave equation for the acoustic case is given by:

$$\frac{\partial^2 p}{\partial x^2} = \frac{1}{c^2}\frac{\partial^2 p}{\partial t^2}. \tag{2.5}$$

In orden to solve Equation (2.5), either time and space are discretized:

$$t_n = n\Delta t,$$
$$x_i = i\Delta t.$$

It is possible to define the numerical approximation of $p(x;t)$ at the grid point $(x_n;t_n)$ as follows :

$$p(xi;tn) \approx p_i^n.$$

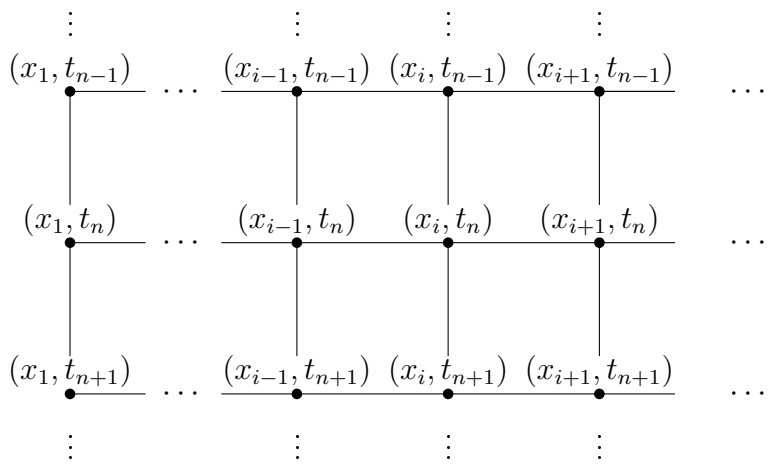

Figure 2.1: 1D grid for wave fields in the time-space domain.

A Taylor series expansion of the right side of the Equation (2.5), which is the second derivative of the pressure with respect to time, yields to:

$$\frac{\partial^2 p}{\partial t^2} \approx \frac{{p_i}^{n+1} - 2{p_i}^n + {p_i}^{n-1}}{\Delta t^2}. \tag{2.6}$$

It is important to highlight that a smaller time step leads to grater accuracy for computing temporal derivatives. Notice that Equation (2.6) requires wavefield values at the current time step, past time step and a future time step at a given spatial point. Such a scheme is called an explicit scheme in time (Liu et al; 2008 [20]). Similarly, the second order Taylor expansion, for evaluating the spatial derivative in the x-direction, is given by

$$\frac{\partial^2 p}{\partial x^2} \approx \frac{p^n_{(i+1)} - 2p^n_i + p^n_{(i-1)}}{\Delta x^2}, \tag{2.7}$$

which will require the wavefield values at the current grid position and its neighboring grid positions, at a given time step.

Substituting the approximations obtained in Equation (2.6) and Equation (2.7) into Equation (2.5), the wave equation now can be writen as:

$$p^{n+1}_i = 2{p_i}^n + {p_i}^{n-1} + c_i \Delta t^2 \left(\frac{p^n_{(i+1)} - 2p^n_i + p^n_{(i-1)}}{\Delta x^2}\right). \tag{2.8}$$

Equation (2.8) is the recursion formula for solving 1D wave equation by finite-difference method. The recursion starts with the wave field values known at two succesive time steps. The wavefield values at a future time step at all the spatial locations are computing using this equation.

In addition, we introduce the 2-D constant density wave equation for the acoustic case

$$\frac{\partial^2 p}{\partial x^2} + \frac{\partial^2 p}{\partial z^2} = \frac{1}{c^2}\frac{\partial^2 p}{\partial t^2}. \tag{2.9}$$

Similarly to Equation (2.6) the temporal derivative is given by

$$\frac{\partial^2 p}{\partial t^2} \approx \frac{p^{n+1}_{(i,k)} - 2p^n_{(i,k)} + p^{n-1}_{(i,k)}}{\Delta t^2}. \tag{2.10}$$

In the same way, the spacial derivative in the x-direction and z-direction for the 2-D wave equation can be written as follows:

$$\frac{\partial^2 p}{\partial x^2} \approx \frac{p^n_{(i+1,k)} - 2p^n_{(i,k)} + p^n_{(i-1,k)}}{\Delta x^2}, \tag{2.11}$$

$$\frac{\partial^2 p}{\partial z^2} \approx \frac{p^n_{(i,k+1)} - 2p^n_{(i,k)} + p^n_{(i,k-1)}}{\Delta z^2}, \tag{2.12}$$

respectively.

The solution of Equation (2.9) is given by the substitution of Equations (2.10, 2.11, 2.12) into Equation (2.9).

$$p^{n+1}_{(i,k)} = 2p^n_{(i,k)} + {p_{(i,k)}}^{n-1} + c_i \Delta t^2 \left(\frac{p^n_{(i+1,k)} - 2p^n_{(i,k)} + p^n_{(i-1,k)}}{\Delta x^2} + \frac{p^n_{(i,k+1)} - 2p^n_{(i,k)} + p^n_{(i,k-1)}}{\Delta z^2}\right). \tag{2.13}$$

2.3 Grid dispersion

The numerical phenomenon called *dispersion*, means that the phase speed of a wave is a function of the frequency, even when the material properties are not frequency dependent. The dispersion velocity[1]($v_{FD} = \frac{\omega}{k}$) is a function of the medium velocity, grid size, time step, wave number and finite-different coefficients. Thus, frequency-dependent numerical dispersion is observed due to inadequate sampling of wavefields in space and time. Furthermore, errors may appear due to truncation of higher order terms in the Taylor serie expansion.

As stated above, it is necessary to select a correct grid size in order to avoid numerical dispersion. It is possible to defined how many grid points are needed in terms of wavelength at the upper half-power frequency (Alford et al; 1974 [19]). The best results for coarse grids, using a second-order explicit method, are obtained having at least 10-11 gridpoints per wavelength. Whereas for fourth-order schemes, or implicit methods it is possible to use a fine grid containing around 5 points wavelength.

On the other hand, one should ensure that the ratio between temporal sampling and spatial sampling is limited. For the 2^{nd} order scheme discussed here, the ratio can be choosen according to the Courant-Friedrichs-Levy condition:

[1] Velocity which the wave propagates through the numerical grid.

$$\frac{v_{max}\,\Delta t}{\Delta x} \leq C_{max}, \tag{2.14}$$

where v_{max} is the maximun velocity in the model, Δt is the time step, and Δx is the grid space. The values of C_{max} changes with the method used to solve the discretised equation.

2.4 Absorbing boundary conditions

For avoid undesired reflections coming from the bounds of the model, it is required to set a non-free surface boundaries (absorbers). In this way, the incidents ray waves upon one of the absorbing sides would be approximately attenuated. Since reflections coming from the free surface are part of the real seismic experiment, no absorber surface should be placed at the upper border.

Chapter 3

Seismic Techniques

3.1 Refraction seismic methods

The seismic methods are the most widely used of all the geophysical methods in petroleum exploration. The objective of seismic methods is to analize the rock behavior from measured arrival times, amplitude, frequency, and wavefrom. The main advantage of this method, is that it provides the most accurate rendition of the geometry of subsurface layers.

Seismic techniques involve measuring the travel time of seismic energy, which is generated artificially at the near surface. In the subsurface, seismic energy travels in waves that spread out as hemispherical wavefronts. The energy arriving at a geophone is described as having traveled a ray path perpendicular to the wavefront. The acoustic waves propagate into the subsurface at a velocity dependent on the elastic properties of the material, where they travel. When the waves reach an interface where the density or velocity changes significantly, a portion of the energy is reflected back to the surface, and the remaining energy is transmitted into the lower layer. If the waves reach an interface with a positive velocity contrast, a portion of the energy is also critically refracted along the interface. Critically refracted waves travel along the interface at the higher velocity and are continually refracted back to surface. The receivers, that laid out in linear array on the surface, record the incoming *refracted* and *reflected* waves (traveltimes and amplitudes).

The knowledge of travel times in various receivers and the velocity of waves in various media enable us to reconstruct the paths of seismic waves. Structural information is derived from reflected and refracted paths. In seismic reflection method, the waves travel downward initially and are reflected at some point back to the surface, with the overall path being essentially vertical. Whereas in seismic refraction method, the principal portion of the wave-path is

along the interface between the two layers and hence, is approximately horizontal. Since the refraction method required larger offsets than the reflection method, stronger sources are used. The refraction data has generally low frequency content compare to the reflection data, due to a longer travel path absorbs higher frequencies.

3.1.1 Refraction travel time

Refraction seismic is well known for the measurement of near surface seismic velocities. Seismic refraction is generally applicable only where the seismic velocities of layers increase with depth. Seismic refraction involves measuring the travel time of the component of seismic energy which travels down to the top of a fast layer, is refracted along the top of that layer, and returns to the surface as a head wave. The waves returning from the top of the rock are *refracted waves*, and for geophones located at a distance x from the shot point, always represent the first arrival of seismic energy (Dubucq et al; 2010 [1]).

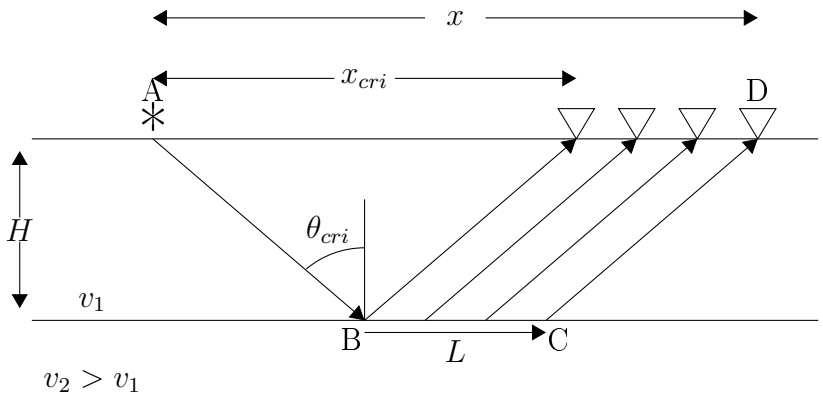

Figure 3.1: Travel path for a wave refracted through the earth.

Figure (3.1) illustrates progressive positions of the ray path from a seismic source at "A". The ray travels from the source until the receiver placed at "D", which is located at a distance "x" from the source. The energy is critically refracted in the lower layer located at a depth "H". The velocities "v_1" and "v_2" represent the P-wave velocity above and below the refracted interface, respectively.

The refracted ray travels down to the interface and back up to the surface with a velocity "v_1" along paths $\overline{AB}$ and $\overline{CD}$ that are inclinated at the critical angle (θ_{cri}), and travels along distance L ($\overline{BC}$) with a the higher velocity "v_2". The total travel time along the refracted ray path $\overline{ABCD}$ can be written as follows:

$$t = t_{\overline{AB}} + t_{\overline{BC}} + t_{\overline{CD}}, \tag{3.1}$$

$$t = \frac{H}{v_1 \cos(\theta_{cri})} + \frac{L}{v_2} + \frac{H}{v_1 \cos(\theta_{cri})}, \qquad x > x_{cri} \tag{3.2}$$

$$t = \frac{2H}{v_1 \cos(\theta_{cri})} + \frac{x - x_{cri}}{v_2}, \qquad x > x_{cri} \tag{3.3}$$

$$x_{cri} = 2Htan(\theta_{cri}). \tag{3.4}$$

If we consider a refracting layer as sketched in Figure (3.1), sin and cos at the critical angle (θ_{cri}) according to the Snell's law are given by

$$\sin(\theta_{cri}) = \frac{v_1}{v_2}, \tag{3.5}$$

$$\frac{1}{\cos(\theta_{cri})} = \frac{v_2}{\sqrt{v_2^2 - v_1^2}}. \tag{3.6}$$

Using Equations introduced above, Equation (3.4) leads to:

$$x_{cri} = \frac{2Hv_1}{\sqrt{v_2^2 - v_1^2}}. \tag{3.7}$$

Substituting Equation(3.7) and Equation (3.6) into Equation (3.3) leads to:

$$t = t_0 \left(\sqrt{1 - \frac{v_1^2}{v_2^2}} + \frac{x}{2H} \frac{v_1}{v_2} \right), \qquad x > x_{cri} \tag{3.8}$$

where $t_0 = \frac{2H}{v_1}$, is the zero offset two-way travel time.

3.2 Time-lapse seismic monitoring

Time-Lapse Seismic monitoring, popularly known as 4D seismic is a repeated 2D/3D conventional seismic data or repeated 4C seismic at different time intervals, wherein the 4^{th} dimension is calendar time. 4D seismic measures changes, either for the reflections or refractions events. In time-lapse seismic, the difference between two seismic surveys (base and monitor) acquired at different time under same acquisition parameters, gives information on the variation of reservoir properties due to hydrocarbon production. However, the subtraction process exhibits residual energy, which is not related to the time-lapse signal such as: random noise, acquisition related noise and signal bandwidth variation. This energy often limits the resolution of the 4D signal (Vedanti et al; 2009 [16]).

Once multiple seismic volumes (baseline, and monitor surveys) are acquired and processed, 4D seismic difference maps are generated. The difference map helps to identify zones of 4D anomalies. The conventional way of analyzing 4D seismic data is to look for the timeshifts and amplitude changes between base and monitor surveys (Vedanti et al; 2009 [16]). Also, based on sensitivity of seismic parameters to saturation and pressure, it is possible to identify whether a given 4D anomaly is due to saturation change or pressure change (Landrø and Stammeijer, 2004 [14]).

4D seismic provides an opportunity to image the fluid flow in volumetric region not sampled by wells. Fluid flow is thus directly mapped by the seismic data rather than solely predicted by the fluid simulation (Lumley, 2001 [3]). With well logs being very expensive, 4D seismic proposes to be the cheap and reliable solution for reservoir monitoring.

From the latest research it is possible to say that convetional 4D seismic monitoring is more succesfull in high-porosity sandstone reservoirs than in carbonate reservoir. The main reason behind this, is that expected velocity and density changes due to production are very low for carbonate reservoirs compared to clastic reservoirs. The need of estimate accurately velocity changes, brings to the scenario time-lapse refraction seismic as such tool. Furthermore, in orden to discriminate between pressure and saturation changes in a reservoir during production stages, a method that allow the estimation of velocity changes only, is vital and again time-lapse refraction seismic offers us a precise tool for accomplish such target.

3.2.1 Post-critical time-lapse seismic

Conventional time-lapse seismic or time-lapse reflection uses pre-critical offset data to analyze variations. However, it is interesting analyze the time-lapse changes of post-critical data as well. The pos- critical time-lapse data is mainly divided in two groups of interest: Critical angle monitoring and Post-critical timeshift monitoring. The first one, monitors the changes in critical angle, which correspond a changes in critical offset.

If the P-wave velocity in the reservoir change in Δv_2 during production, the critical angle given in Equation (3.5) will also change as follows:

$$\sin(\theta'_{cri}) = \frac{v_1}{v_2 + \Delta v_2}, \tag{3.9}$$

and correspondingly the new critical offset is given by:

$$x_{cri} = \frac{2H}{\sqrt{\frac{(v_2+\Delta v_2)^2}{v_{RMS}^2} - 1}}. \tag{3.10}$$

The only approximation used in the derivation of Equation (3.10), is that the overburden is treated as one homogeneous medium with an effective velocity equal to the root mean squared velocity v_{RMS}. The velocity and thickness for the overburden are assumed as unvariable during production. Figure (3.2) illustrates how a velocity change leads to a variation in critical angle and critical offset, repectively.

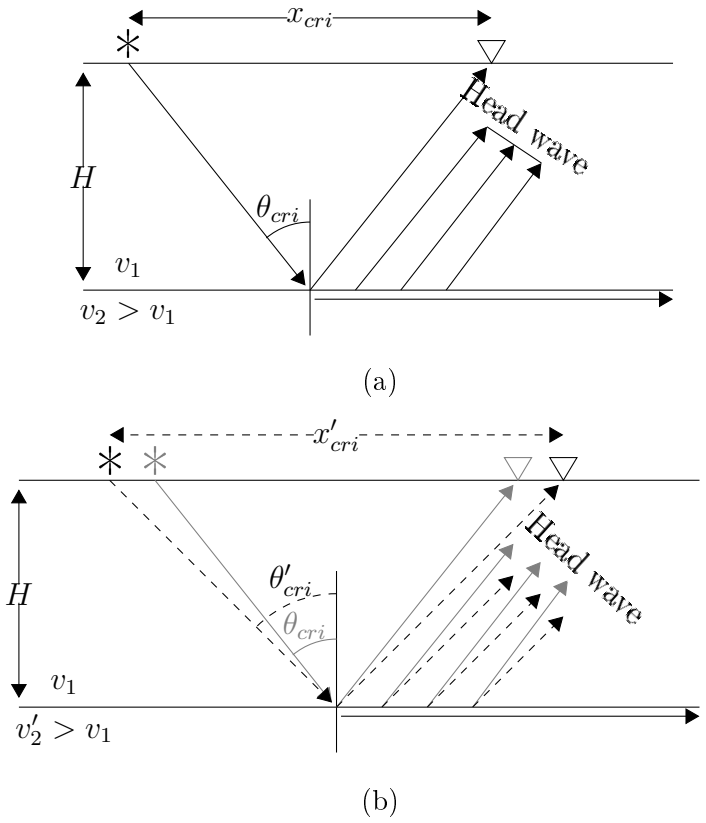

Figure 3.2: Principle of critical offset monitoring. Notice from (b) that if the velocity in the second layer changes from v_2 to v'_2 the critical offset is also changed from x_{cri} to x'_{cri}.

Post-critical timeshift monitoring can be subdivided into two type of analysis (Zadeh, 2011 [5]). The first case considers anomalies just under the refracting interface. The head wave passes through the anomaly, Figure (3.3b) (bottom). This case requires a positive velocity contrast at the interface placed above the anomaly to generate head waves. The second method is suitable for the anomalies over the refractating interface, Figure (3.3c) (bottom). This case requires a positive velocity contrast at the interface beneath the anomaly.

When an anomaly is placed below the refracting interface as in Figure (3.3b) (bottom), timeshift increase monotonically after critical offset. The timeshift is a linear function of the

offset, this dependency is due to the refraction timeshift is a function of the horizontal distance that the refracted ray travels along the interface. From Figure (3.3b) (top), it is possible to observe a change in the slope for the refracted event where the anomaly has taken place.

On the other hand, for the case ilustrated in Figure (3.3c) (bottom), the refraction timeshift remains always constant. The refracted event is pull up in time, without changes in its slope, see Figure (3.3c) (top). For such case, the timeshift is meanly a function of the vertical distance travelled by the refracted ray.

Time lapse refraction seismic has potential for accurate estimation of reservoir velocity changes (Landrø et al; 2004 [11]). Variations in reservoir properties can be detected by measuring timeshifts on first arrival head-waves from refracting layers at the top reservoir. In other words, this technique aims to detect changes and inverts them to reservoir parameters.

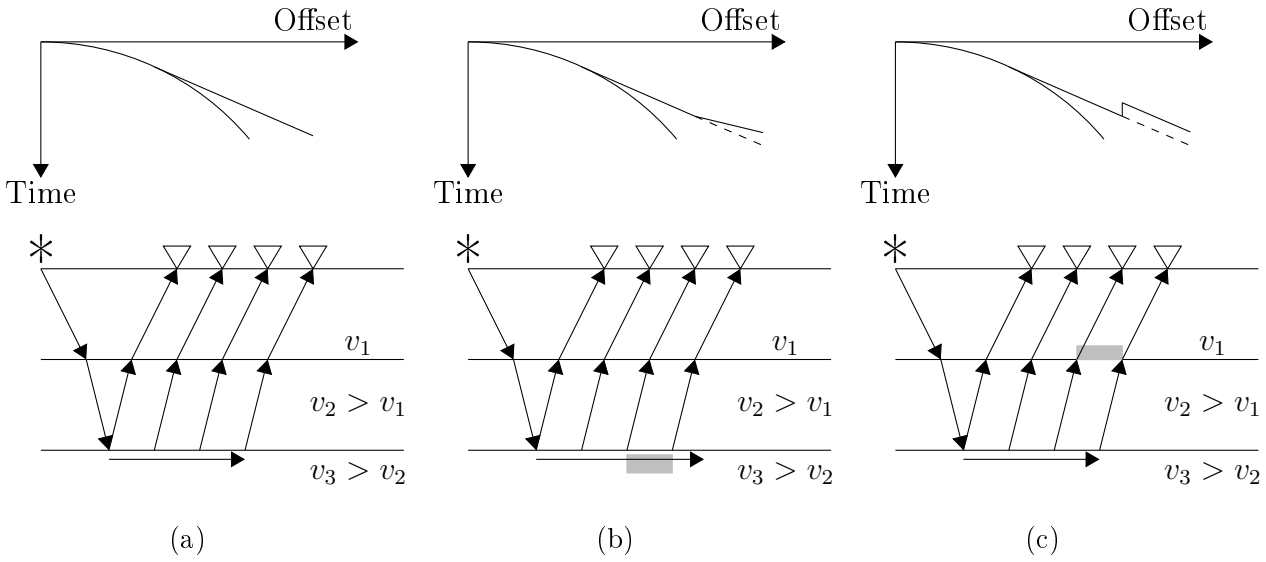

Figure 3.3: Different critical timeshifts. Top figures show the travel time curve and the bottom figures the corresponding geological model. (a) Base case, before production. (b) Effect of an anomaly placed under the refracting interface. (c) Effect of an anomaly placed above the refracting interface.

3.2.2 Refraction timeshift

Assuming a small velocity change bellow the refracting interface, and performing the derivation of Equation (3.8), refraction timeshift can be written as follows:

$$\Delta t \approx ax + b, \tag{3.11}$$

where, a and b are defined as:

$$a = -\frac{\Delta v_2}{v_2^2},$$

and

$$b = -\frac{2Hv_1\Delta v_2}{\sqrt{v_2^2 - v_1^2 v_2^2}}.$$

Equation (3.11) can be written as:

$$\Delta t \approx -\frac{\Delta v_2}{v_2^2}\left(x - \frac{2Hv_1}{\sqrt{v_2^2 - v_1^2}}\right), \tag{3.12}$$

Equation (3.12) estimates the refraction timeshift for a velocity change in the whole layer. For a velocity anomaly with a limited extension (l_a), two different monitor travel time scenarios can happen. Figure (3.4) :

- First case: $\frac{x_{cri}}{2} + l_a > x - l_1 > +\frac{x_{cri}}{2}$

$$t' = t'_{down} + t'_L + t'_{up} \tag{3.13}$$

$$t' = \frac{\sqrt{\left(\frac{x_{cri}}{2}\right)^2 + H^2}}{v_1} + \frac{l_1 - \frac{x_{cri}}{2}}{v_2} + \frac{x - l_1 + \frac{x'_{cri}}{2}}{v'_2} + \frac{\sqrt{\left(\frac{x'_{cri}}{2}\right)^2 + H^2}}{v_1} \tag{3.14}$$

$$\Delta t \approx \left(x - l_1 - \frac{Hv_1}{\sqrt{v_2^2 - v_1^2}}\right)\frac{\Delta v_2}{v_2^2} \tag{3.15}$$

- Second case $x - l_1 > +\frac{x_{cri}}{2} + l_a$

$$t' = t'_{down} + t'_L + t'_{up} \tag{3.16}$$

$$t' = \frac{\sqrt{x_{cri}^2 + 4H^2}}{v_1} + \frac{l_1 + l_2 - x_{cri}}{v_2} + \frac{l_a}{v'_2} \tag{3.17}$$

$$\Delta t \approx l_a \frac{\Delta v_2}{v_2^2} \tag{3.18}$$

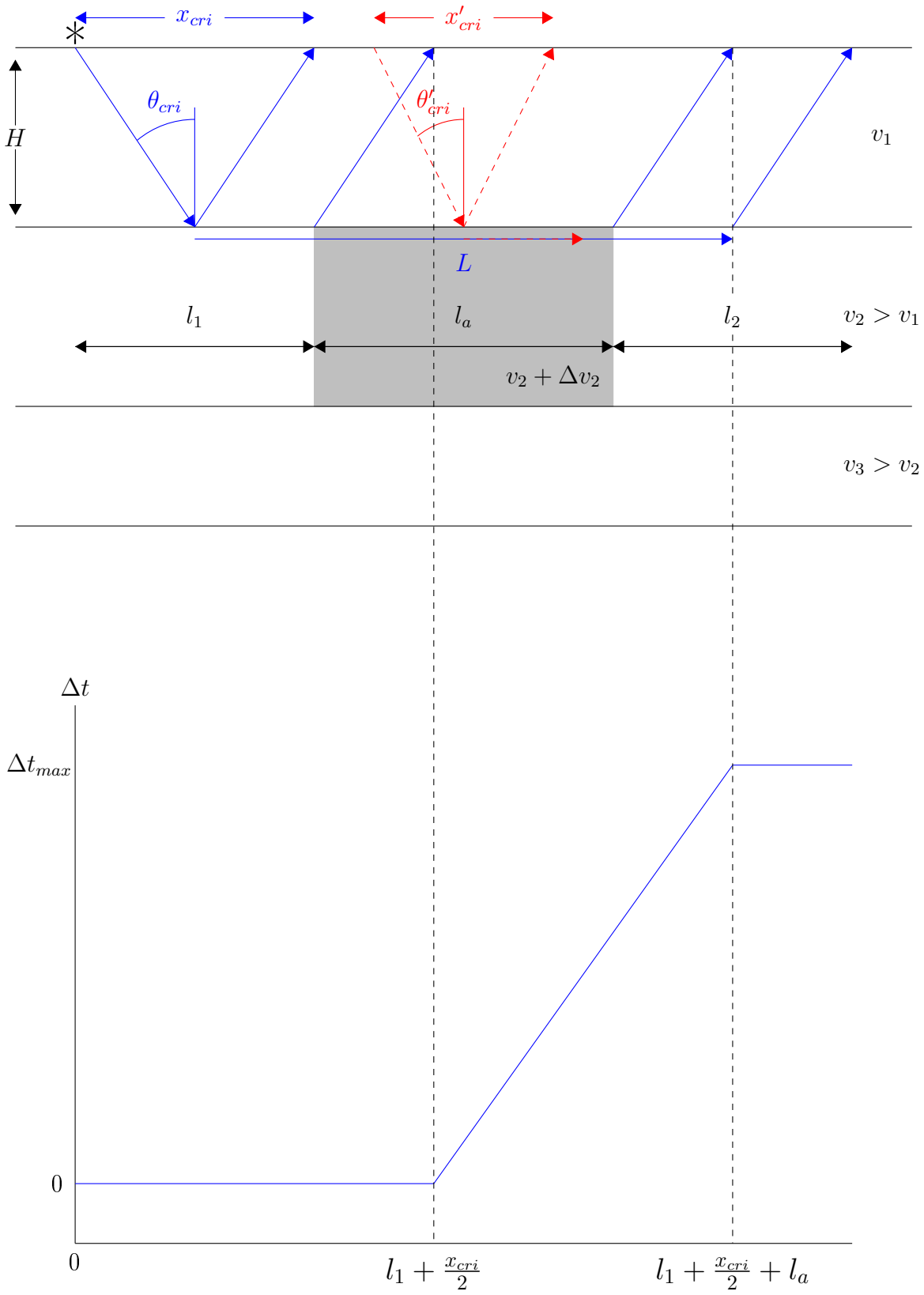

Figure 3.4: Timeshift versus offset for an anomaly placed under a refracting interface.

Chapter 4

Modelling With Seismic Unix

Seismic Unix (SU) is an open source software supported by the Center for Wave Phenomena (CWP) at the Colorado School of Mines (CSM). The package provides a collection of subroutines, libraries, graphics tools, and fundamental seismic data processing applications for users running on all Unix and Unix-like operating systems, which include the operating systems Mac OS X, Linux, Free BSD Unix, and the Cygwin32 system for Windows PCs. Since SU is a open source package, it can be used to craate more complicated aplications. Furthermore, is constantly updated.

When the user runs a terminal window application under a Unix-like environment, that terminal window runs a programm called a shell that gives the user access to the kernel of the operating system. Many of the programs run simply by a command on the terminal. SU applications typically read their input traces from the standard input file (SEG-Y or SU) and write their output to the standard output file (SEG-Y or SU). In this way, the user can create sequences of *Seismic Unix* applications by means of shell script files in which several applications (along with their corresponding parameters) are specified, each one separated from the next by the pipeline operator provided by Unix shells. When the shell script is executed, the output from one application is communicated to the next one through a pipeline file.

4.1 Subsurface mathematical models

4.1.1 Uniformly sampled models. *Unif2*

The command `Unif2` generates 2D uniformly sampled velocity and density profiles from a layered model. In each layer, velocity and density are a linear function of position. The command `Unif2` of *Seismic Unix* allows us to create a model of the subsurface by introducing

a Input file giving the shape of each interface. This command generates a binary file, which represents a uniform spaced grid. For each point of the grid a value of velocity and density is assigned.

The input file for `Unif2` is a `ASCII` file, which contains coordinates (x, z) of a point series that define the trend for each interface in the model. It consists of two columns, the values in the column on the left are horizontal positions (x) and the values on the right are depths (z). The `ASCII` file uses the ordered pair (1, -99999) to separate consecutive interfaces. The first and last "x" values must be the same for all boundaries. No boundary may cross another.

The output file is a binary file given by vfile $[nx][nz]$, it contains the generated profile, either for velocity or density. This file is a uniformly sampled grid representing the properties of the subsurface (density and velocity).

In order to view the output file of `Unif2`, a command that allows us to plot binary format files must be used. In this sense, the commands `Ximage` and `Psimage` are the most commonly used in SU environment.

In Appendix A an example to execute the `Unif2` command is given. It shows all the parameters that can be adjusted. This appendix contains Script (A.1), which shows how `Unif2` works. To generate an uniform velocity or density profile of a layered model; first, the input file containing the coordinates of the interfaces, and the amount of samples required to generate the model (nx and nz) have to be introduced. Then, it is also necessary to introduce distance intervals between each grid point (dx and dz). Furthermore, a velocity function ($v00$), which assigns velocity values to each layer have to be introduced. Notice that the number of values for the $v00$ parameter must be equal to the number of layers in the model. If this number is lower, the velocity will be equal to zero in those layers, where the velocity was not assigned. If it is greater, the leftover values will not be taken into account for the model. Finally, the output file, which is going to contain the model must be specified.

To construct the model or profile using `Unif2`, a 2D uniformly spaced grid is created by the interpolation of points (x, y) contained in the input file. In order to effectuate this interpolation it is necessary to introduce the sampling parameters $(nz, dz, nx$ and $dx)$. It is worth to highlight, that the product of the number of samples (nx and nz) and the spacing between them (dx and dz) must be equal to the maximum value of x (distance) in the input file. In the same way, this condition has to be verified for z (depth). If the number of samples and the spacing between them is not equal to the limits of the model, the result may not be as expected. However, *Seismic Unix* will not give any warning or error.

In Figure (4.1) is shown the velocity profile generated by Script(A.1). The input file for

this profile is presented in Table (4.1)

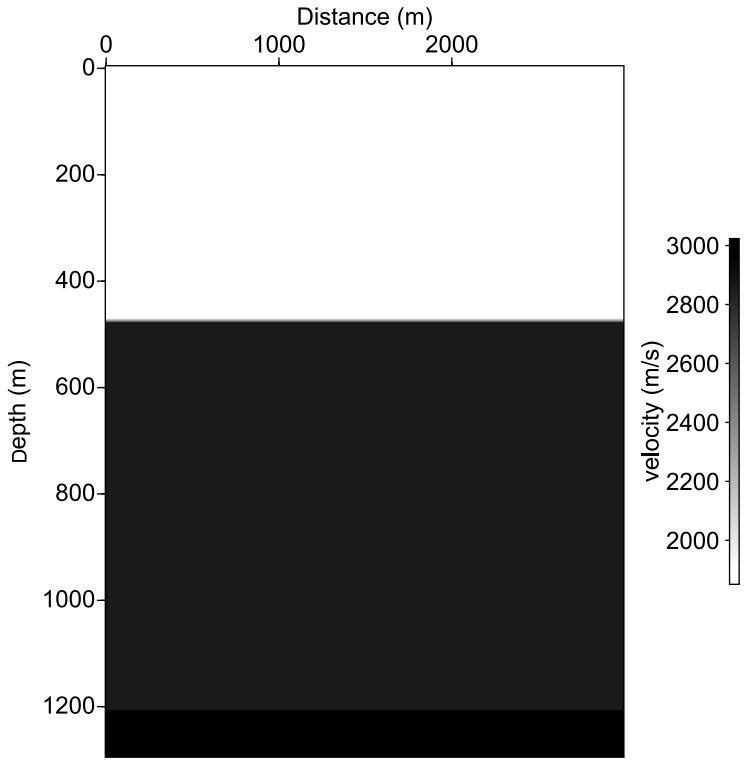

Figure 4.1: Uniform model generated by *Unif2* command. Velocity profile for a simple model with 3 horizontal layers.

X	Y
0	0
3000	0
1	-99999
0	476
3000	476
1	-99999
0	1200
3000	1200
1	-99999
0	1300
3000	1300

Table 4.1: Input file example for the velocity rofile prresented in Figure (4.1)

4.1.2 Triangulated models. *Trimodel*

Since for `Unif2` command the first and last x values must be the same for all boundaries, complicated models can not be created. Therefore, another command is required. `Trimodel` command represents a solution for such target.

`Trimodel` command of SU builds a triangulated model from values of sloth ($1/velocity^2$) or velocity. It is possile to add values of density or Q-factor for the construction. The model is done by interpolating points using the Delaunay triangulation.

To create a model using `Trimodel`, it is necessary to introduce the maximun and minimun values for the lenght and depth (xmin, xmax, zmin and zmax) of the model. It is also necessary to introduce the values (x, z), which describe each surface. This is done by introducing the parameters *xedge* and *zedge*; the numbers of these parameters must be equal. Within each set, vertices will be connected by the parameter *edge*. *Edge* indices in the k array are used to identify interfaces specified by *xedge* and *zedge* parameters. The first k index corresponds to the first interface, the second k index corresponds to the second interface, and so on. After all the vertices have been inserted into the model, the $sfil$l parameter is used to fill with a determinated velocity value closed regions bounded by fixed edges. The (x, z) component of the $sfill$ parameter is used to identify a closed region. Finally, `Sxplot` and `Spsplot` are used to display the model in the screen and to create a Post-script file, respectively.

Appendix A contains Script(A.2), which shows how `Trimodel` works. all the parameters that can be adjusted are showed. In the Figure (4.2) the velocity profile generated by Script(A.2) is shown. The white lines in Figure (4.2) represent the triangles generated by the Delaunay interpolation.

The output file of `Trimodel` is a triangulated file o sloth model file. This kind of file is not accepted by all the functions of seismic unix (for instance, `Sufdmod2`). Then, a convertion to uniformly sampled model is often necessary.

4.1.3 Triangulated models to uniform models. *Tri2uni.*

Despite the fact that triangulated models allow us to create more complicated geological structures than uniformly sampled models. There are some commands of *Seismic Unix* package that require as input uniformly sampled models. However, this is not a limitacion in the use of `Trimodel` command, since it is possible to change from a triangulated interpolation to uniform interpolation and vice-versa. This conversion is done by `Tri2uni` command.

For the `Tri2uni` command, it is necessary to introduce the number of samples in the slow

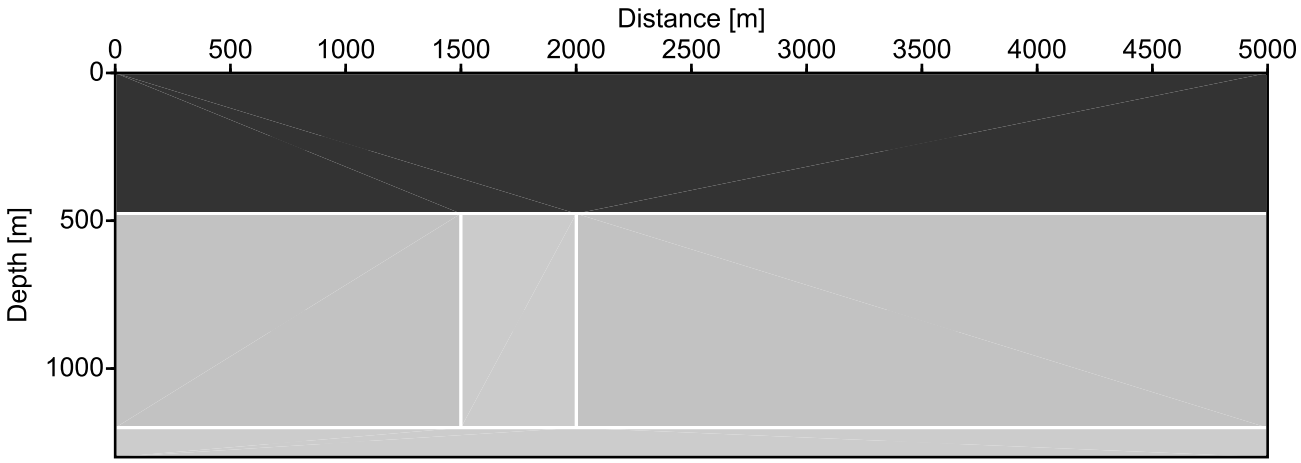

Figure 4.2: Triangulated velocity model generated by *Trimodel* comman. Model with 3 horizontal layers, containing a velocity anomaly with a limited extension.

and fast directions ($n2$ and $n1$) and the sampling intervals ($d2$ and $d1$). The values for n1 and n2 must be calculated using Equations (4.1) and (4.2).

$$n_1 = \frac{z_{max}}{d_1} \tag{4.1}$$

$$n_2 = \frac{x_{max}}{d_2} \tag{4.2}$$

where, $xmax$ and $zmax$ are the maximun length and the maximun depth of the triangulated model, respectively.

Figure(4.3) shows the uniformly sampled model generated by `Tri2uni`. Script (A.3) in Appendix A is used to execute `Tri2uni` command.

4.2 Acoustic wave propagation modelling. Finite difference scheme. *Sufdmod2*

`Sufdmod2` command of *Seismic Unix*, performs a 2^{nd} order finite-difference modelling for the acoustic wave equation over a subsurface model. `Sufdmod2` command gives the numerical solution for the wave equation by carrying out a second-order Taylor series expansion of the equation. The input files of `Sufdmod2` are a uniformly sampled velocity and density models. This command provides two output files, one containing the waves $[nx][nt]$ for time steps, and another for horizontal line of seismograms $[nx][nt]$, containing the Shotgather.

Seismic Unix package offers the possibility to obtain wave propagation movies and Shotgathers, for one, or multiple shots. In those files it is possible to identify different phenomena

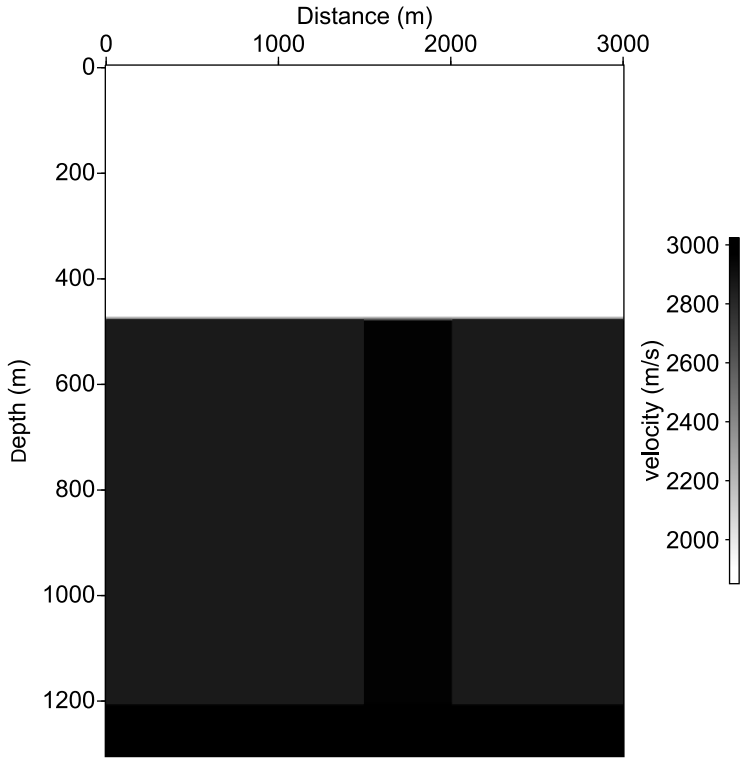

Figure 4.3: Uniform model generated by *Tri2uni* command.

(reflexion, refraction, difraction and interference) along the subsurface models. For that purpose, the user must insert the subsurface models generated using Script (A.1) or (A.2), and the adquisition parameters in Script (A.4), which contains a explanation in detail about the syntax and parameters of `Sufdmod2`. Those Scripts were designed in order to be used over any model. It is required to adjust some parameters related to the model and acquisition. In Figure (4.4) a Shotgather generated by executing Script (A.4) is showed.

A important factor to be aware when using `Sufdmod2`, is the stability of the finite-difference schemes. In this sense, the ratio between temporal sampling and spatial sampling must be limited. In order to ensure the fulfillment of this condition, `Sufdmod2` uses a stability criteria according to the Courant-Friedrichs-Lewy condition, Equation (2.14). The values of v_{max} and Δx are introduced by the user, and the value for C_{max} is set by `Sufdmod2` as $1/2$. It is important to consider appropriate values of dx to ensure that the temporal sampling is within the range of real seismic surveys ($10ms - 1ms$).

Another important parameter to talk about is the maximun frequency (f_{max}). As consequence of the numerical phenomenon socalled *dispersion*, the phase speed of a wave is a function of the frequency, even if the material properties are not frequency dependent. Theoretically, the solutions for the wave equation given by finite-difference modelling represent a good approximation of the continuous solution as long as the spatial sampling is much smaller than the

wavelength. When the wavelength is in the order of spatial sampling, the discrete solutions do not match with the continuous solutions. Therefore, if f_{max} is not adjusted carefully, dispersion will take place. To get a simulated data as similar as possible to reality the values of f_{max} must be chosen in the range of the real seismic surveys $(20Hz - 60Hz)$.

It is important to point out that to minimize undesired reflections coming from the bounds of the model, non-free surface boundaries (absorbers) must be set with the absorption parameter (abs). Since reflections coming from the free surface are part of the real seismic experiment, by setting $abs = 0, 1, 1, 1$ no absorber surface is placed at the upper border. Figure (4.5) shows 4 snapshots from the wave propagation movie. In the upper left snapshot it is possible to see a reflexion event located at approximatly $500m$ of depth. The refraction wave can be detailed in the bottom left figure.

4.3 Modeling of a 2D+1 seismic acquisition.

Acquisition is the generation and recording of seismic data. Acquisition involves many different receiver configurations, which are going to record the acoustic or elastic vibrations generated by a set of sources, such as a vibrators, dynamite shots, or an air guns. To predict the seismic response of the data to be recorded, modelling is done. In modelling for seismic acquisition, the response of each subsurface point is defined by the solution for the acoustic wave propagation experiment in each source position. This experiment requires the velocity and density profiles related to each shot point. Therefore, a iteritive program containg a number of loops equal to the number of shot points is necessary to modelate a seismic acquisition. Script (A.5) have been created in orden to to carry out modeling of seismic acquisition by introducing a few input parameters.

The acquisition geometry implemeted in Script (A.5), is the type Straddle Spread. Hence, the maximun offset ($offset_{max} = 3000m$) is equal to the length of the array ($LT = 3000m$). In contrats with a real acquisition, in this modelling a receiver is located in the same place as a shot point ($Offset = 0$). For this Script the receiver interval (IR) is equal to $10m$, and the total number of receivers (NR) is 301. The position for the first receiver is equal to 0 meters, and the position for the last receiver (limit of the iteration) is given by

$$LIMIT = NS * IS - IS,$$

where NS and IS are the number of shots and the shot interval, respectively.

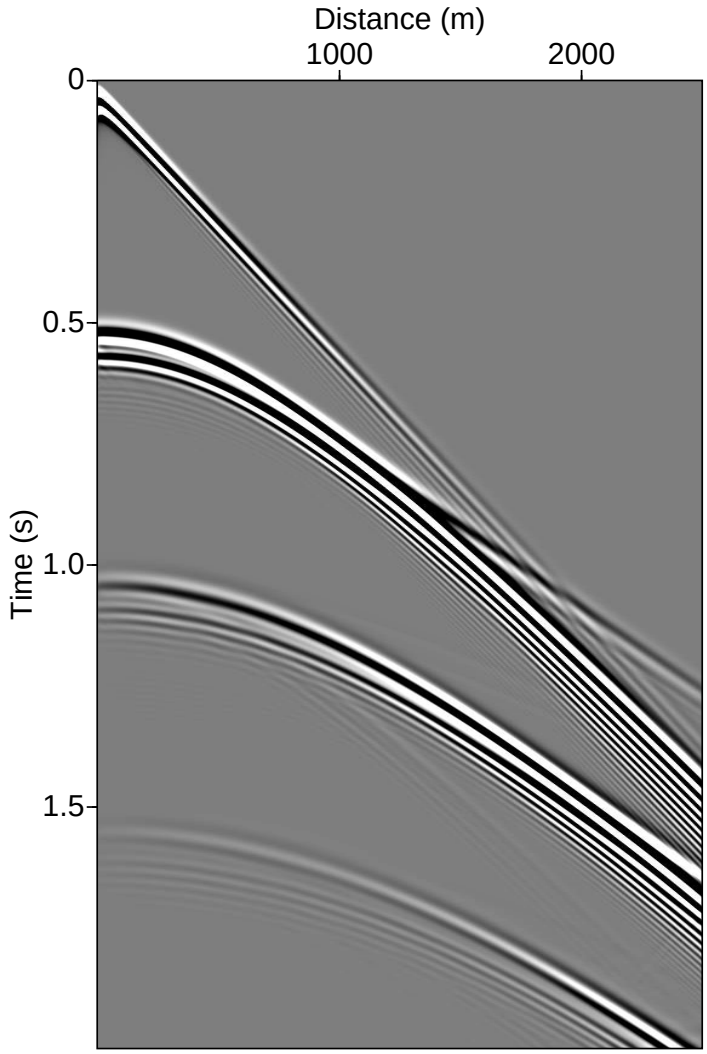

Figure 4.4: Synthetic Shotgather, generated by Sufdmod2 command, over the Uniformly sampled model presented in Figure (4.3).

Implementing the `Unif2` command and by introducing the required values, Script (A.5) generates and plots the velocity and density profiles related to each shot point position. A profile for the shot point placed at $0m$, has information from the receiver located at $0m$ to the receiver at $3000m$. In the same way, if the shot point is located at $50m$, the profile contains information from $50m$ to $3050m$, and so on. Once the subsurface models are done, Script (A.5) generates the Shotgathers and the movies for the wave propagation for aech shot point by executing the Sudfmod2 command. It is important to highlight that a number of files equal to the number of shot points (NS) will be returned. Those files are named according to the shot point position that generated them.

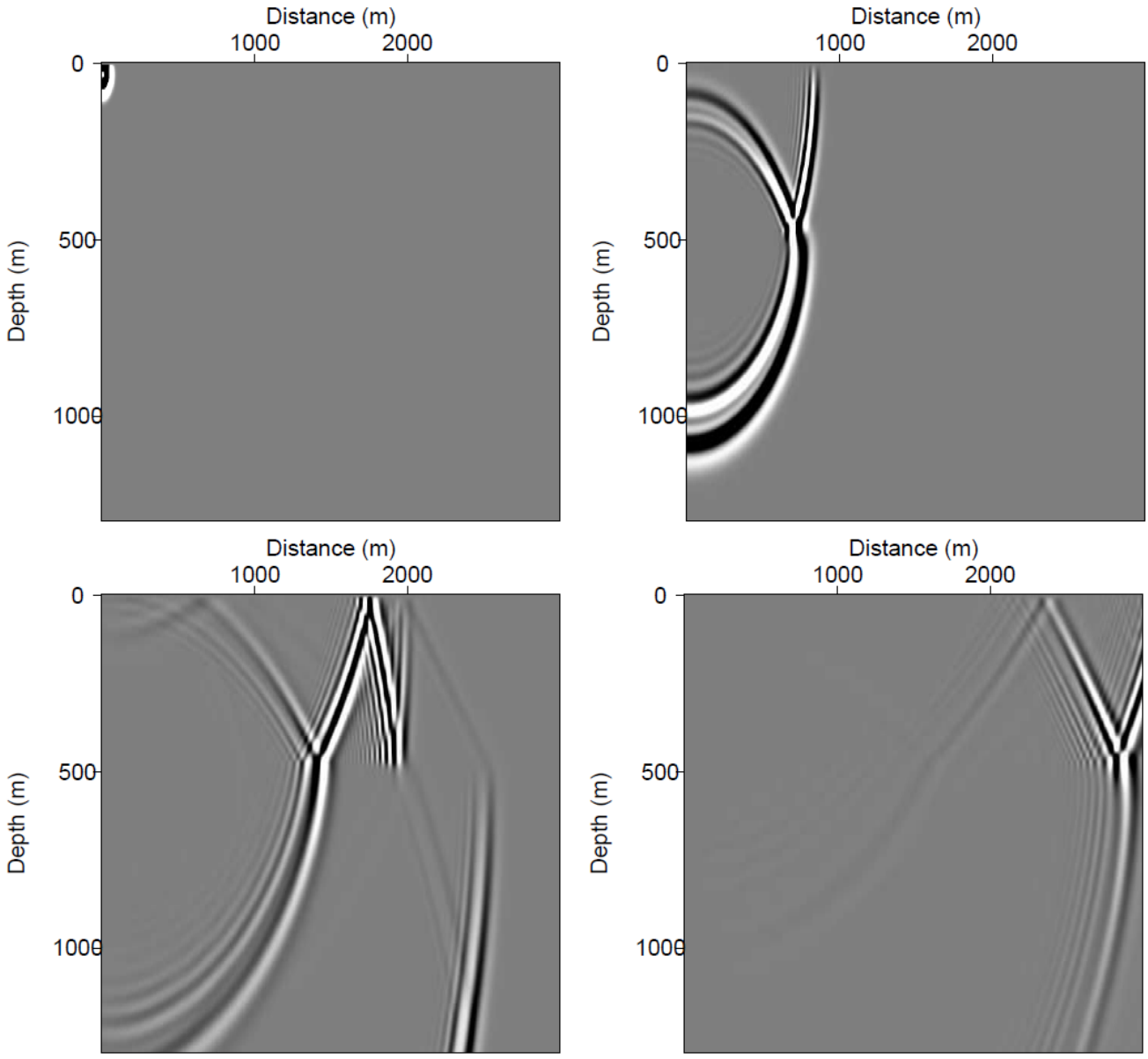

Figure 4.5: Snapshots of the acoustic wave propagation movie.

Another important aspect to be aware when using Script (A.5) is that the values for the sampling parameters nx, nz, dx, and dz used for the generation of the subsurface models must be equal to the acquisition parameters NR and IR. Otherwise, the solutions for the wave propagation generated by the finite-difference scheme implemented by `Sufdmod2` will be wrong.

4.4 Concatenation of Shotgathers, header adjusting and CMP sorting.

In section (4.3), a set of Shotgathers were obtained by using Script (A.5). These Shotgathers represent the acquisition survey of a seismic line. In manipulation of seismic data, the

generation of a Supergather is often necessary. Hence, in order to create a Supershotgather, Script (A.6) utilizes the command `CAT` to combine adjacent Shotgathers and save them in a unique file. It is important to emphasize that all the operations done upon the seismic data are based on the header information. The header parameters in the Shotgathers, define the acquisition geometry. Therefore, If this information is not correct, the procedures will generate erroneous results. Script (A.6) setups the header values for the Supergather by using `Sushw` command. This configuration is made according to the acquisition parameters. In Table (4.2) the header parameters, for the simulated acquisition survey, are summarized. Once the header is configured, it is possible to extract a single Shotgather from the complete seismic line by using the command `Suwind`, as each seismic trace has various parameters in the header, a key word to select the desired data must be used. Figure (4.6a) shows 4 Shotgathers selected from the concatenated file by using `Suwind` command. Notice that the distance within Shotgathers (i.e distance between shot points, IS) is $50m$.

Common-midpoint gathers CMP (also called common-depth point CDP) are required for velocity analyses, Normal Moveout Correction (NMO), stacking, among other techniques. In this sense, the data in the Supershotgather previously created, can be sorted by CDP using the command `Susort`. It sorts the data by increasing or decreasing CDP points using the key words cpd and -cdp, respectively. In the same way, the traces are sorted by increasing or decreasing offset for each CDP point using the key words offset and - offset, respectively.

Once the data is sorted by CDP, using `Suwind` it is possible to pick out the desired CMPgahter by introducing the values min and max for the keywords. In Figure (4.6b) 4 CMPgathers with full-fold are showed.

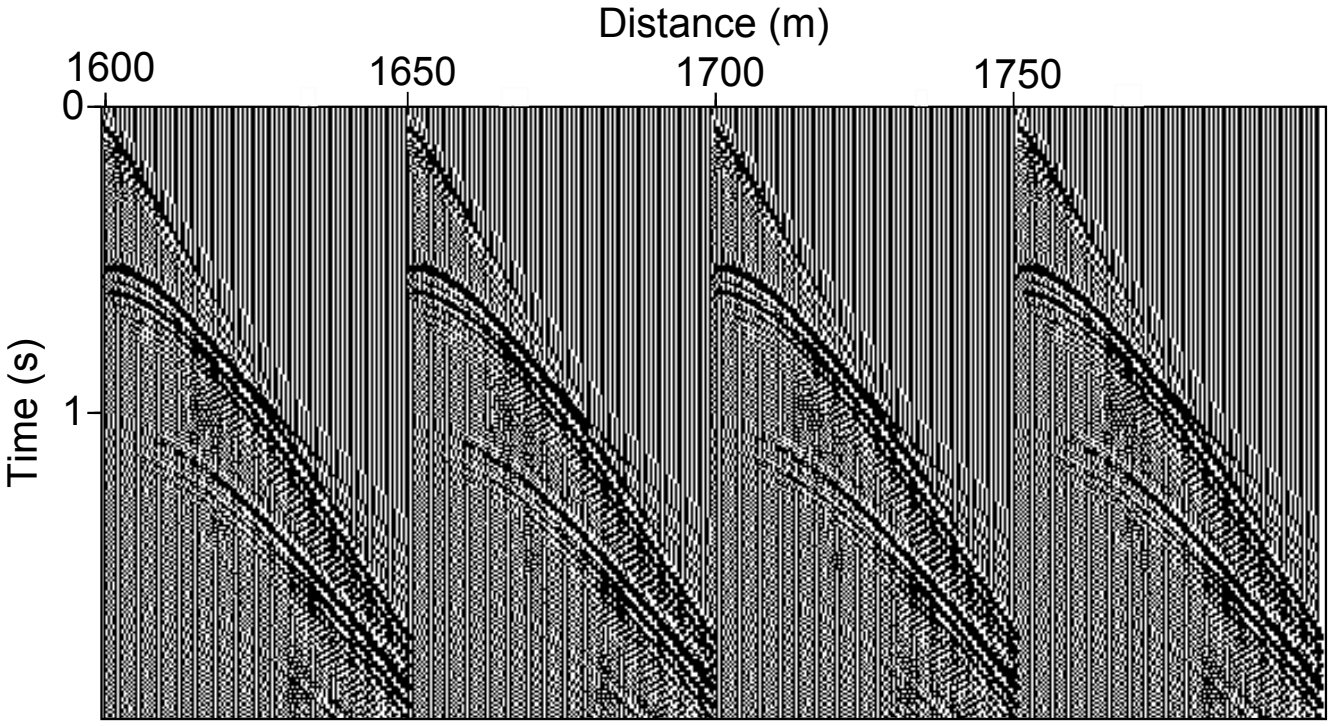

(a)

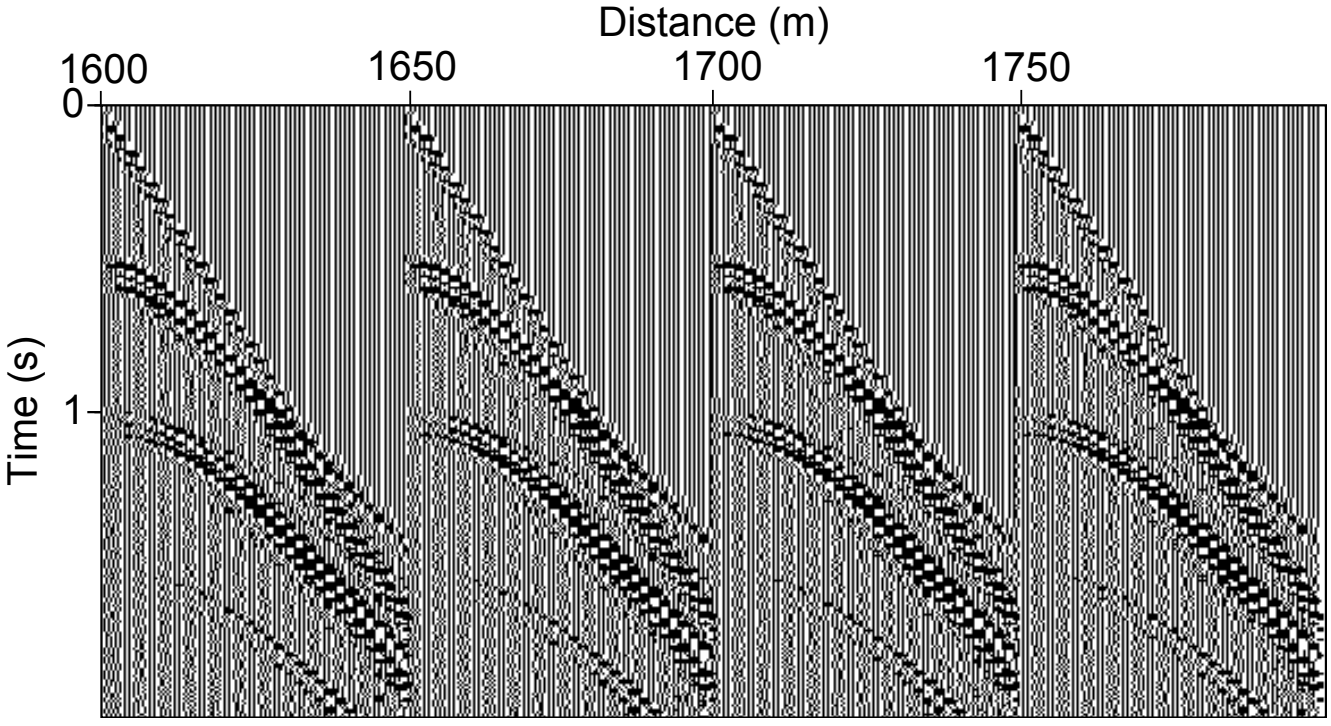

(b)

Figure 4.6: (a)Shotgathers from the synthetic acquisition.(b)CMPgathers from the synthetic acquisition. The common mid points were picked each $50m$, this distance is equal to the distance between shot points.

Key	Value
$tracl$	1 - 12040
$tracr$	1 - 12040
$fldr$	1 - 40
$traf$	1 - 301
cdp	0 - 3450
$trid$	1
$offset$	0 - 3000
$sdepth$	50
sx	0 - 1950
gx	0 - 4950
ns	1189
dt	1683

Table 4.2: Header of shotgather for model 1.

Chapter 5

Refraction timeshift due to modeled gas leakage

Landrø et al. (2004 [12]), introduced a method for more accurate estimation of velocity changes in high velocity reservoirs. An interesting property of the method is that it is a pure velocity estimator. The proposed time-lapse refraction technique works by measuring timeshifts on first arrival head-waves from the reservoir layer. The method assumes that the dominant time-lapse effects are confined to the reservoir. The main requirements for the method are acquisition of long offset data, typically one to two kilometer beyond the critical offset, and increasing velocity across the interface to be analyzed (e.g. at top interface of the reservoir.).

In order to understand the effect of changes in seismic properties on the refraction timeshift, simple geological models are created. Figure (5.1) shows velocity and density profiles, for the base case. The parameters used for the base model are summarized in Table (5.1). Synthetic time-lapse seismic data was generated by performing a 2^{nd} order finite-difference algorithm over the geological models. Only the acoustic case was modeled, due to the fact that no reliable shear velocity data was available. The signal used for the finite-difference modelling scheme is a ricker wavelet, with a peak frequency of 30Hz. Absorbing boundaries were used in all directions except the free surface, thus, multiples are present.

The modeled data were used to identify the presence of refracted energy. Since refracted energy is weak compared to reflected energy, a high gain had to be applied to the gathers in order to see the head wave. Figure (5.2) shows the same Shotgather, in two different color scales for the base case model.

In this study, refracted timeshift is used as an alternative method to estimate small velocity changes due to *gas leakage*. In order to evaluate the feasibility of using refraction

timeshif as gas leakage detector, two velocity variation scenarios have been modeled. For the first case, a velocity variation of $60m/s$ in the whole reservoir layer is used. While a velocity variation of $60m/s$ with a length of $500m$ (i.e a velocity anomaly with limited extension) was modeled for the second case.

Layers	Thickness (m)	Base Depth (m)	v_p (m/s)	ρ (g/m^3)
Layer 1	476	476	1904	1.75
Layer 2	724	1200	2900 (base) 2960 (monitor) 2960 (monitor anomaly)	1.8
Layer 3	100	1300	2970	1.8

Table 5.1: Parameters describing the layered model of Test 1 for finite difference modelling. v_p and ρ represent the P-wave velocity and density, respectively.

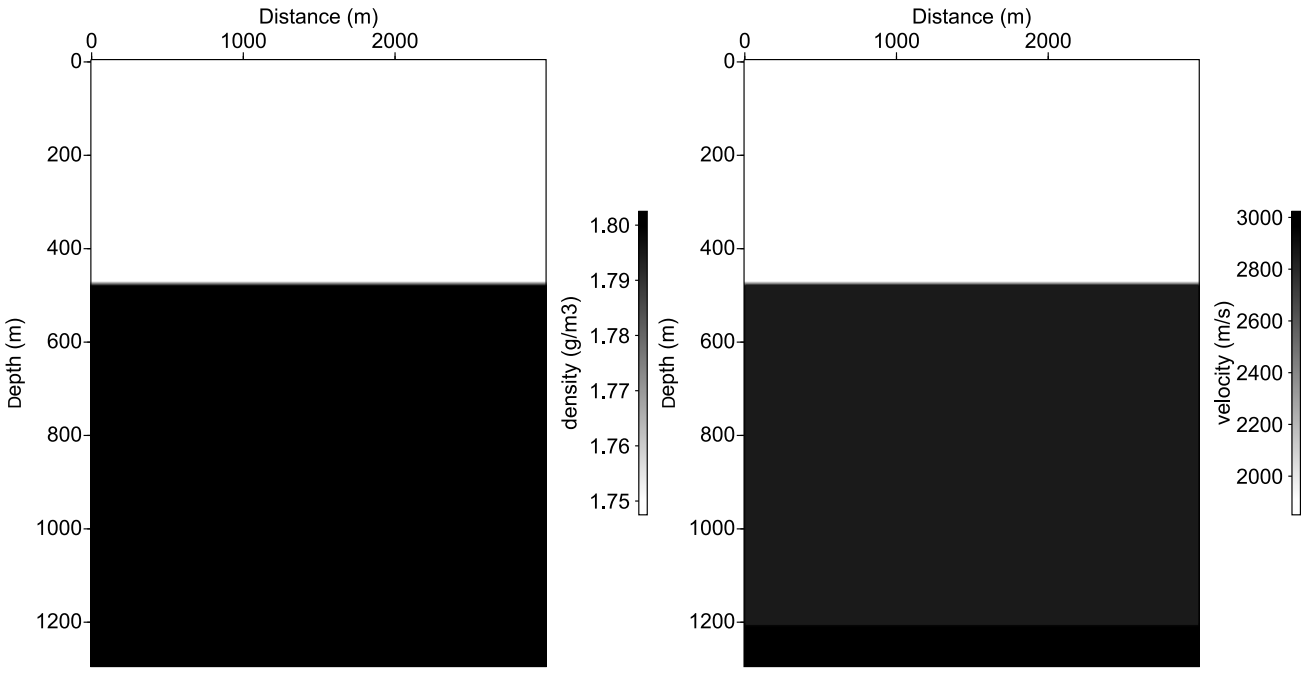

(a) (b)

Figure 5.1: Uniform models generated by *Unif2* command.(a) Density and (b) Velocity profiles for a simple model with horizontal layers.

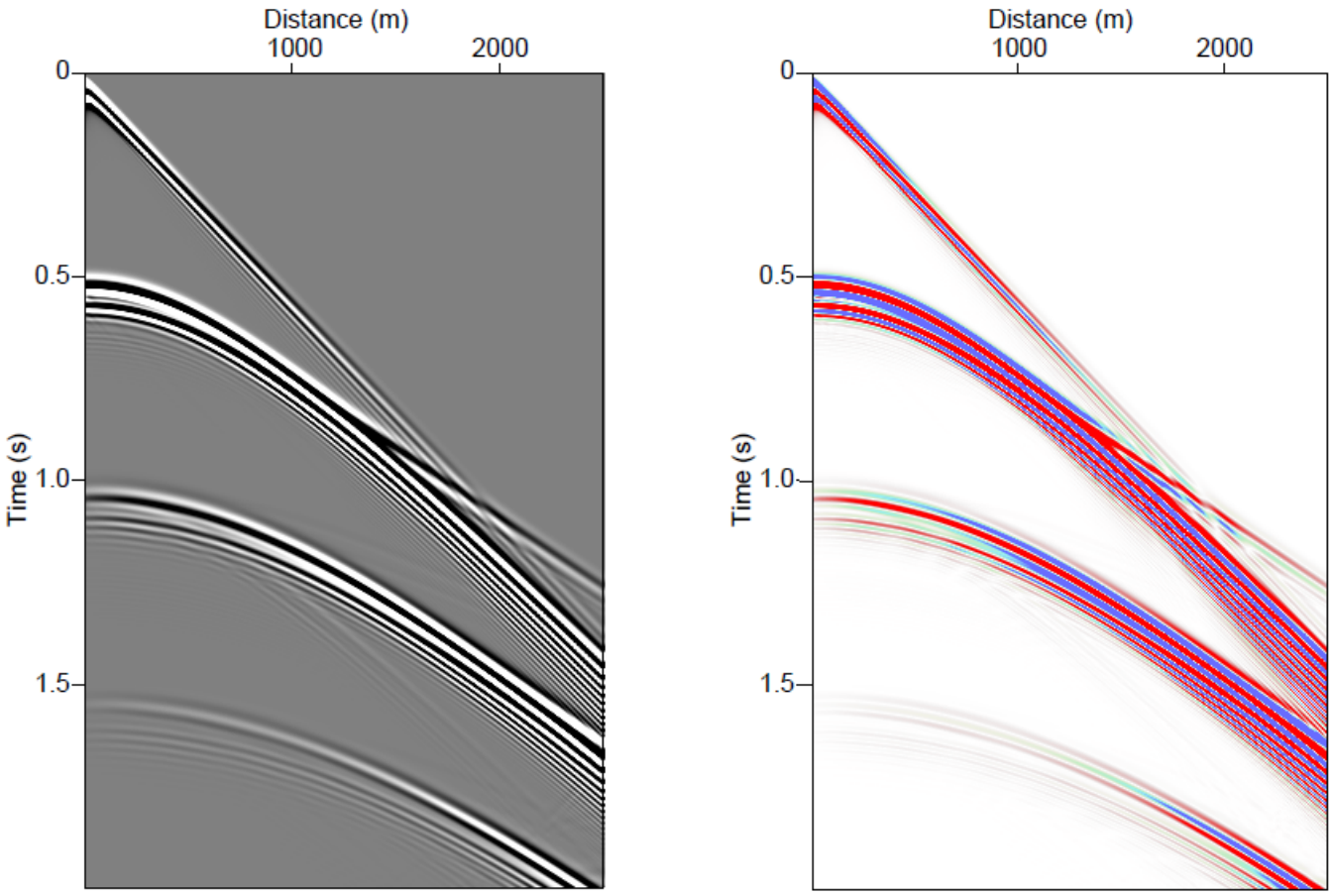

(a) (b)

Figure 5.2: Synthetic Shotgather generated using *Sufdmod2* command, data for base case. (a) grey scale colormap, (b) hsv4 colormap.

5.1 Test 1: Refraction timeshift for a velocity change in the whole reservoir layer

In this model, the top reservoir is located at $H = 476m$, the velocity of the reservoir layer is $2900m/s$ for the base survey, and $2960m/s$ for the monitor survey. Considering the overburden as one homogeneous medium with its thickness remaining constant, and with a velocity of $v = 1904m/s$, it is possible to compute the critical offset for the top reservoir using Equation (3.7). Thus, the critical offsets for for the base and monitor surveys are $830m$ and $800m$, respectively. However, the reservoir refractions are visible as first arrivals over a distance of more than one kilometers, starting at about $1400m$ away from the shot (maximun amplitude offset).

Figure (5.3a) shows the FD result for base survey. In Figure (5.3b) the difference data between the base and monitor surveys, is presented. The P-wave velocity change between the

surveys is +2.06%; this velocity variation was modelled for the whole reservoir layer. Notice that the difference section shows high amplitude changes at offsets larger than the critical offset (i.e. maximum amplitude offset). It is obvious from this figure that the 4D differences are significantly larger for refracted signals compared to reflected signals.

It is important to emphasize that synthetic data was modeled as pre (base) and post (monitor) gas leakage. The difference between the base and monitor survey, Figure (5.3b), gives us a qualitative perspective about the potential of the time-lapse refraction to monitor small velocity changes (2.06%) in the reservoir layer.

To quantify the changes due to simulated gas leakage, base and monitor data are merged and interleaved in the same gather, Figure (5.4). In this figure, the recorded travel time differences due to gas leakage are observable as timeshifts on first-arrival head waves. A timeshift around $10ms$ can be observed in a detailed comparison in Figure (5.5).

Script (B.2) was used to calculate the refraction timeshift, subtracting traveltime values from the baseline survey (red line in Figure 5.4) and values from monitor survey (blue line in Figure 5.4). Only timeshifts associated with head wave (i.e. beyond the maximum amplitude offset) were considered. The computed timeshift versus offset is shown in Figure (5.6).

In Figure (5.6), blue circles represent the exact measured timeshift from the Shotgathers, cyan line indicates the linear interpolation for the measurement and green line indicates the theoretical timeshift. The timeshift predicted by Equation (3.12) and the timeshift measured from synthetic data, match reasonably well. Notice that timeshift curve increases monotonically after critical offset, this is due to the refraction timeshift is a function of the horizontal distance that the refracted ray travels along the interface.

Considering a 3-layer simple model as shown in Figure (5.1), if one of the layers (upper layer in this case) remains unchanged during the variation in the medium below, then the relative timeshift is only a function of P-wave velocity below the interface (i.e. v_p in the reservoir only). Under these conditions, and asuming no change in the thinkness, it is feasible to invert the timeshift, using Equation (3.12), back to the P-wave velocity change of the medium below the interface. Picking an ordered pair (timeshift,offset) from Figure (5.6), the estimated P-wave velocity change is 60.5 m/s. This corresponds to 1% of error compared to the modeled velocity change of 60 m/s. However, for real data, is expected that other issues like noise, location accuracy, source strength etc. will affect the repeatability of the seismic data; therefore, the accuracy of the proposed method.

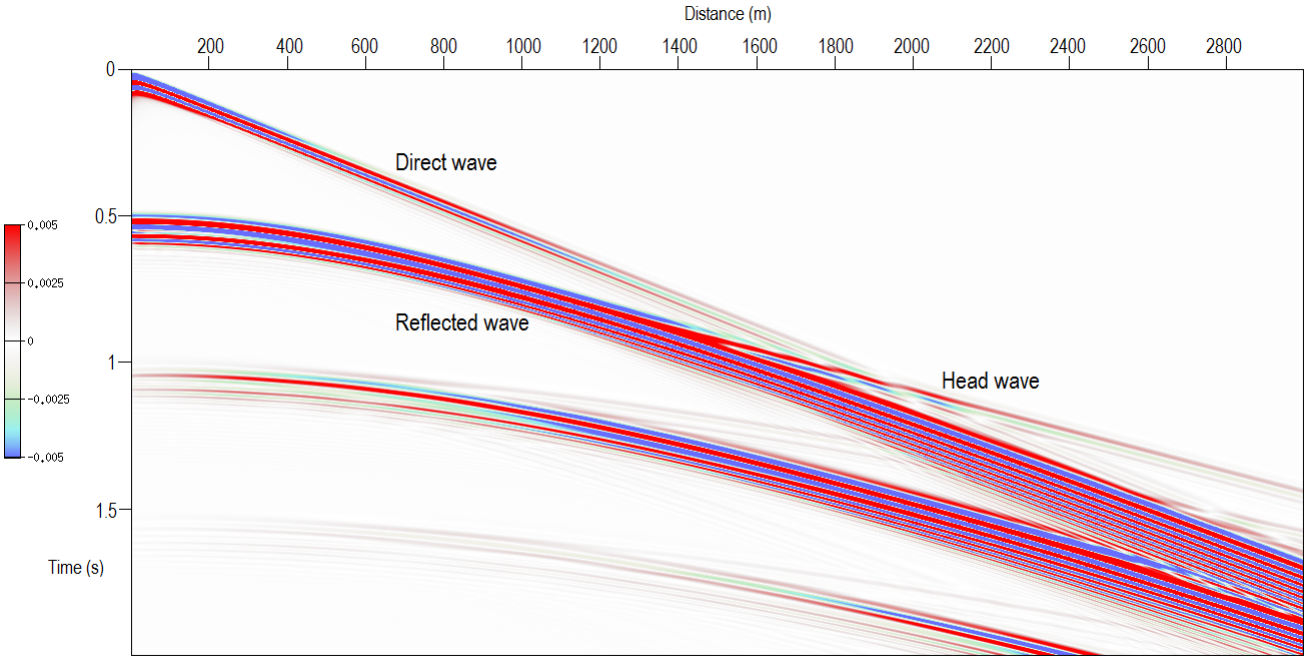

(a)

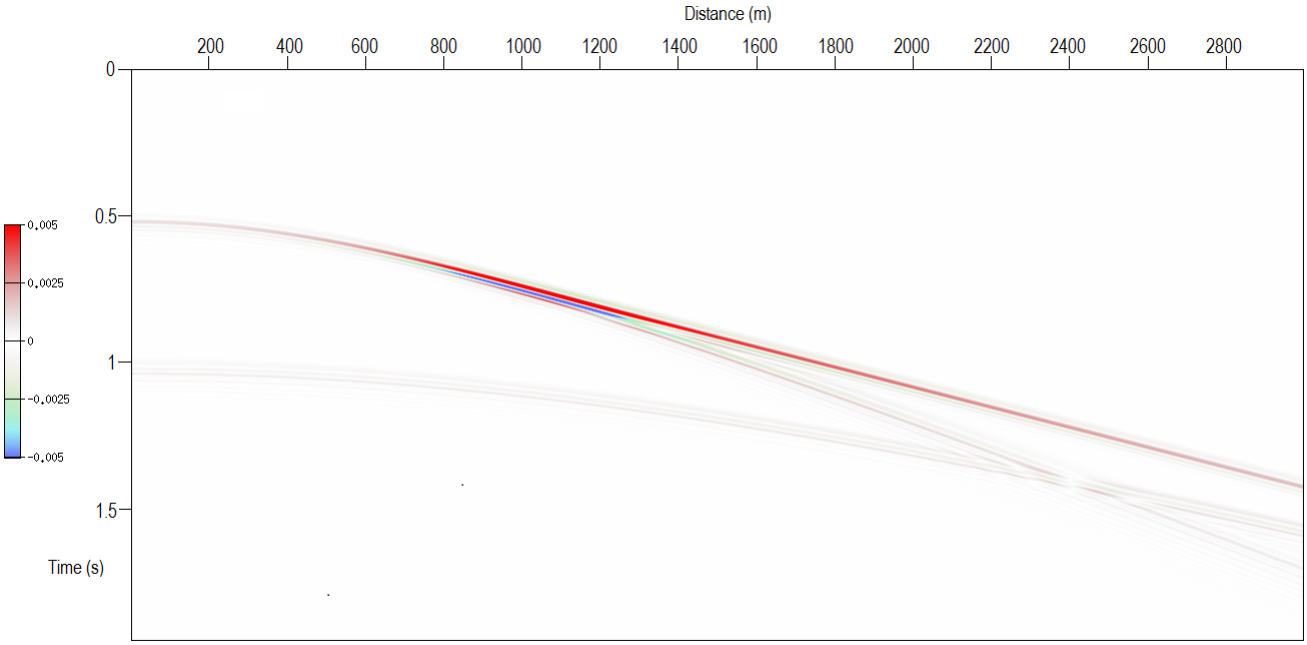

(b)

Figure 5.3: Synthetic Shotgather generated using *Sufdmod2* command. (a) Data for base case, the target interface is located around 0.5s. (b) Difference between base and monitor data. For the monitor model, P-wave velocity was increased in the reservoir layer (second layer) by 2.1% (60m/s). Notice that he 4D differences are significantly larger for refracted wave than for reflected wave.

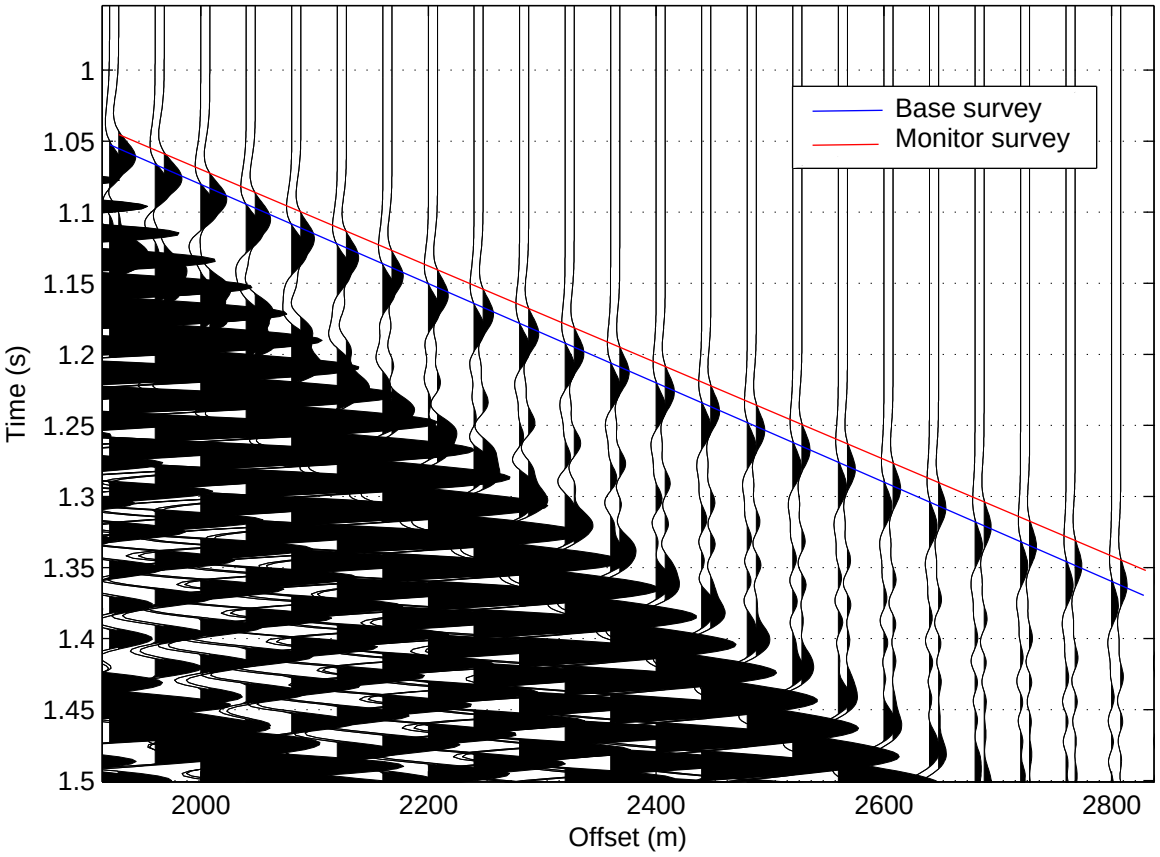

Figure 5.4: Refraction timeshift data. Base and monitor data were merged and intervaled. Blue and red lines indicate the refraction event for the base and monitor case, respectively. Notice that the separation between the two lines is increasing with offset.

5.2 Test 2: Refraction timeshift for a model including a velocity anomaly with a limited extension

When a velocity anomaly with a limited extension (l_a) is placed below a refracting interface, it is possible to observe a change in the slope for the monitor refracted event. This change generates a timeshift, which becomes greater with offset until it reachs a maximum. Two different monitor travel time scenarios can happen. Therefore, the timeshift is described by two different equations:

- First case: $\frac{x_{cri}}{2} + l_a > x - l_1 > +\frac{x_{cri}}{2}$

$$\Delta t \approx \left(x - l_1 - \frac{H v_1}{\sqrt{v_2^2 - v_1^2}} \right) \frac{\Delta v_2}{v_2^2} \tag{5.1}$$

- Second case: $x - l_1 > +\frac{x_{cri}}{2} + l_a$

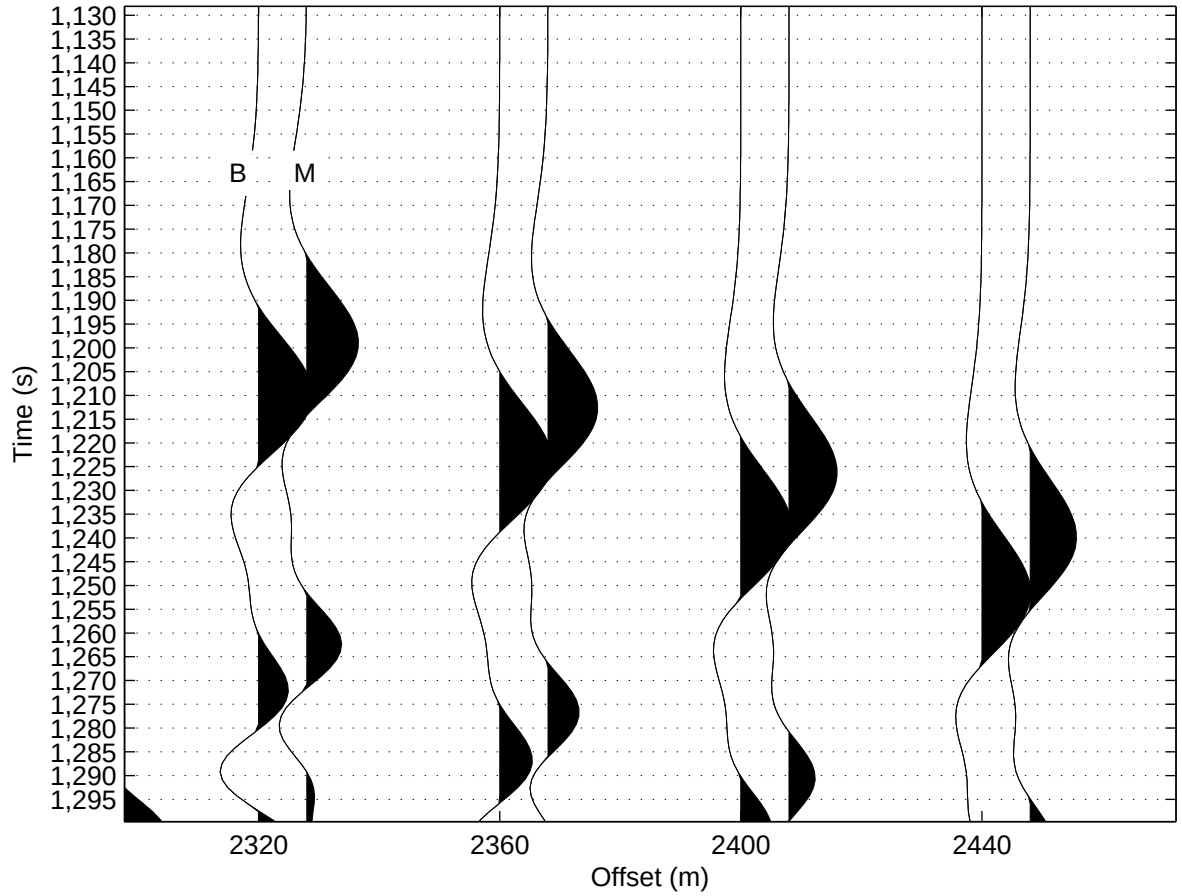

Figure 5.5: Zoom from previous figure. Detail comparison between base and monitor surveys. A timeshift around 10 ms can be observed.

$$\Delta t \approx l_a \frac{\Delta v_2}{v_2^2} \tag{5.2}$$

In the first case, described by Equation (5.1), the timeshift is a function of the horizontal distance that the head wave travels along the anomaly. Hence, the timeshift increases monotonically with offset, while the rays are still traveling inside the anomaly. On the other hand, in the second case, described by Equation (5.2), the head wave has passed through the whole anomaly and timeshift reaches a maximum. Thus, the timeshift is independent of the horizontal distance travelled by the rays and remains constant.

In order to understand the effect of a confined velocity change due to gas leakage on the refraction timeshift, a simple geological model for the monitor case containing a velocity anomaly was created. Figure (5.7) shows velocity and density profiles. This monitor model, preserves all the parameters of the monitor model for Test 1, save that the velocity change is restricted in lenght. This case considers an anomaly placed under the refracted interface (top

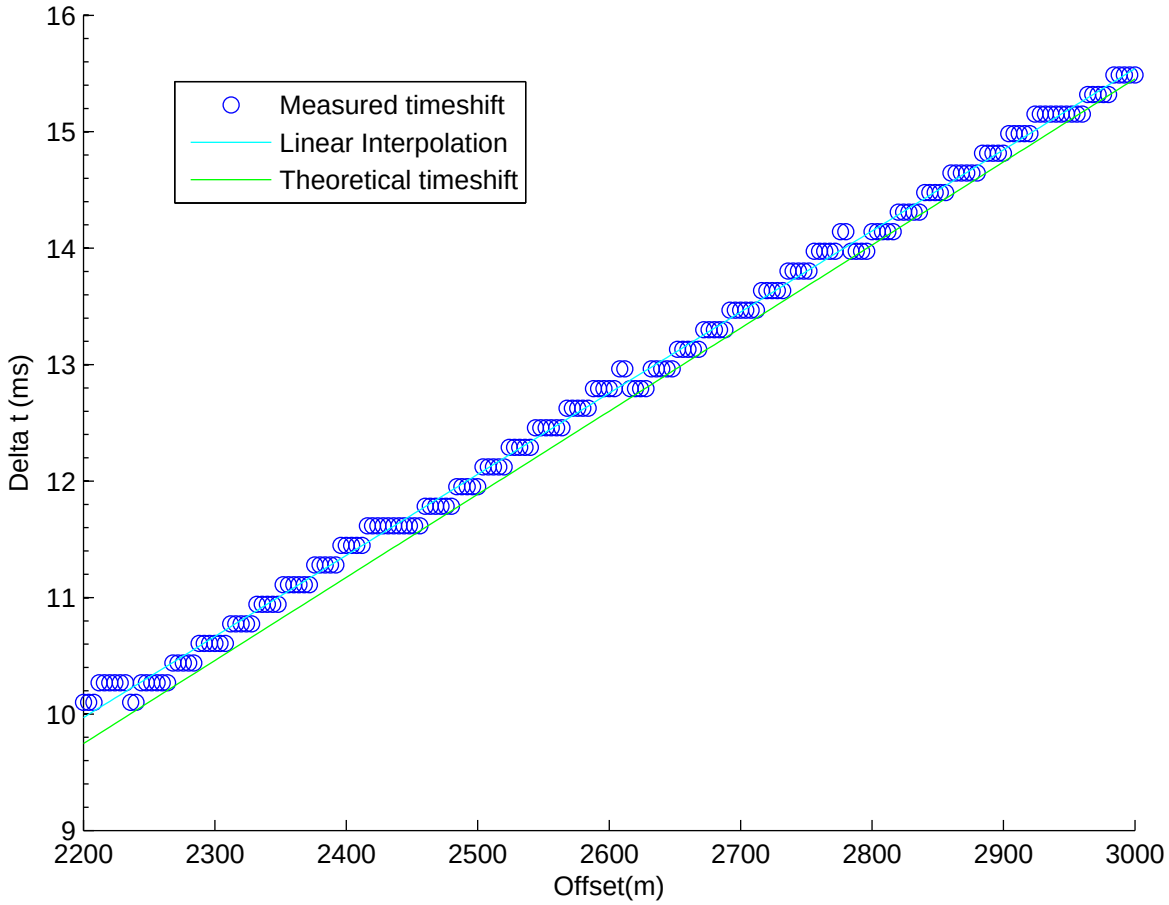

Figure 5.6: Timeshift between base and monitor data versus offset. Blue circles represent the measured timeshift from Shotgathers, cyan line indicates the linear interpolation for the measurement and green line indicates the theoretical timeshift. Timeshift increases monotonically with offset.

reservoir). The positive velocity contrast at the interface placed above the anomaly generates head waves.

Due to lateral P-wave velocity variation in the reservoir ($\Delta v_{res} = 60m/s$), the critical angle is changed; this change in the critical angle leads to a variation in the critical offset. For this model, the top reservoir is located at $H = 476m$ and the velocity for the reservoir layer is $2900m/s$. Considering, the overburden as one homogeneous medium with a velocity of $v = 1904m/s$ and its thickness remaining constant, it is possible to compute the critical offset for the top reservoir and its respective variation. Using Equations (3.7) and (3.10) the critical offsets are 800m outside the anomaly and, 830m in the center of the anomaly.

This study aims to use timeshift of shallow refraction events, from the reservoir layer, to identify shallow 4D anomalies caused by an underground hydrocarbon flow (gas leakage).

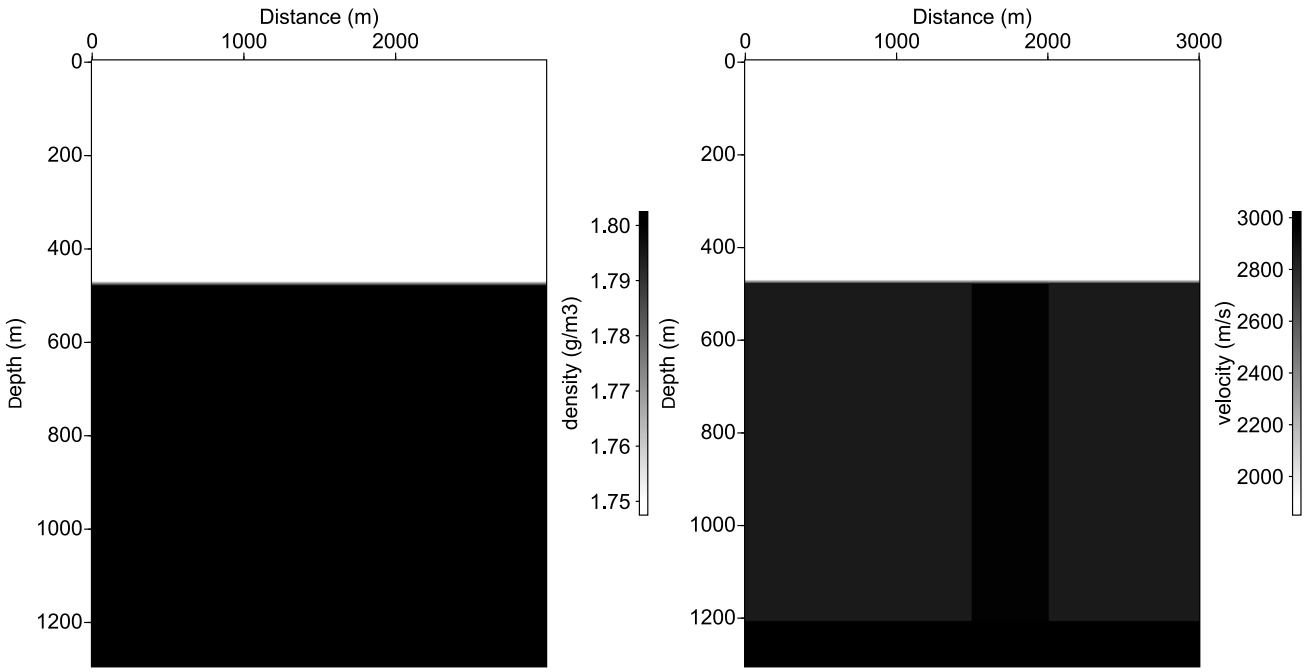

(a) (b)

Figure 5.7: Uniform models generated by *Unif2* and *Tri2uni* commands. (a) Density and (b) Velocity profiles including an anomaly with extension $l_a = 500m$ and $\Delta v = 60m/s$.

The underground flow variation can be considered as the modeled limited velocity anomaly of $500m$. The location and extension of the anomaly is shown in Figure (5.8).

To quantify the changes due to simulated gas leakage, base and monitor data are merged and interleaved in the same gather. Figure (5.9a) shows a CMP (1800) at the center of the high velocity anomaly and Figure (5.9b) shows a CMP(2400) outside the anomaly. Blue and red lines indicate the refraction event for the base and monitor case, respectively. In Figure (5.9a) it is possible to observe timeshift due to gas leakage on first-arrival head waves. Notice that for the reflected events (stronger in amplitude and present at a later time) no timeshift is observed in contrast to the refracted event.

Figure (5.10) shows a detail comparison between base and monitor case for a CMPgather (a) at the center of the anomaly and (b) outside the anomaly. A timeshift around $3.5ms$ can be observed in Figure (5.10a). However, no timeshift is observed in Figure (5.10b). Script (B.2), was used to calculate the exact refraction timeshift against the offset. This Script subtracts traveltime values from the baseline survey and values from monitor survey. As in Test 1, only timeshifts associated with head wave (i.e beyond the maximum amplitude offset) were considered. The computed timeshift versus offset is shown in Figure (5.11).

In Figure (5.11) blue circles represent the exact timeshift measured from the Shotgathers, and green line indicates the theoretical timeshift. The timeshift predicted by Equations (5.1)

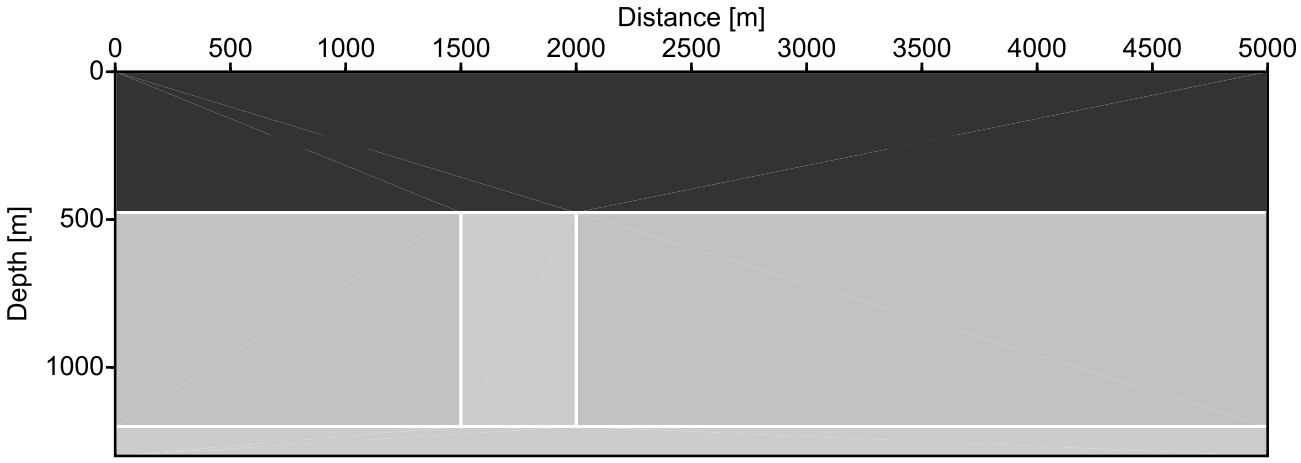

Figure 5.8: Triangulated velocity model generated by *Trimodel* command. Velocity profile for the model summarized in Table (5.1), including a velocity anomaly with extension of $l_a = 500m$ and $\Delta v = 60m/s$.

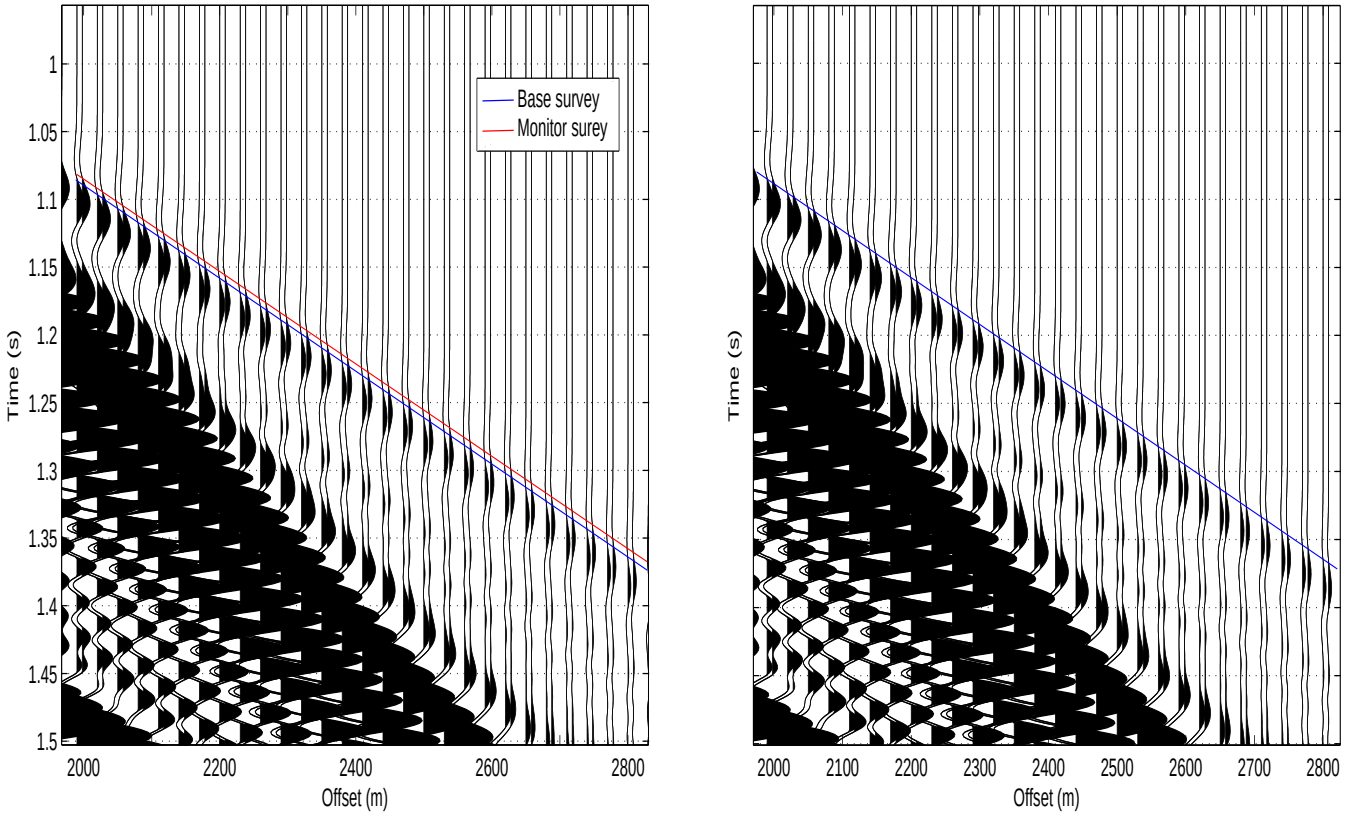

(a) (b)

Figure 5.9: Refraction timeshift generated by the model presented in Figure (5.7b). Base and monitor data are merged and intervaled. (a) shows a CMP (1800) at the center of the high velocity anomaly, (b) shows a CMP(2400) outside the anomaly. Blue and red lines indicate the refraction event for the base and monitor case respectively.

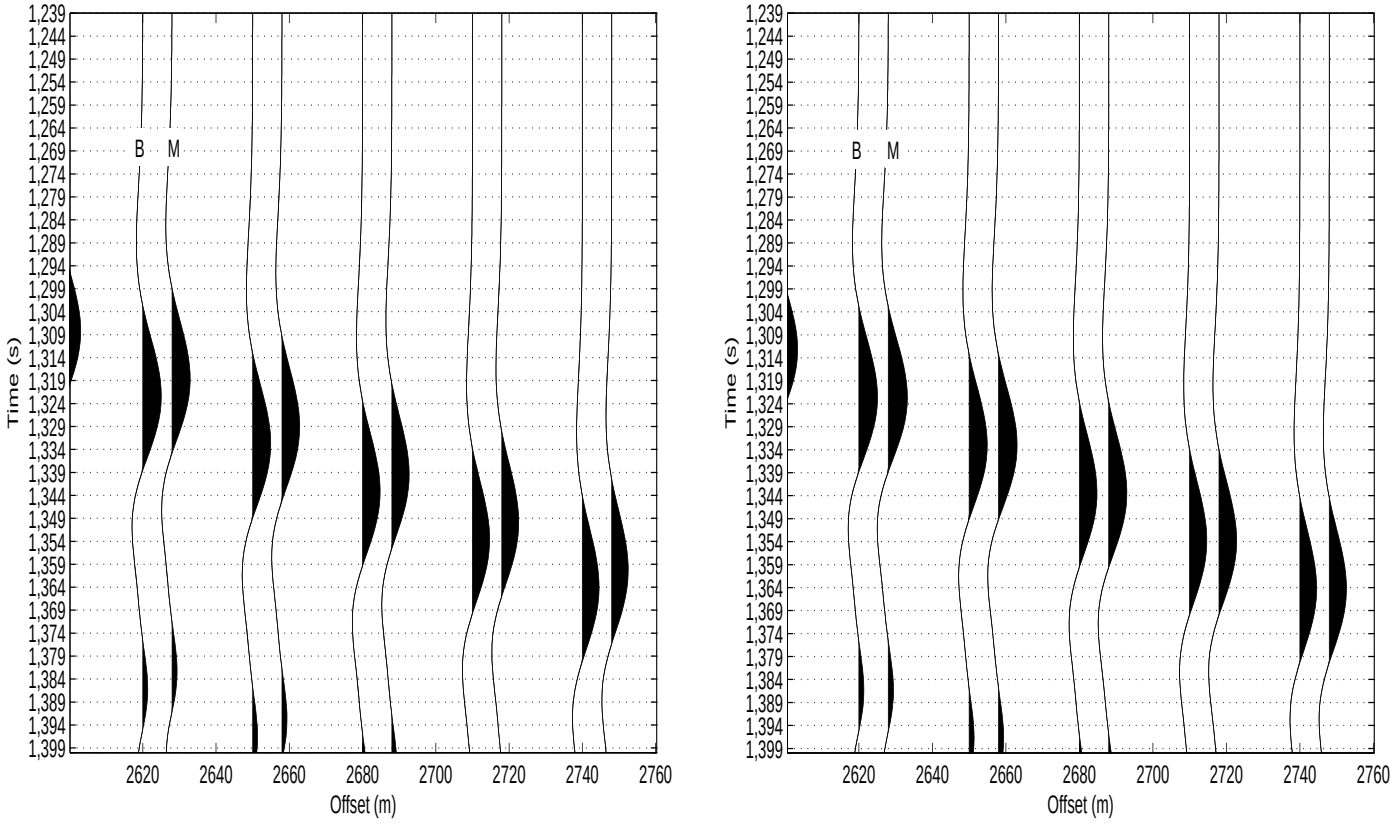

(a) (b)

Figure 5.10: Zoom from previous figure. Detail comparison between base and monitor data for a CMPgather (a) at the center of the anomaly and (b) outside the anomaly. A timeshift around 3.5 ms can be observed in left figure, while no timeshift is observed in right figure.

and (5.2), and the timeshift measured from synthetic data, match reasonably well. Notice that timeshift becomes non zero after $l_1 + \frac{x_{cri}}{2} = 1915m$ and increases with offset, but once the head waves travel along the whole anomaly at $l_1 + \frac{x_{cri}}{2} + l_a = 2415m$ timeshift reach a maximum and becomes constant, this is confirmed by Equation (5.2).

Since the relative timeshift is only a function of lateral velocity variation below the refracted interface (Δv_p for the limited extension anomaly), and assuming no change in the thinkness, Equation (5.2) can be used to invert timeshift back to P-wave velocity change. In this way, the velocity change can be computed using the maximum timeshift observed from the crossplot in Figure (5.11). In this sense, using the Equation (5.2), the estimated P-wave velocity change is 59 m/s. This corresponds to 1.6% of error compared to the modeled velocity change of 60 m/s. It is important to realize that the actual lateral extension of the anomaly can be obtained from Figure (5.11) by the subtraction of limit values that separate each trend

(i.e. 2415m – 1915m).

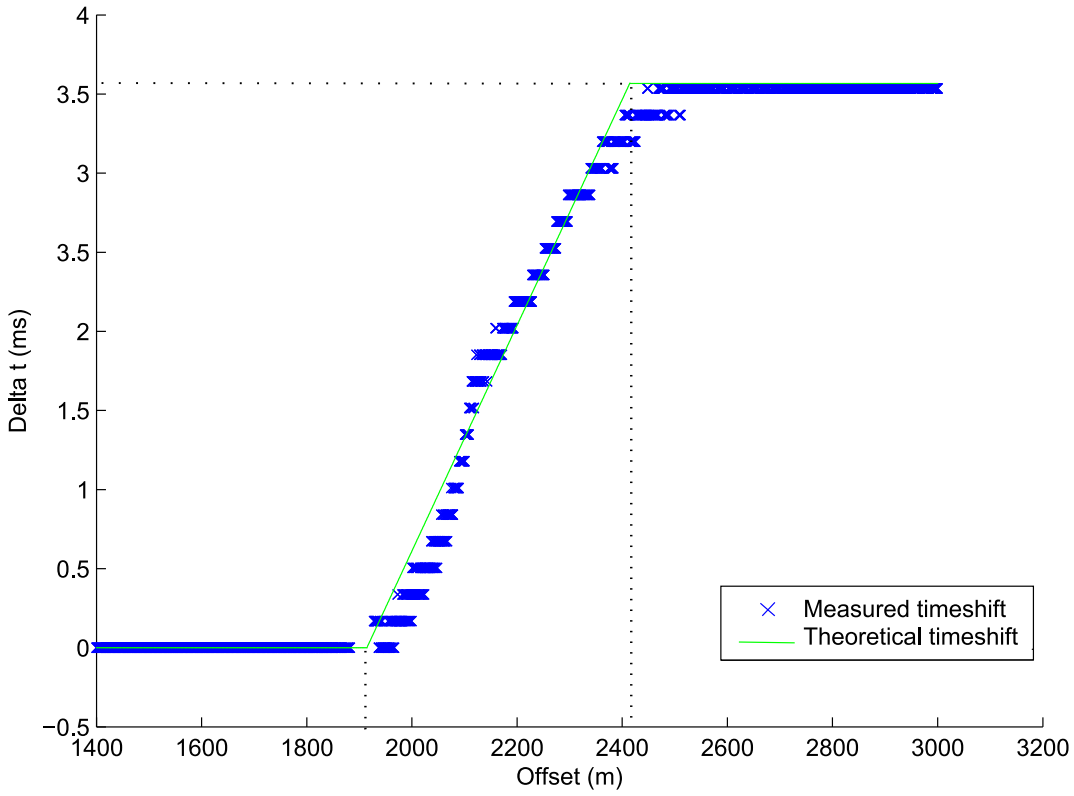

Figure 5.11: Timeshift between base and monitor data versus offset at the center of the anomaly. Timeshift increases monotonically with offset after $offset = 1915m$ $(l_1 + \frac{x_{cri}}{2})$. The maximun timeshift is reached when the refracted rays travel along the whole anomaly at $(l_1 + \frac{x_{cri}}{2} + l_a)$.

5.3 Timeshift due to a cylindrical velocity anomaly

Consider a cylindrical velocity anomaly, where the cylinder height is equal to the thickness of the reservoir layer ($h = 724m$) and diameter equal is to $500m$, as sketched in Figure (5.12). The velocity variation in the anomaly respect to the surroundings ($\Delta v_2 = 60m/s$) remains constant through the whole volume (i.e. is homogenous).

The synthetic acquisition of some 2D lines over the subsurface model containing the cylindrical velocity anomaly, will allow us to establish a clear perspective about how powerful is the time-lapse refraction technique for the detection of velocity changes, and to find out if it is possible to define its length and position. A wide range of azimuth values for the 2D lines must be used to map the whole anomaly area in a correct way.

A top view for the velocity anomaly is presented in Figure (5.13). The colour lines indicate the different 2D seismic lines with its respective azimuthal angles. Notice that the dotted lines

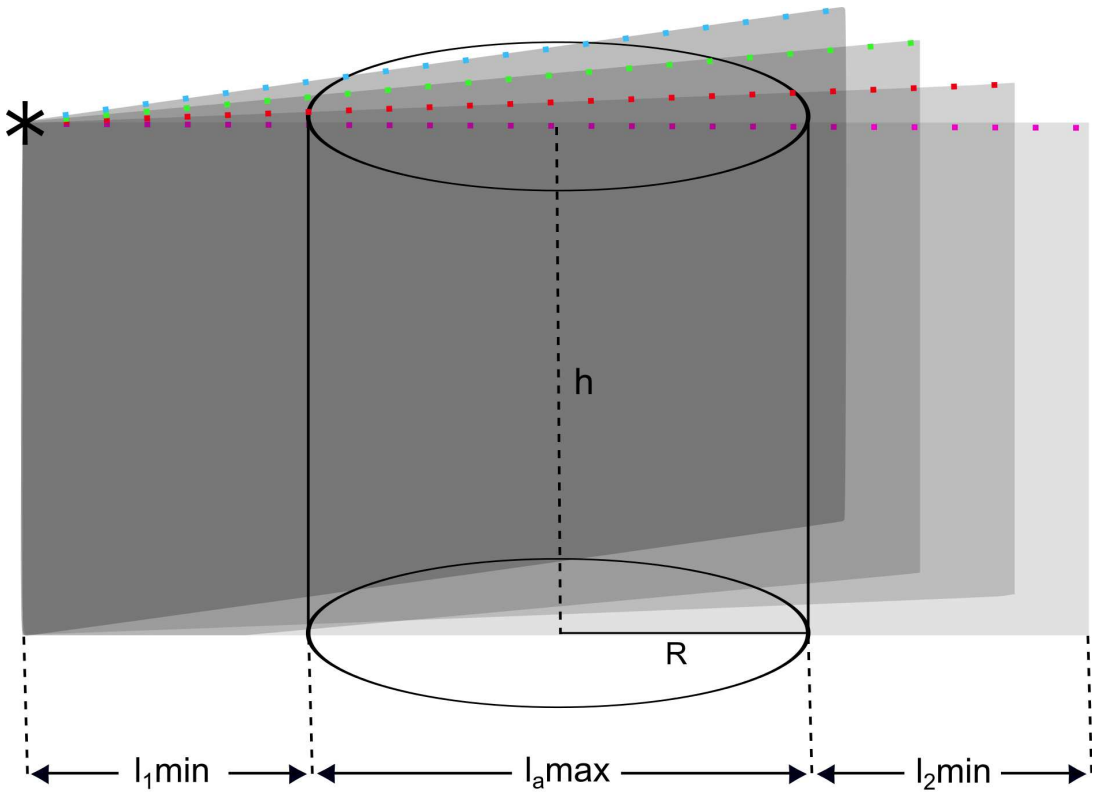

Figure 5.12: Cylindrical velocity anomaly, with $h = 724m$, $R = 250m$ and $\Delta v_2 = 60m/s$. Notice that the maximun extension of the anomaly is equal to 2R. Dotted lines represent the geophone arrays.

represent the geophone arrays planted along the lines, with a group interval of 10 meters. Each 2D line passes across a section of the velocity anomaly. As the anomaly has a cylindrical shape, as soon as the azimuthal angle increases, the anomaly extension decreases; until an azimuthal angle where no velocity anomaly can be detected, is reached.

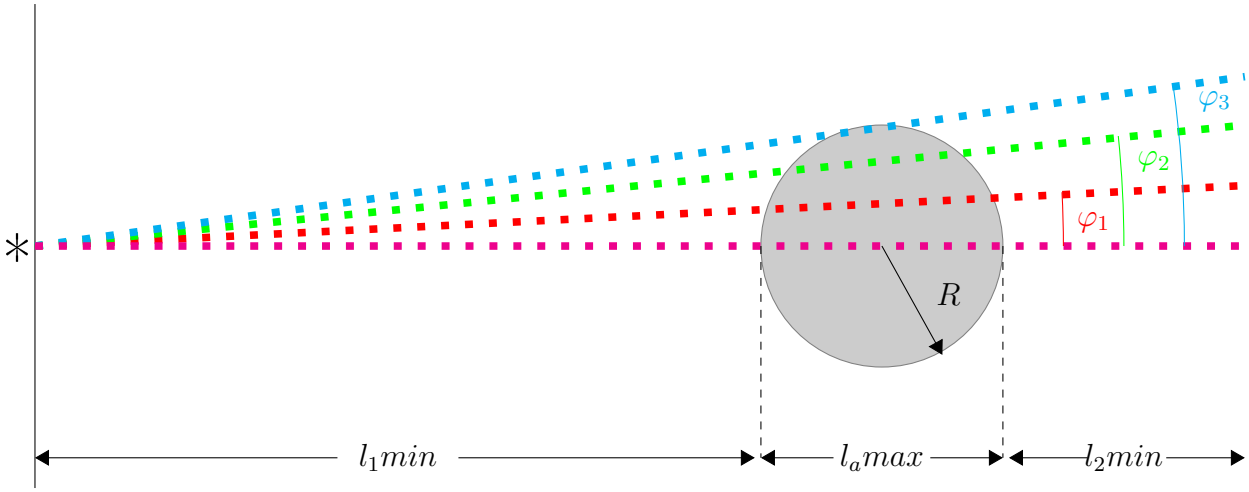

Figure 5.13: Top view for the cylindrical velocity anomaly presented in Figure (5.12). Dotted lines represent the geophone arrays.

The values for the left and right limits of the cylindrical anomaly, are the intersection points (x_1 and x_2) between the lines and the anomaly. The first solution "x_1" corresponds to the value "l_1" (location of the anomaly repect to the source), and the second solution "x_2" represents the right border of the anomaly ($l_1 + l_a$). Hence, by subtracting the two solutions it is possible to obtain the anomaly extension "l_a" for each 2D line.

According to the values " l_1" and "l_a" obtained from the solution of the systems of equations between each line and the anomaly, 4 velocity profiles containing a small section of the whole anomaly have been constructed, see Figure (5.14). Those models were constructed assuming a 3-layer simple model as in Section (5.2), with all the seismic properties remaining constant. The position for each profile is given by the azimuthal angle of each line. Position parameters and anomaly extensions are summarized in Table (5.2).

$\varphi(^\circ)$	$r(m)$	x_1(m)	$x_2(m)$	l_1	l_a
0	250	1500	2000	1500	500
6.58	250	1623	1923	1623	300
7.84	250	1707	1857	1707	150
8.17	250	1761	1811	1761	50

Table 5.2: Position parameters and anomaly extensions for the acquisition model presented in Figure(5.13)

Following the same procedure as in Section (5.2), the timeshift generated by each section of the cylindrical anomaly is calculated by using Script(B.2). The computed timeshifts versus offset are presented in Figures (5.15), (5.16), (5.17) and (5.18).

Notice that from each plot, the synthetic results match reasonably well with the theory. It is possible to observe a decrement in the seperation between the limit points, which define each trend. This decrement is due to the fact that, at each time, a 2-D seismic line is passing through a smaller section of the anomaly. In the same way, the maximun timeshift for each plot is decreasing, because the maximun timeshift is a function of the anomaly lenght. In other words, for an homogeneous velocity anomaly, as in our case, if the 2-D seismic lines pass through a smaller section of the anomaly, the maximun recorded timeshift will be lower. It is important to reiterate that the theoretical timeshift can be predited by Equation (5.2).

From the results, it is possible to say that the refraction timeshift method is a good tool to

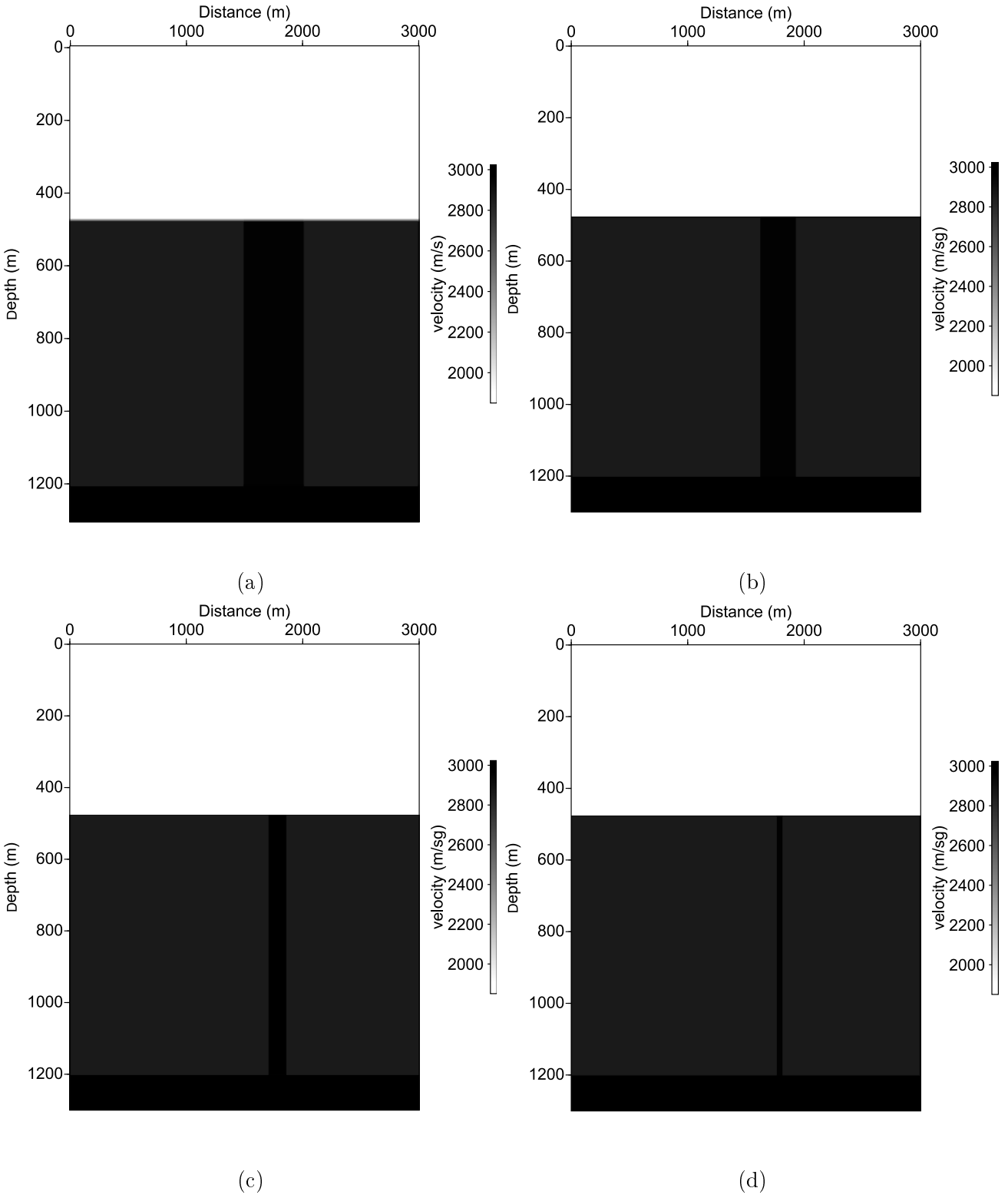

Figure 5.14: Velocity profiles including an anomaly of $\Delta v = 60m/s$, with an extension of (a) $l_a = 500m$, (b) $l_a = 300m$, (c) $l_a = 150m$ and (a) $l_a = 50m$.

monitor velocity changes due to gas leackage in shallow layers, even when the lateral extension of the anomaly is a couple of hundred meters. If the lateral extension of the anomaly is in the range of $500m - 50m$, as in our case, even a minor velocity change ($60m/s$) will lead to

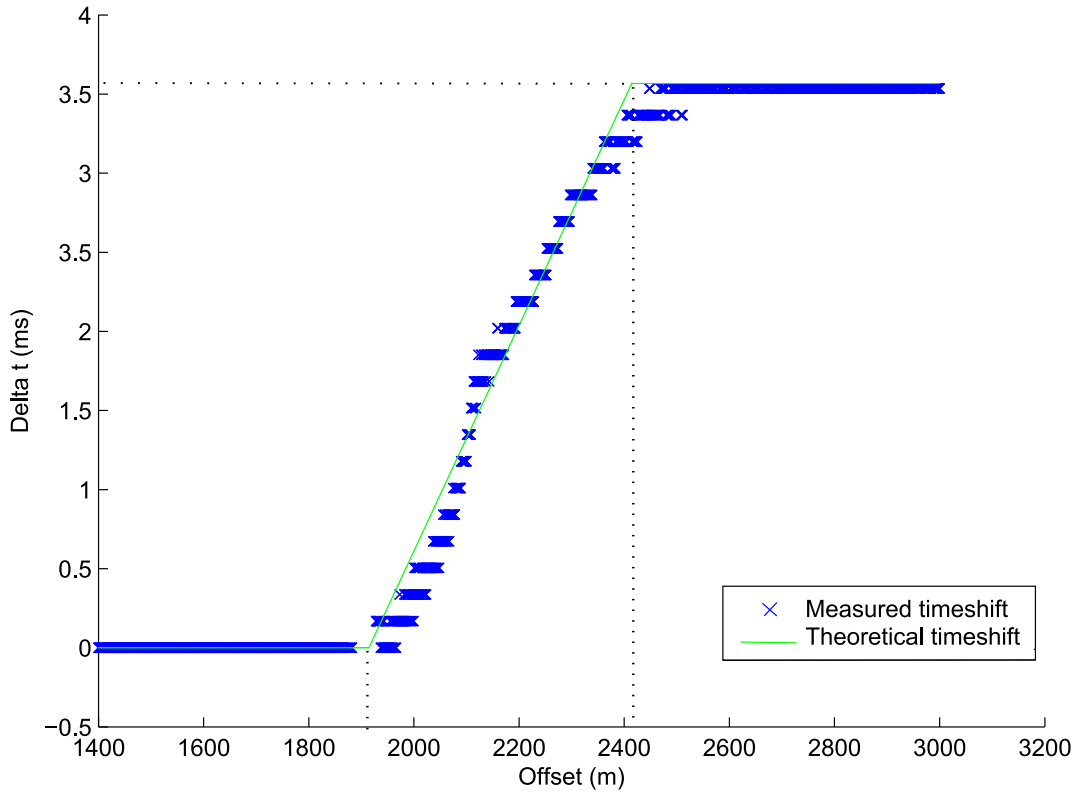

Figure 5.15: Timeshift vs offset for $\varphi = 0°$. The maximun timeshift is reached at $(l_1 + \frac{x_{cri}}{2} + l_a)$

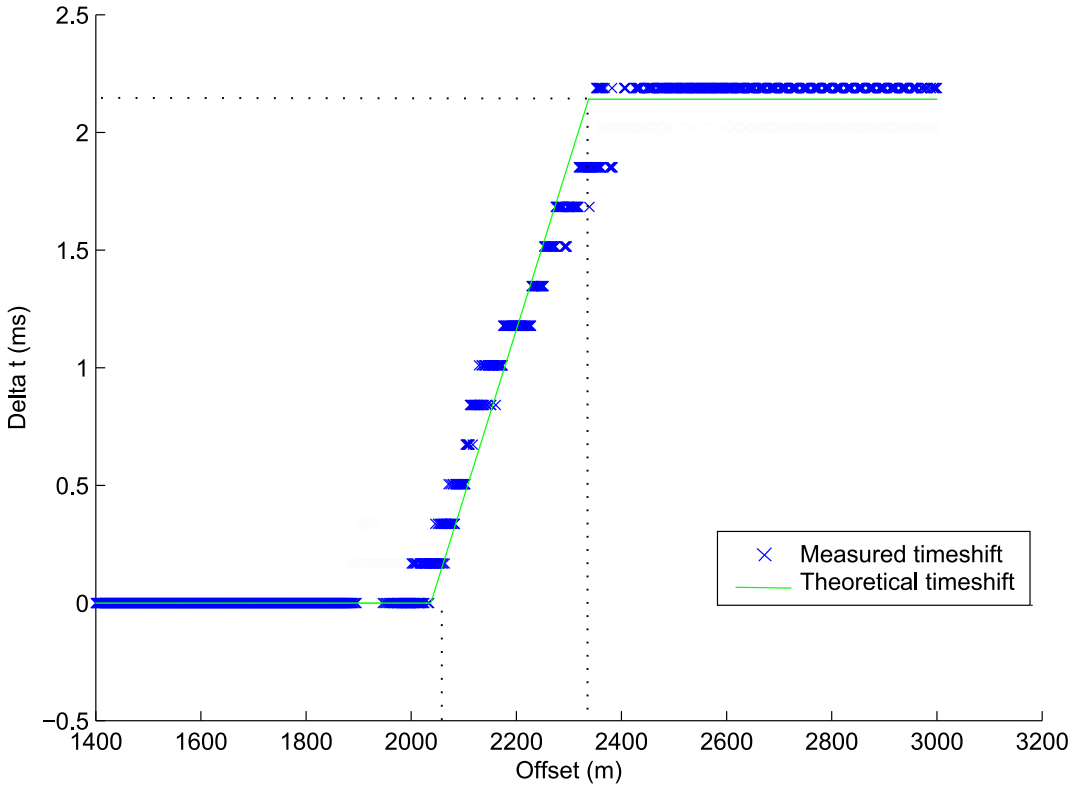

Figure 5.16: Timeshift vs. offset for $\varphi = 6.6°$. The maximun timeshift is reached at $(l_1 + \frac{x_{cri}}{2} + l_a)$

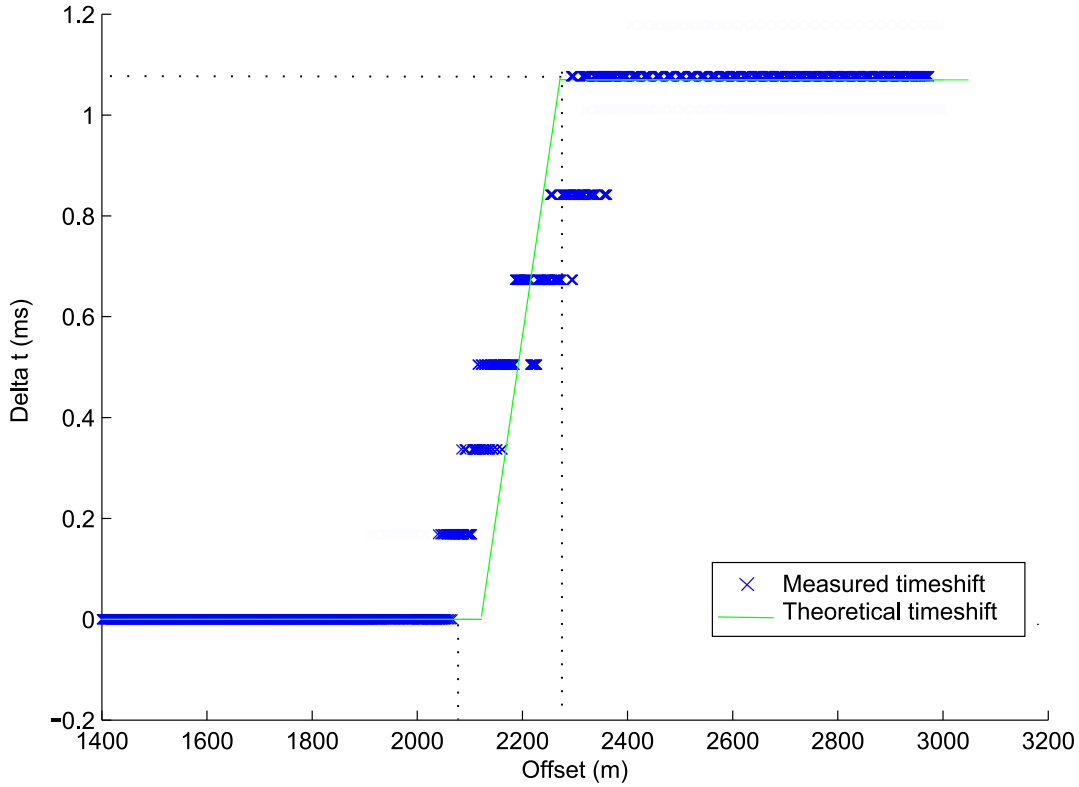

Figure 5.17: Timeshift vs. offset for $\varphi = 7.8°$. The maximun timeshift is reached at $(l_1 + \frac{x_{cri}}{2} + l_a)$

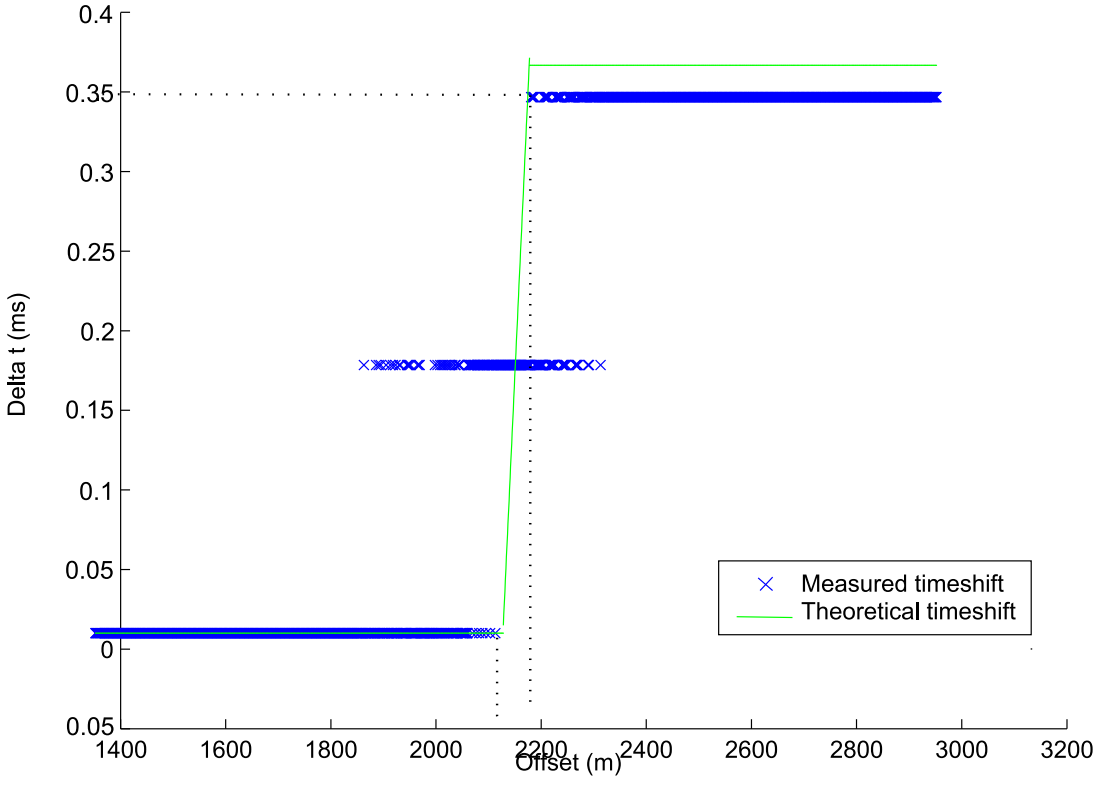

Figure 5.18: Timeshift vs. offset for $\varphi = 8.2°$. The maximun timeshift is reached at $(l_1 + \frac{x_{cri}}{2} + l_a)$

significant 4D refraction timeshift. Limitations of this method are related with the existence of positive velocity contrast in the reservoir layer, existence of long-offset data and repeatability of the seismic. Further investigation is needed, in order to identify crucial bottlenecks that are likely to meet for a real data case.

5.4 Refraction timeshift measurement using a permanent receiver system.

The potential of the refraction time-lapse technique was explored in the Section (5.3), where the feasibility of velocity change detection has been proven. Even under subtle velocity changes (e.g. due to a cylindrical velocity anomaly) the technique allows to map the velocity anomaly, giving its location (l_1), and its extension (l_a). However, the deployment of the receiver arrays for the method proposed in Section (5.3) is time consuming and may be really expensive. Hence, a simplified acquisition design for monitoring the same velocity anomaly is given in Figure (5.19). Notice that now a simple array composed by 9 receivers is used. The receivers are deployed in a perpendicular line to the source, $2700m$ away (i.e $Offset = 2700m$ for the central line). The position parameters and anomaly extensions are summarized in Table (5.3).

$\varphi(^\circ)$	$r(m)$	x_1(m)	$x_2(m)$	l_1	l_a
11	250	1761	1811	1761	50
8.17	250	1761	1811	1761	50
7.84	250	1707	1857	1707	150
6.58	250	1623	1923	1623	300
0	250	1500	2000	1500	500
- 6.58	250	1623	1923	1623	300
-7.84	250	1707	1857	1707	150
- 8.17	250	1761	1811	1761	50
- 11	250	1761	1811	1761	50

Table 5.3: Position parameters and anomaly extensions for the acquisition model presented in Figure(5.19)

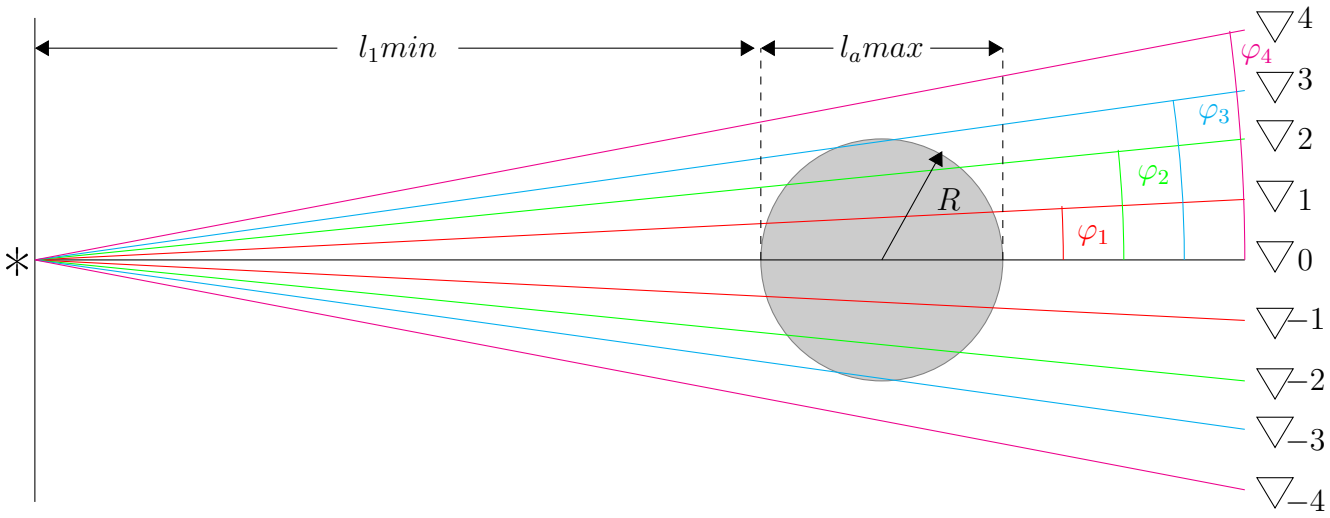

Figure 5.19: Top view for the cylindrical velocity anomaly presented in Figure (5.12). An array composed by 9 receivers is used. Notice that the position of each receiver is given by the value for the azimuthal angle respect to the horizontal line.

In orden to quantify the timeshift recorded by each geophone in the array, a specific ordered pair from the plots presented in Figures (5.15), (5.16), (5.17) and (5.18) is taken. This ordered pair (Offset, timeshift) is chosen according to the position of each receiver in the array presented in Figure (5.19). Notice that the position of each receiver is given by the value for the azimuthal angle respect to the horizontal line.

The computed timeshift versus azimuth is showed in Figure (5.20). Notice that as soon as the azimuthal angle increases (absolute value), the timeshift decreases. This is due to the fact that rays recorded by each receiver travel through a smaller section of the anomaly, until a azimuthal angle where no velocity anomaly can be detected, is reached ($\varphi = 11°$). It is not straightforward to estimate the extension and velocity change of the anomaly. However, for this monitoring system, it is possible to detect relative values in a given area, and know where the anomaly is relatively greater ($\varphi = 0°$, for our case). According to the results, for low acquisition costs, it is possible to say that is feasible to monitor the shallow subsurface layers in a producing hydrocarbon field, despite of the fact that no absolute values can be estimated. This problem can be solved by using the technique proposed in Section (5.3); always keeping in mind that the acquisition costs will be higher.

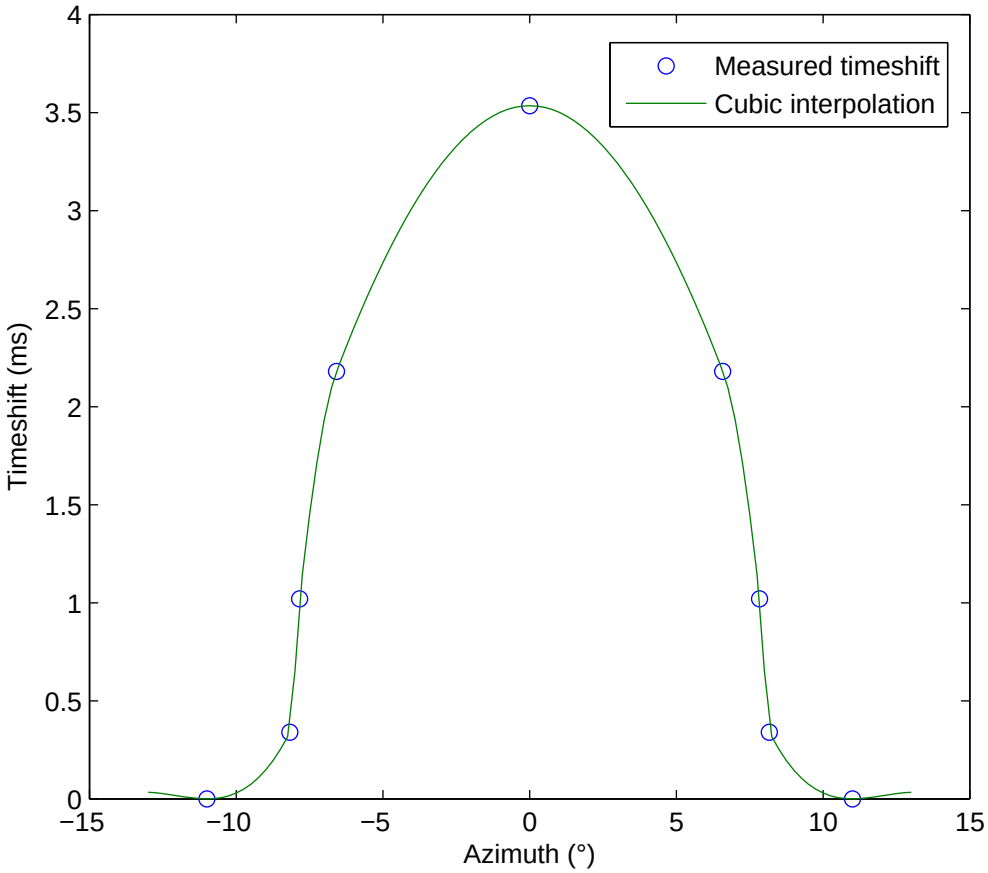

Figure 5.20: Timeshift between base and monitor data versus azimuth. The maximum timeshift is reached when the receiver is alienated with the maximum extension of the anomaly at $\varphi = 0°$.

Chapter 6

Time-lapse Refraction in Snorre Field

6.1 Snorre Field

The Snorre field is located in the Norwegian part of the North Sea, covering an area of approximately $200km^2$. It is situated in the southern part of the block 34/4, and the northern part of the block 34/7, Figure (6.1). It belongs to the prolific hydrocarbon province on the wertern margin of the Viking graben. The Snorre field was discovered in 1979 and its production started in 1992. It total stratigraphic reservoir thickness is approximately $1km$, and 17 zones with varying fluvial styles have been identified, Figure (6.2).

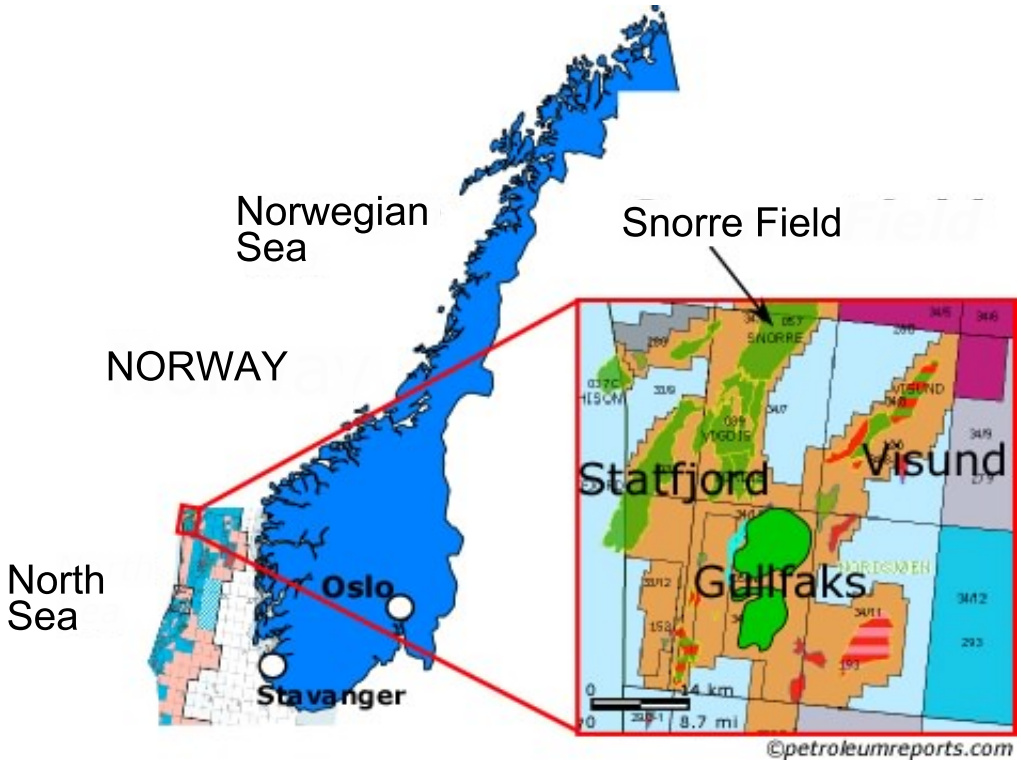

Figure 6.1: Location of Snorre Field in offshore. (Petroleum Safety Authority Norway, [18])

The reservoirs at Snorre are very complex with thin layers, sand connectivity, and communication across faults. The Snorre Field has two main reservoirs- Triassic Lunde Formation and Triassic-Jurassic Statfjord Formation, Figure (6.3). Each of these reservoir consists of a network of fluvial sand bodies in a mudstone matrix, deposited in alluvial setting (Thompson et al; [8]).

The water depth in snorre field is around $300m$. Both Statfjord and Lunde reservoirs are truncated by the Kimmerian unconformity, and overlain by Jurassic and Cretaceous shales. This feasibility study for refraction time-lapse was performed on the Statfjord Formation. The average porosity for the formation is 18-25%. The oil -water contact for Statfjord Formation varies from $2561m$ on the crest to $2599m$ in the western region (Smith et al; [17]) .

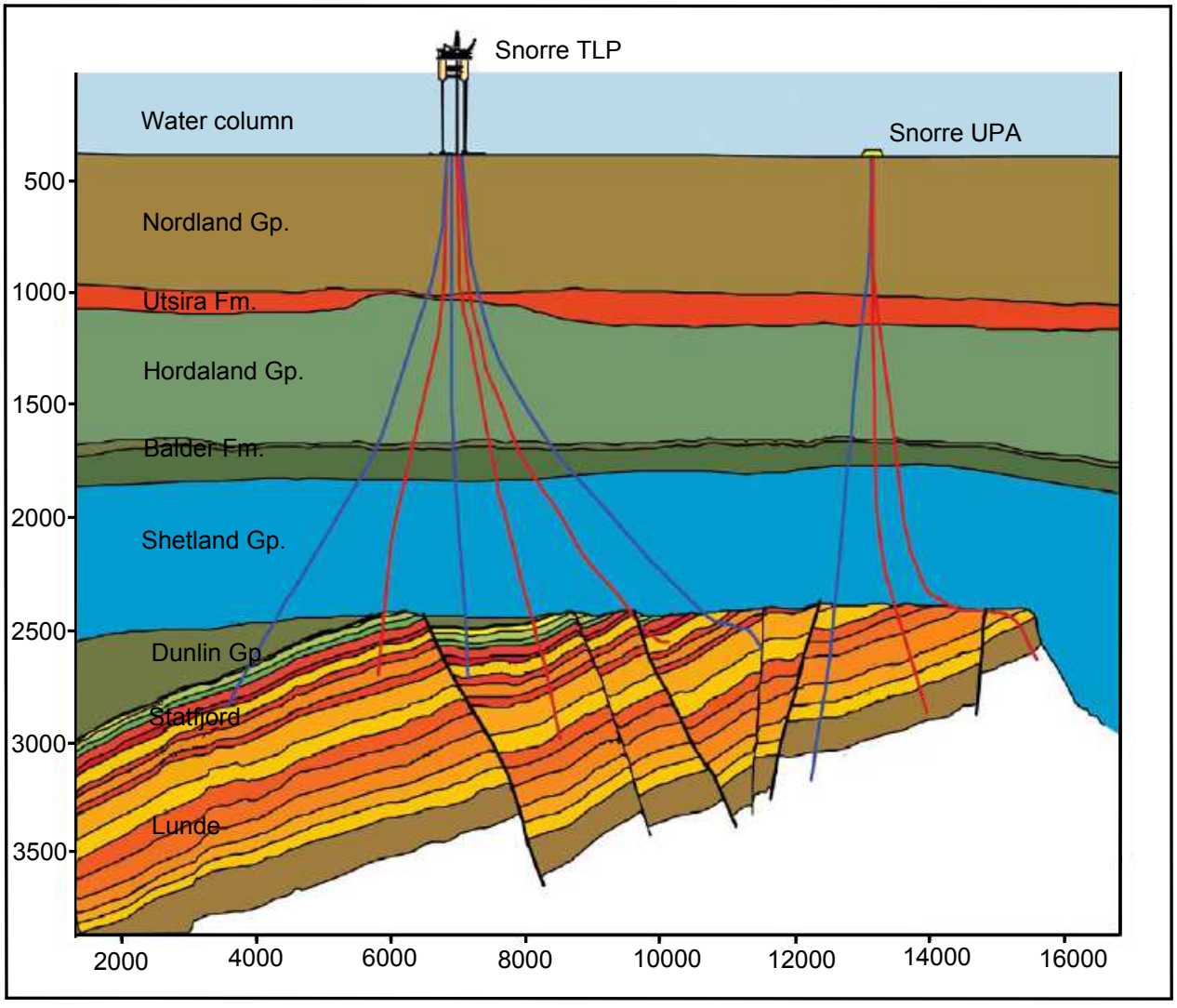

Figure 6.2: Model of Snorre Field illustrating the structural complexity of the reservoir. (Thompsom et al; [8])

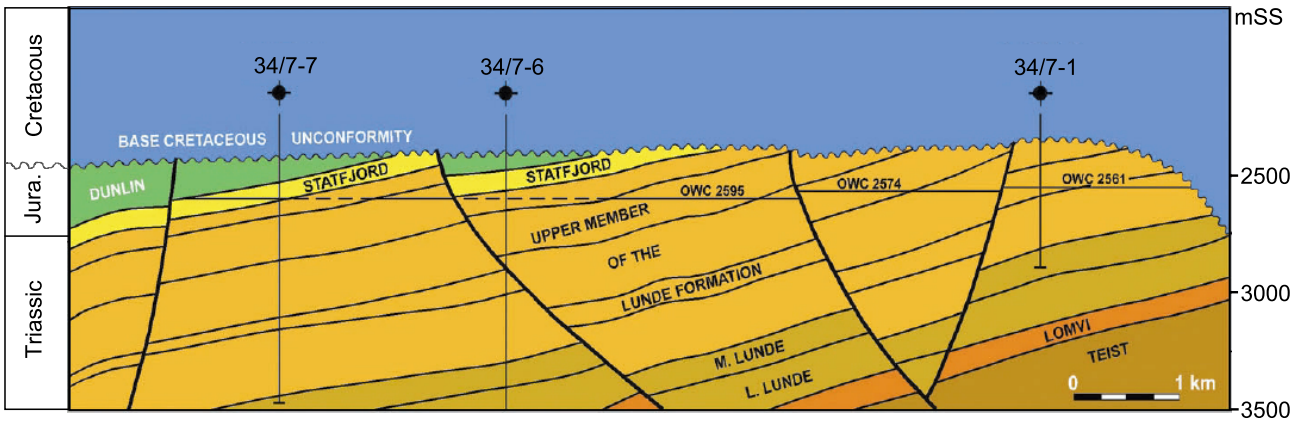

Figure 6.3: Cross-section through Snorre Field. (Smith et al; [17])

6.2 Refraction time-lapse seismic modelling in Snorre Field.

Considerable effort has been dedicated for a number of years to find out under what circumstances 4D seismic monitoring would provide useful information on reservoir dynamics. There is a general consensus among researchers that 4D seismic monitoring is particularly effective in high-porosity sandstone reservoirs. Nonetheless, when the variations in the reservoir properties are small and the depths are large, the scenario is less favorable for the conventional time-lapse seismic. In Chapter (5) the time-lapse refraction was introduced as a tool to detect changes in reservoir properties, especially for small velocity variations.

From the results in Chapter (5), it is possible to say that the velocity variations in the reservoir can be quantitatively determined from changes in the arrival times for the head waves. One important aspect in the study of this technique is to establish until what point it is possible to detect a timeshift due to small velocity variations, when the reservoir layer is located at large depths. To accomplish this task, a 10-layer simplified model of Snorre field was used to study the effect of different velocity increases in the reservoir layer. Figure (6.4) shows velocity and density profiles, for the base case .

The subsurface model for Snorre field focuses on the upper part of the reservoir, which correspond to the Statfjord Formation, see Figure (6.3). The top of Statfjord is located at $H = 2500m$, The OWC is located at a depth of $2600m$ for Statjord Formation. Therefore, the pay thickness of the reservoir is $100m$. A velocity of $2900m/s$ for the reservoir layer, was obtained by performing a fluid substitution using Gassmann's equation, all the values related to the calculation were chosen considering Sandstone as lithology. The model parameters, for the base case, are summarized in Table (6.1).

In the same way as in Chapter (5), Synthetic data was generated by performing a 2^{nd} order finite-difference modeling for the acoustic wave equation. Only the acoustic case was

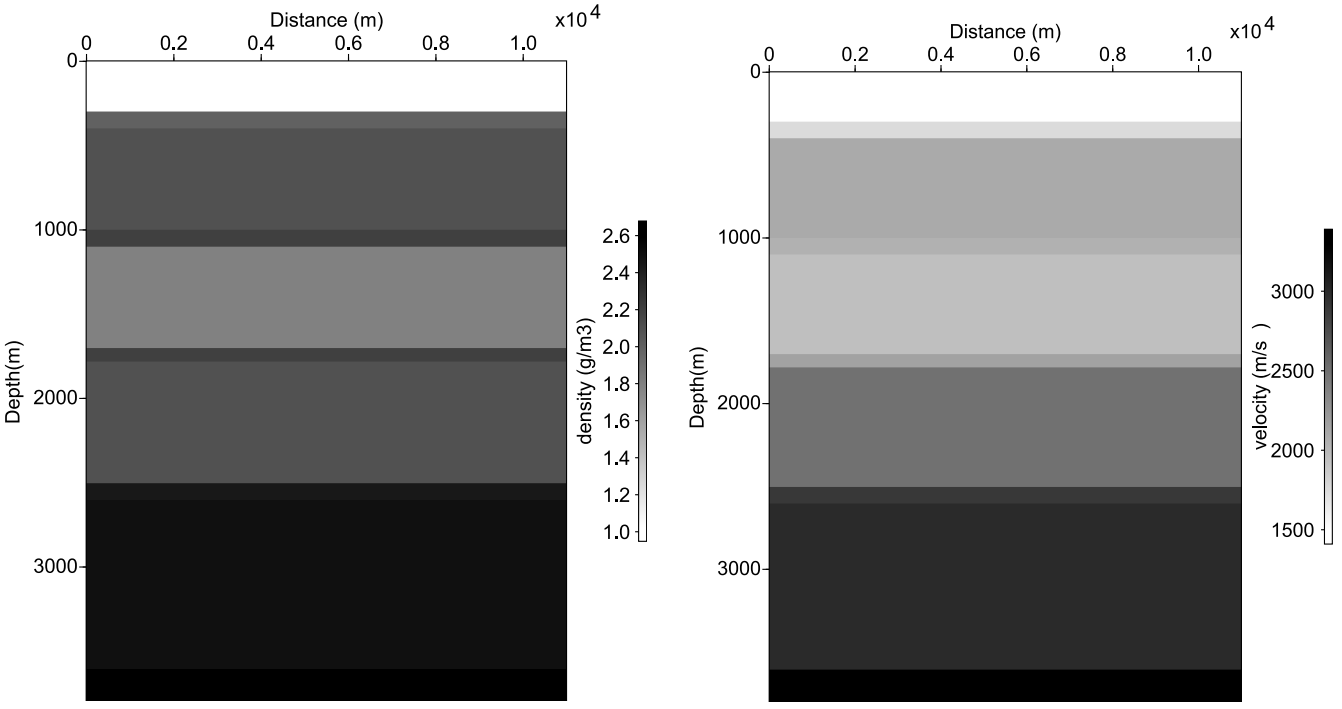

(a) (b)

Figure 6.4: Uniform models generated by *Unif2* command. (a) Density and (b) Velocity Profiles for a simplified model of *Snorre Field* presented in Table (6.1).

Layers	Thickness (m)	Base Depth (m)	V_p (m/s)	ρ (g/m^3)
Layer 1 (Water)	300	300	1500	1.027
Layer 2	100	400	1750	2
Layer 3	600	1000	2100	2.1
Layer 4	100	1100	2050	2,2
Layer 5	600	1700	1950	1.8
Layer 6	80	1780	2100	2.2
Layer 7	670	2500	2500	2.1
Reservoir	100	2600	2900	2.45
Layer 8	1000	3600	3000	2.5
Layer 9 (Half plane)	200	3800	3300	2.6

Table 6.1: Parameters describing a simplified model of *Snorre Field* for finite difference modelling (Base case). V_p and ρ represent the P-wave velocity and density respectively.

modeled, due to the fact that no reliable shear velocity data was available. Since refracted energy is weak compared to reflected energy, a high gain had to be applied to the gathers in order to see the head wave. The signal was modeled for the finite difference modelling scheme as a ricker wavelet with a maximum frequency of 60Hz, and a peak frequency of 20Hz. Absorbing boundaries was used in all directions except the free surface, thus, multiples are present.

Assuming the overburden as one homogeneous medium with its thickness remaining constant during production, and a root mean square velocity for the overburden of $v_1 = 2065m/s$, it is possible to compute the critical offset for the reservoir top using Equation (3.7). In this sense, the critical offset of the reservoir, for the base case, is 5073m. In the synthetic Shot-gather presented in Figure (6.5), the refracted events can be observed over a distance of five kilometers, starting about 6500m away from the shot (maximum amplitude offset).

To achieve a clear understanding of how sensitive is the timeshift to small velocity variations, 10 different monitor scenarios have been modeled. For the monitor surveys 1, 2 , 3, 7 and 9 a velocity variation for the whole reservoir layer was used. While a velocity anomaly with limited extension was used for monitors 4, 5, 6, 8 and 10. From Figure (6.6) to Figure (6.10) differences between base and monitor data, and their respective velocity profiles are shown. Table (6.2) summarized changes in the seismic parameters. Notice that the amplitude values in the sections showing the difference between monitor and base surveys, remain in the same range that the original amplitudes until an anomaly with limited extension began to be used. At this moment, the amplitudes values become 10 times (monitors 4, 5 and 6) and 5 times (monitors 8 and 10) smaller than the original amplitudes. From the results, it is possible to conclude that the amplitude values for the difference due to velocity changes, become smaller when the velocity anomaly is smaller and is located at deeper layers. However, the variations between the two sections (base and monitor) are still detectable. For real data case, noise, location accuracy, source strength etc. will affect the repeatability of the seismic data. Therefore, those issues (especially the noise) may mask the signal variation, making the velocity changes in the reservoir undetectable.

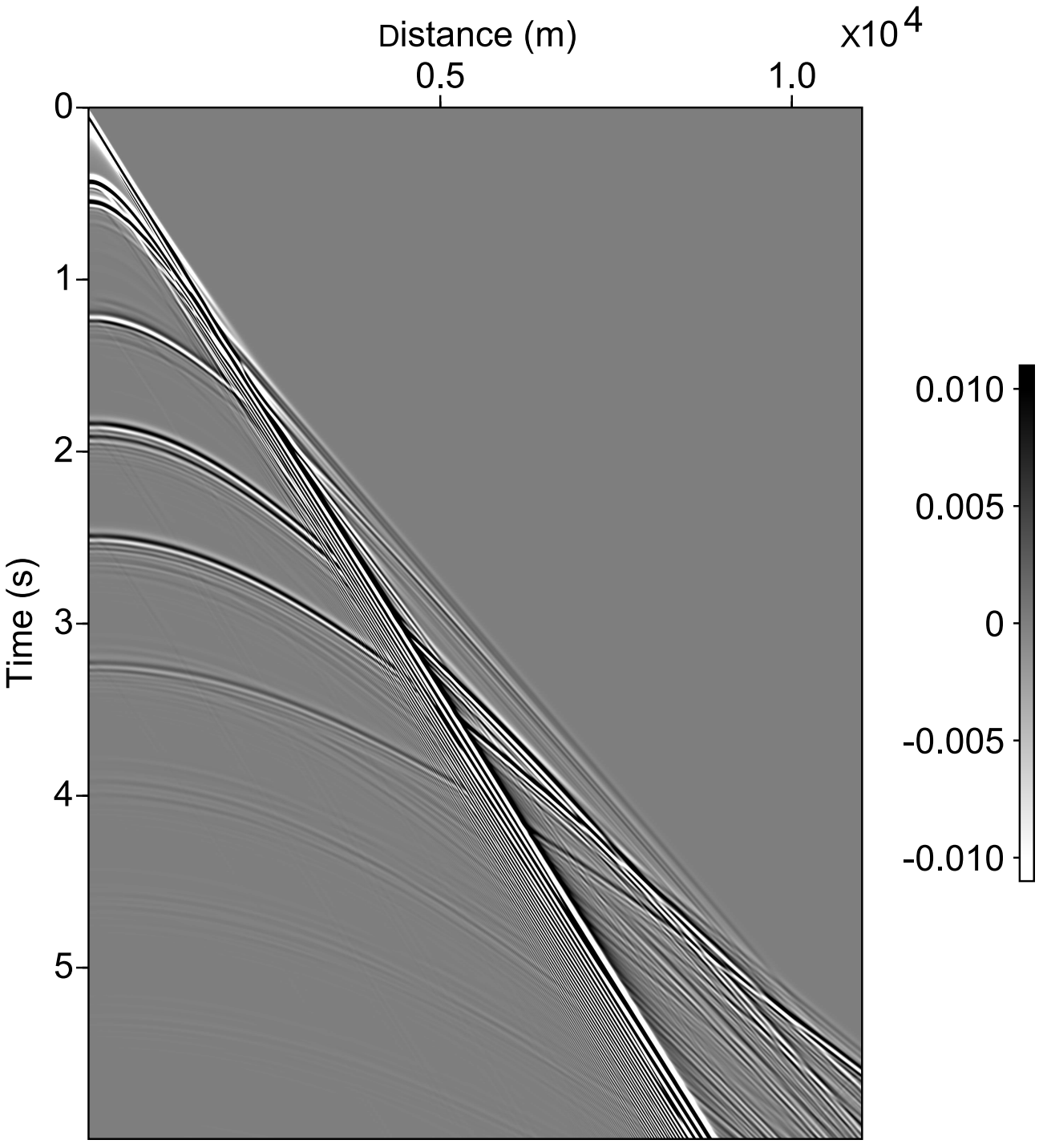

Figure 6.5: Synthetic Shotgather generated using *Sufdmod2* command. Data for a simplified model of *Snorre Field* (Base case).

Model	v_{pres}	v_{p6}	v_{p7}	$l_a(m)$
Base	2900	2100	2500	
M-1	+1.72%			
M-2	+3.31%			
M-3	-1.72%			
M-4	+1.72%			2000
M-5	+1.72%			1000
M-6	+1.72%			500
M-7		+2.38%		
M-8		+2.38%		1000
M-9			+2%	
M-10			+2%	1000

Table 6.2: Changes in seismic properties for different monitor models in comparison to base model for *Snorre Field*.

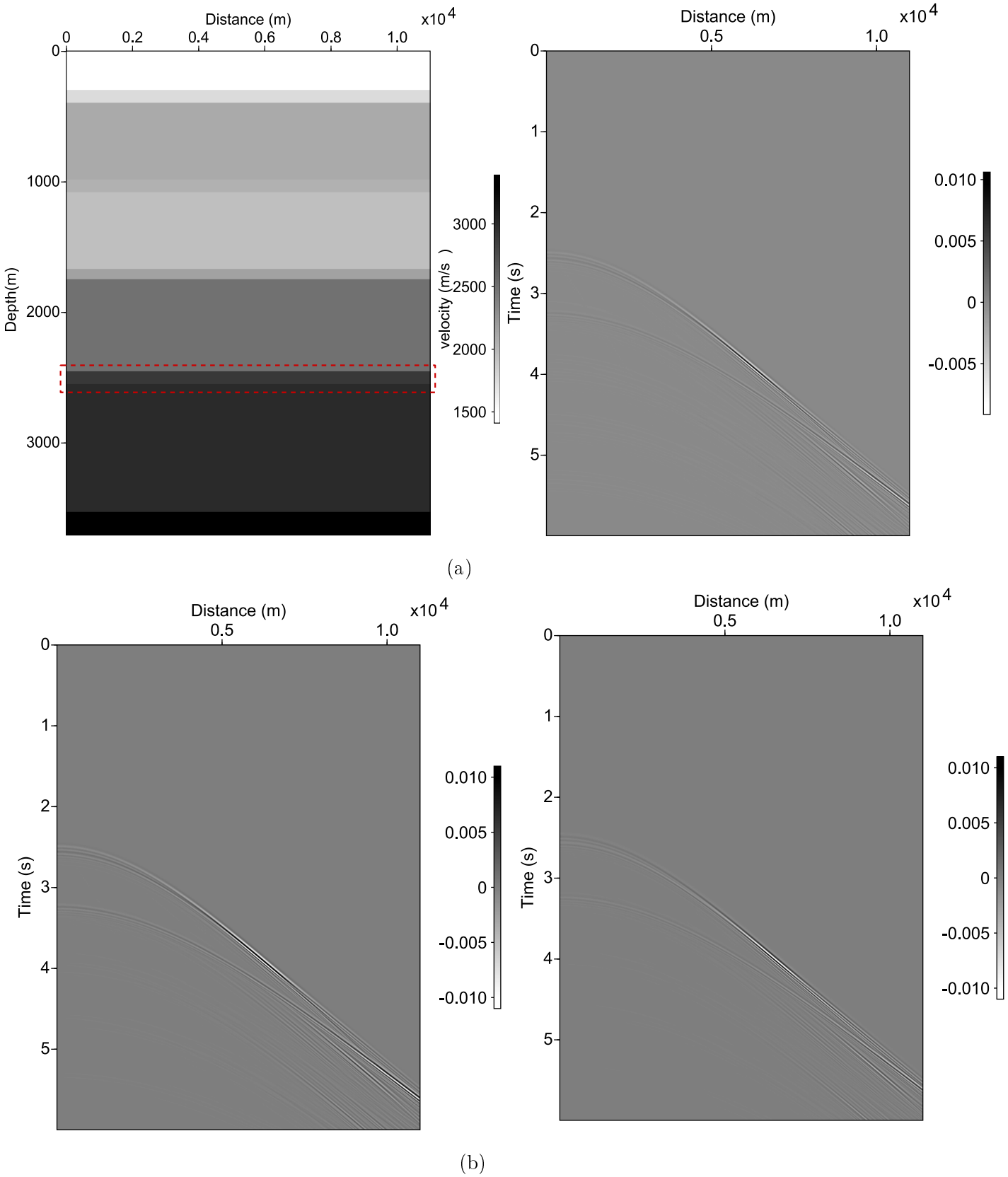

Figure 6.6: (a) Velocity profile indicating a velocity change (left), and difference between base and monitor 1 (right). (b) Difference between base and monitor data for monitor 2 (left) and monitor 3 (right). Table (6.2) summarized the changes in the seismic parameters.

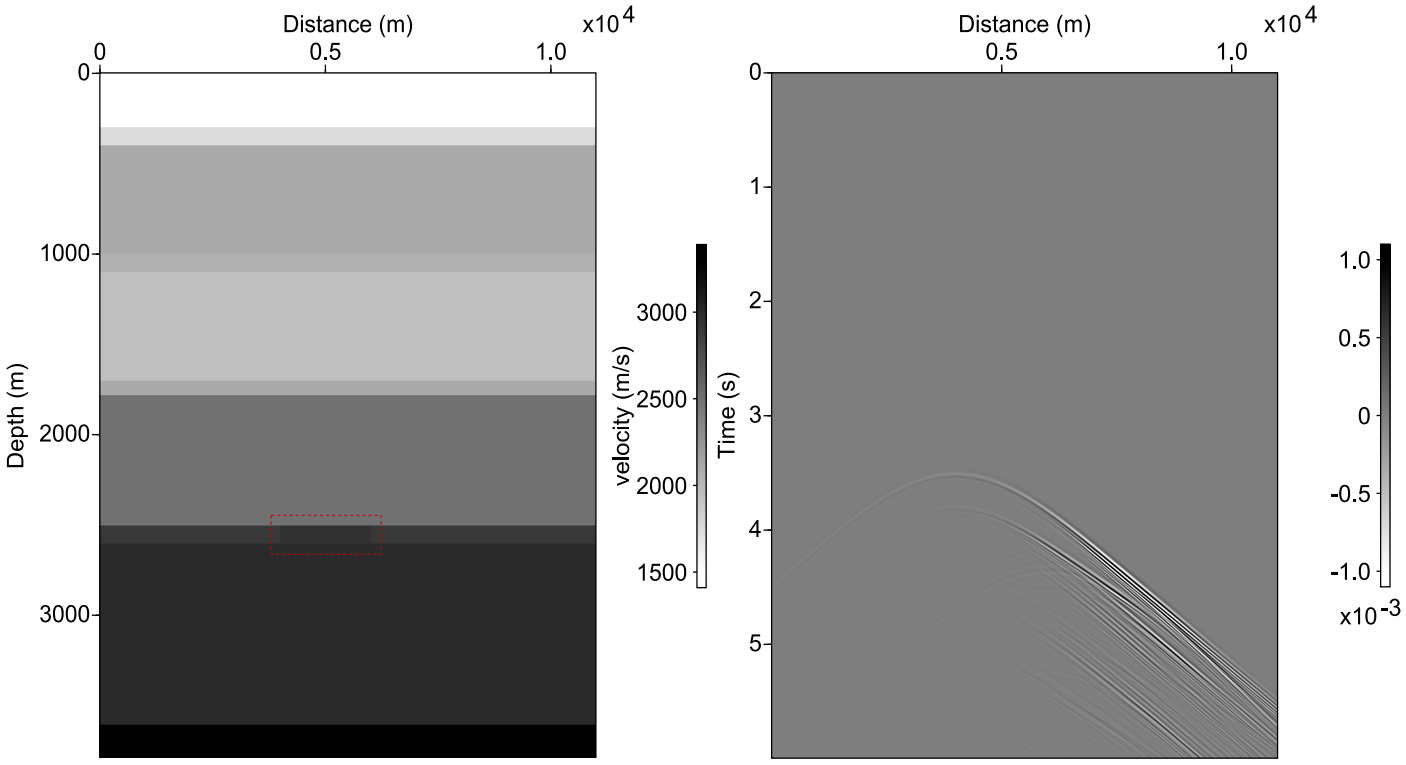

(a)

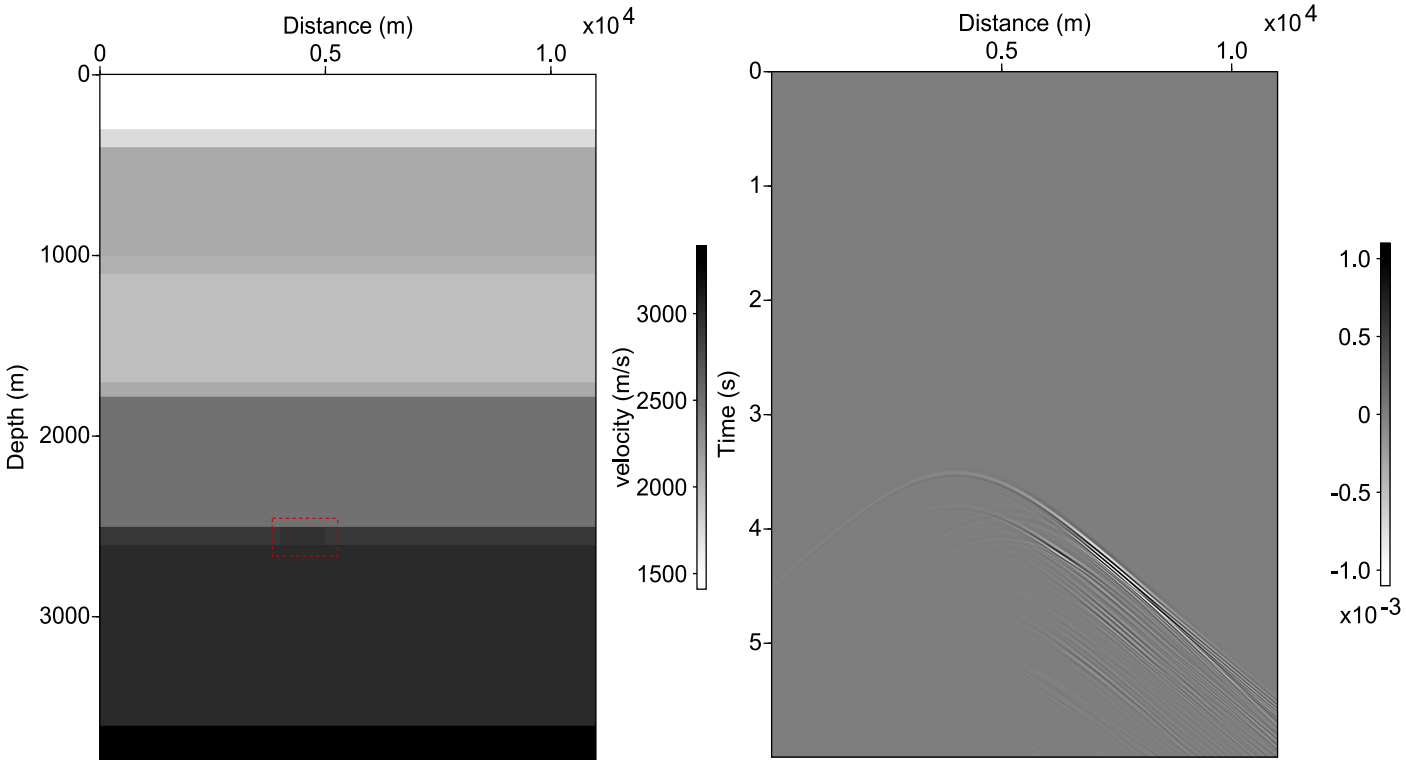

(b)

Figure 6.7: Velocity profiles containing a velocity anomaly, for monitor cases (left). The right figures show the difference between base and monitor data for (a) monitor 4 and (b) monitor 5. Table (6.2) summarized the changes in the seismic parameters.

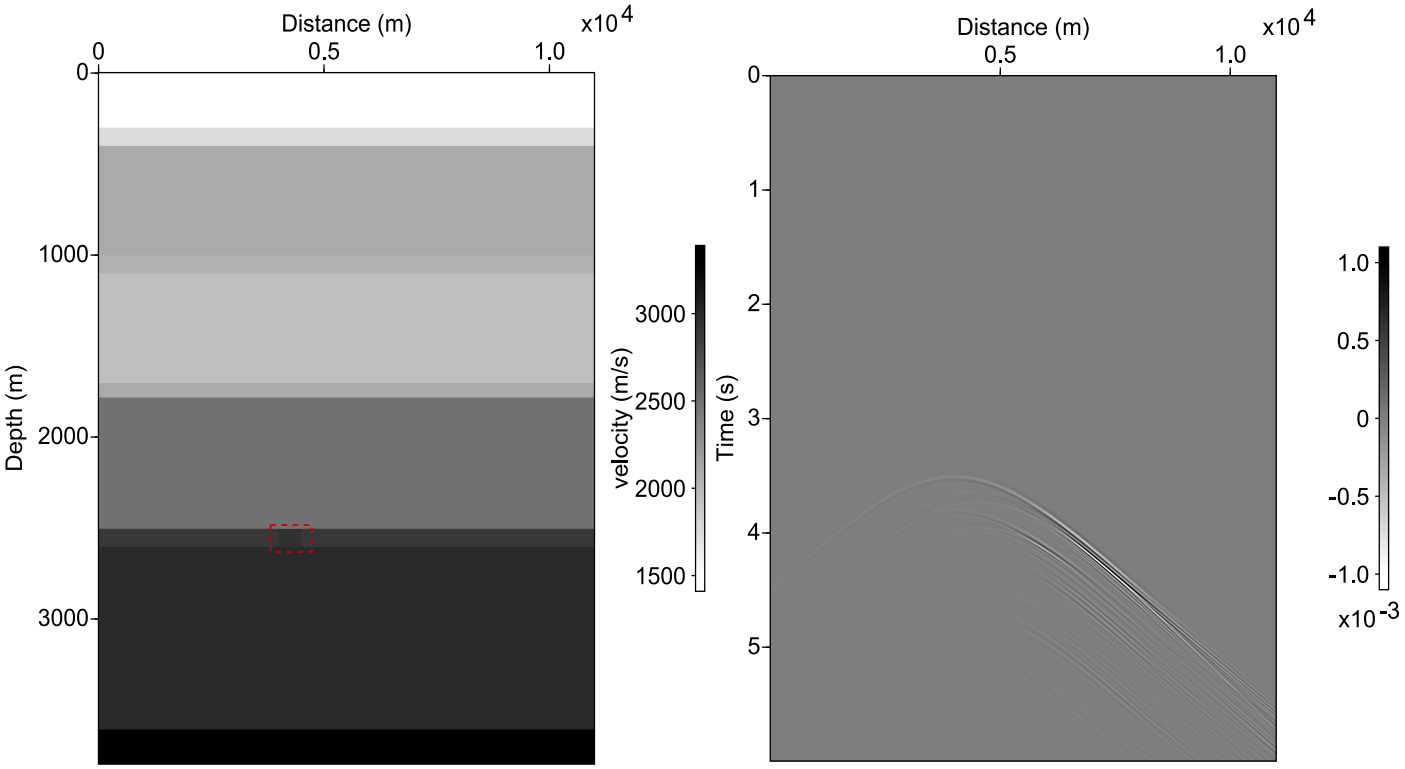

Figure 6.8: Velocity profile containing a velocity anomaly, for monitor 6 (left). The right figure shows the difference between base and monitor 6 data. Table (6.2) summarized the changes in the seismic parameters.

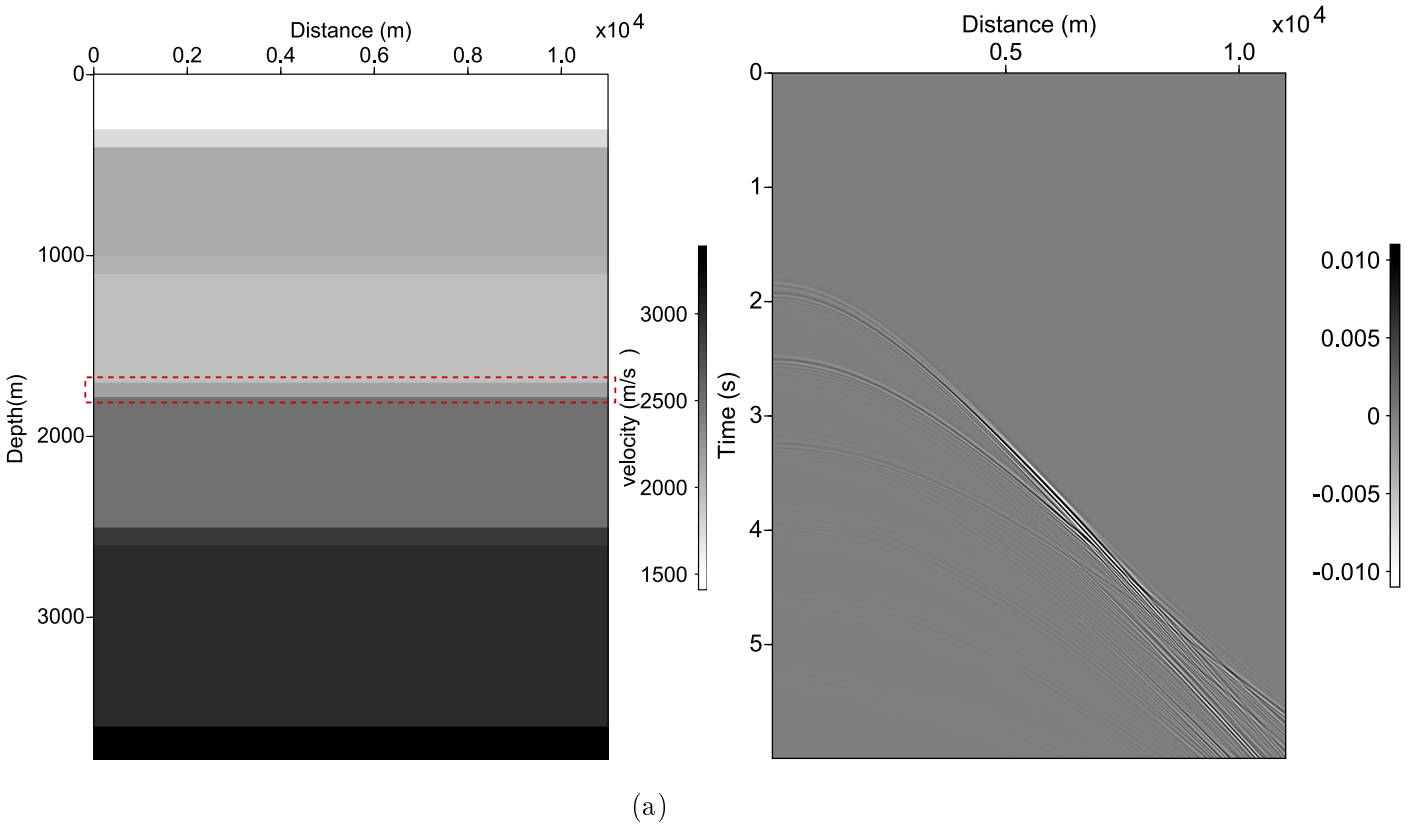

(a)

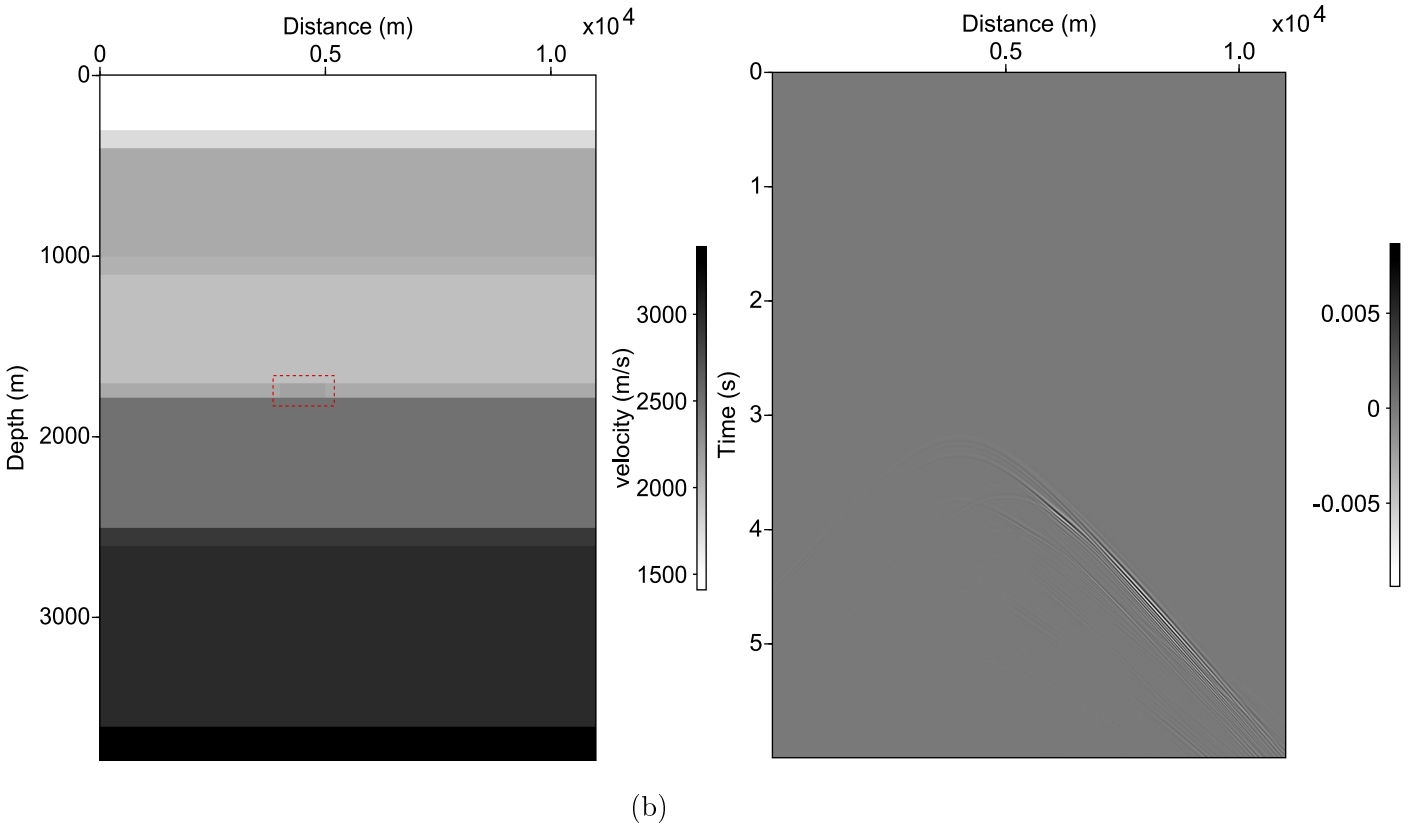

(b)

Figure 6.9: Velocity profiles, for monitor cases (left). The right figures show the difference between base and monitor data for (a) monitor 7 and (b) monitor 8. Table (6.2) summarized the changes in the seismic parameters.

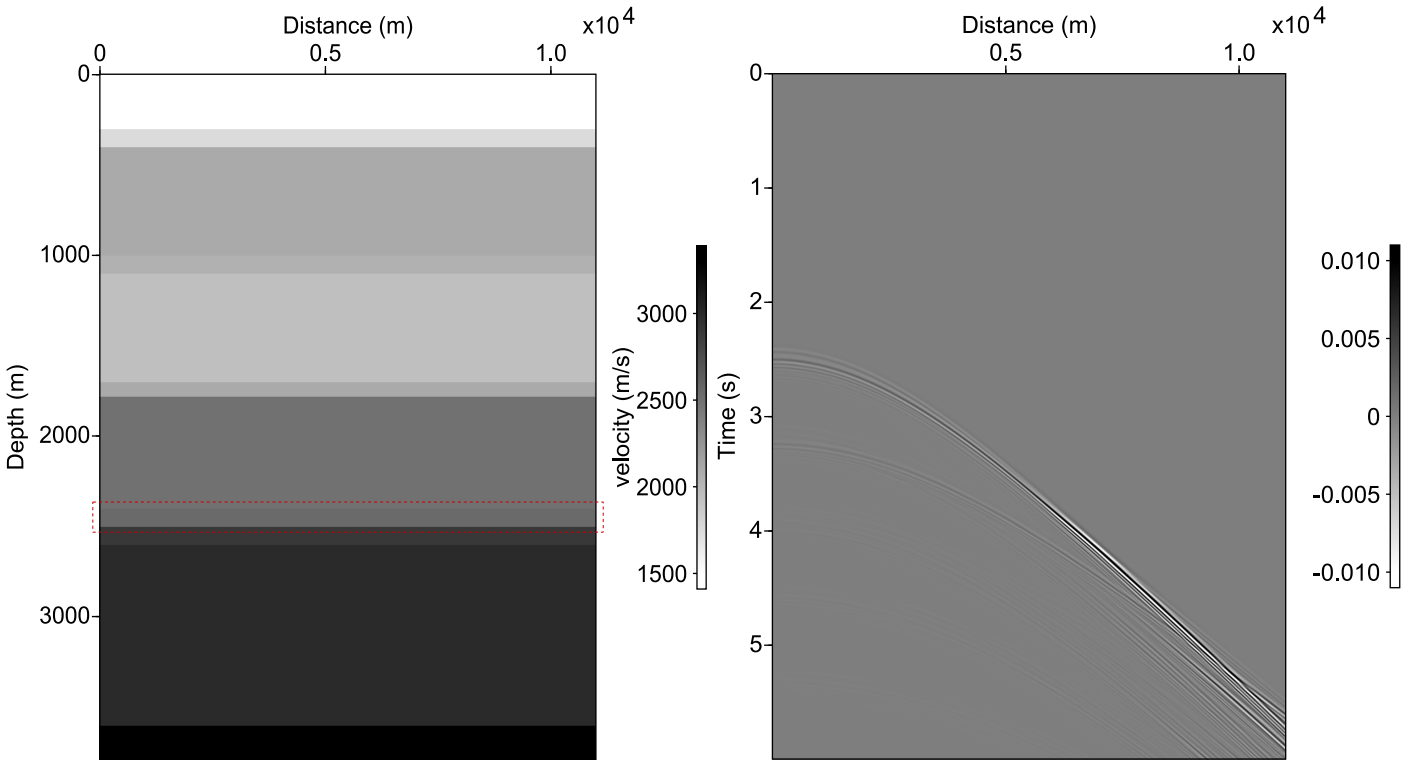

(a)

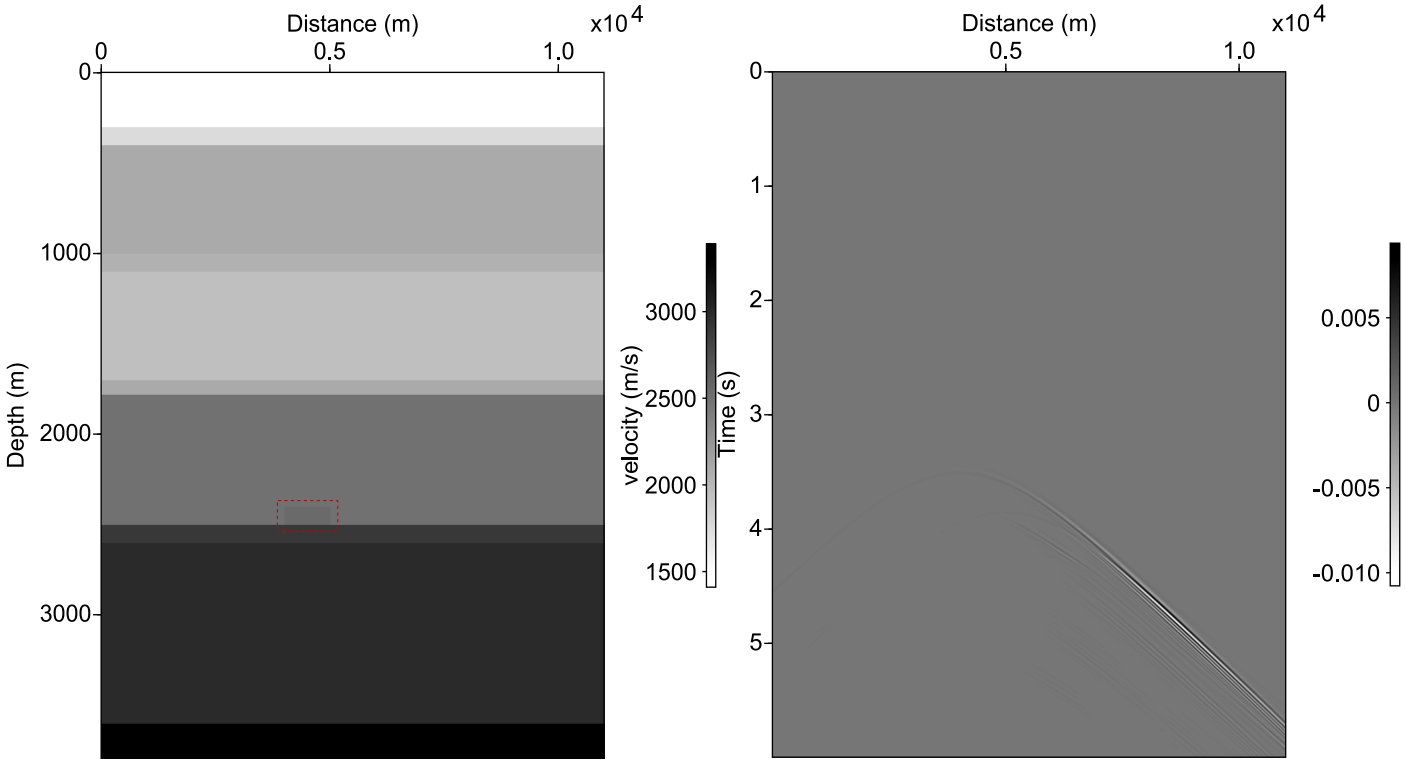

(b)

Figure 6.10: Velocity profiles, for monitor cases (left). The right figures show the difference between base and monitor data for (a) monitor 9 and (b) monitor 10. Table (6.2) summarized the changes in the seismic parameters

6.3 Refraction timeshift measurement using a permanent receiver system for Snorre Field.

The potential of the time-lapse refraction technique was explored in the Chapter (5), where in Section (5.4) was introduced the possibility of monitoring shallow subsurface layers by a low cost acquisition design. In this section, further investigation is done using a cylindrical anomaly located at a larger depth and with a smaller extension than in Section (5.4). In this model, the cylinder height is equal to the thickness of the reservoir layer ($h = 100m$) and diameter equal to $300m$. The velocity variation in the anomaly respect to the surroundings ($v_{res} = 50m/s$) remains constant through the whole volume (i.e. is homogenous).

A top view for the velocity anomaly, and acquisition design is presented in Figure (6.11). A simple array composed by 9 receivers is used. The receivers are deployed in a perpendicular line to the source, $9km$ away (i.e. $offset = 9000m$ for the central line). The position parameters are summarized in Table (6.3).

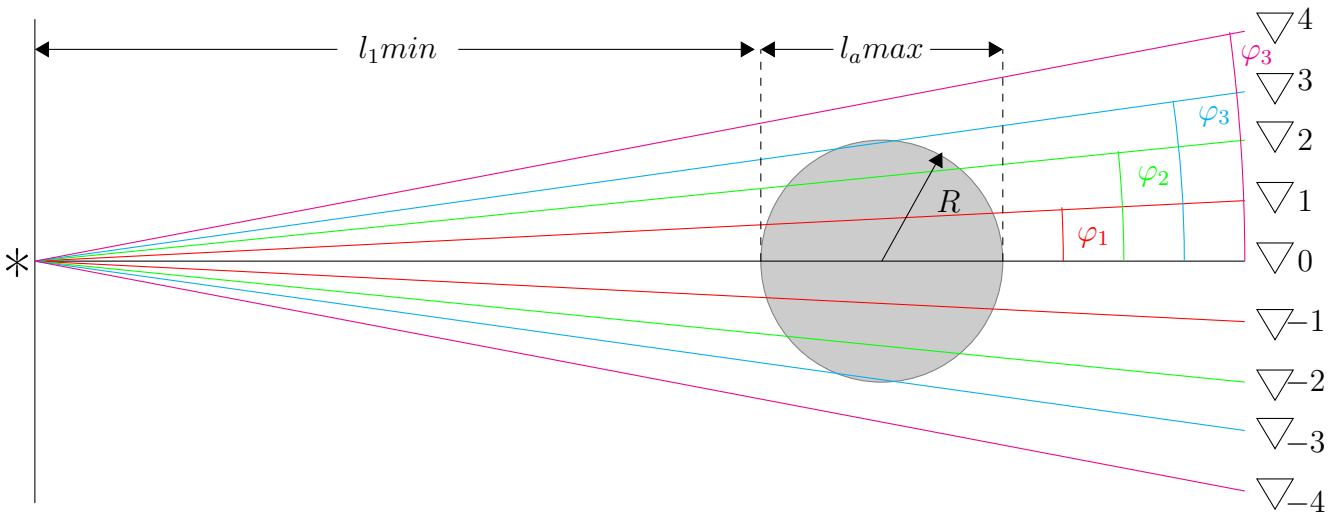

Figure 6.11: Top view for a cylindrical velocity anomaly, with $h = 100m$, $R = 150m$ and $\Delta v_{res} = 50m/s$. An array composed by 9 receivers is used. Notice that the position of each receiver is given by the value of the azimuthal angle respect to the horizontal line.

According to the values " $l1$" and "la" obtained from the solution of the systems of equations between each line and the anomaly, 4 velocity profiles were constructed, containing a small section of the whole anomaly. Those models were constructed assuming a 10-layer simple model as shown in Figure (6.4), with all the seismic properties remaining constant. The position for each profile is given by the azimuthal angle of each line.

Base and monitor data were merged and interleaved in the same gather. Figure (6.12)

$\varphi(^\circ)$	$r(m)$	x_1(m)	$x_2(m)$	l_1	l_a
1.378	150	1761	1811	1761	50
1.21	150	1707	1857	1707	150
0.77	150	1623	1923	1623	250
0	150	1500	2000	1500	300
-0.77	150	1623	1923	1623	250
-1.21	150	1707	1857	1707	150
-1.378	150	1761	1811	1761	50

Table 6.3: Position parameters and anomaly extensions for the acquisition model presented in Figure(6.11).

shows the difference between the data, with amplitudes 10 times smaller than the original. A timeshift around $1ms$ can be observed in a detailed comparison in Figure (6.13). Following the same procedure as in Section (5.4), Script (B.2) was used to calculate the refraction timeshift, subtracting traveltime values from base survey and values from monitor survey (containing the cylindrical anomaly).

The computed timeshift versus azimuth is shown in Figure (6.14). Notice that in contrast with the plot presented in Figure (5.20), this timeshift curve does not present a gaussian distribution shape. However, the trend remains the same; when the azimuthal angle increases (absolute value), the timeshift decreases. According to the results, the anomaly is expected to have its greater extension in the azimuth range ($\varphi = -0.77^\circ$ to $\varphi = 0.77^\circ$). It is important to point out that the timeshift for the model containing an anomaly of 50m ($\varphi = 1.378^\circ$) is equal to zero, the resolution of the method does not enable the detection of this section of the anomaly. Nevertheless, it has been proved that refraction timeshift method is a good estimator of velocity changes if the lateral extension of the anomaly is larger than $100m$.

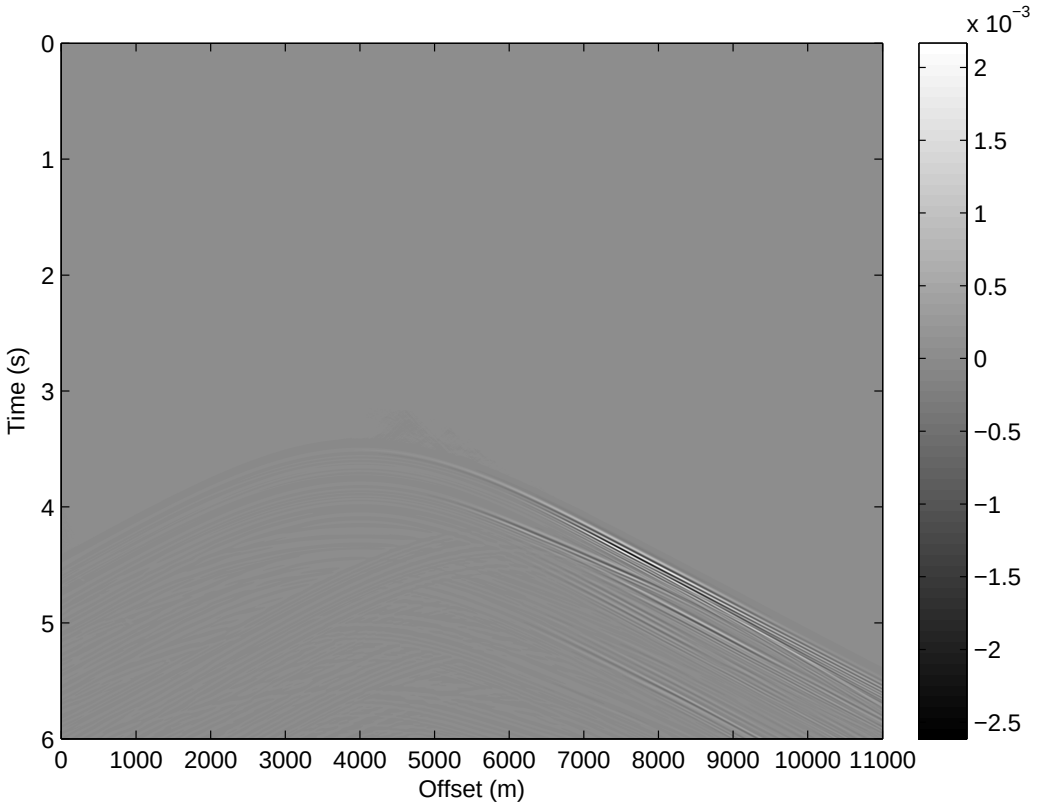

(a)

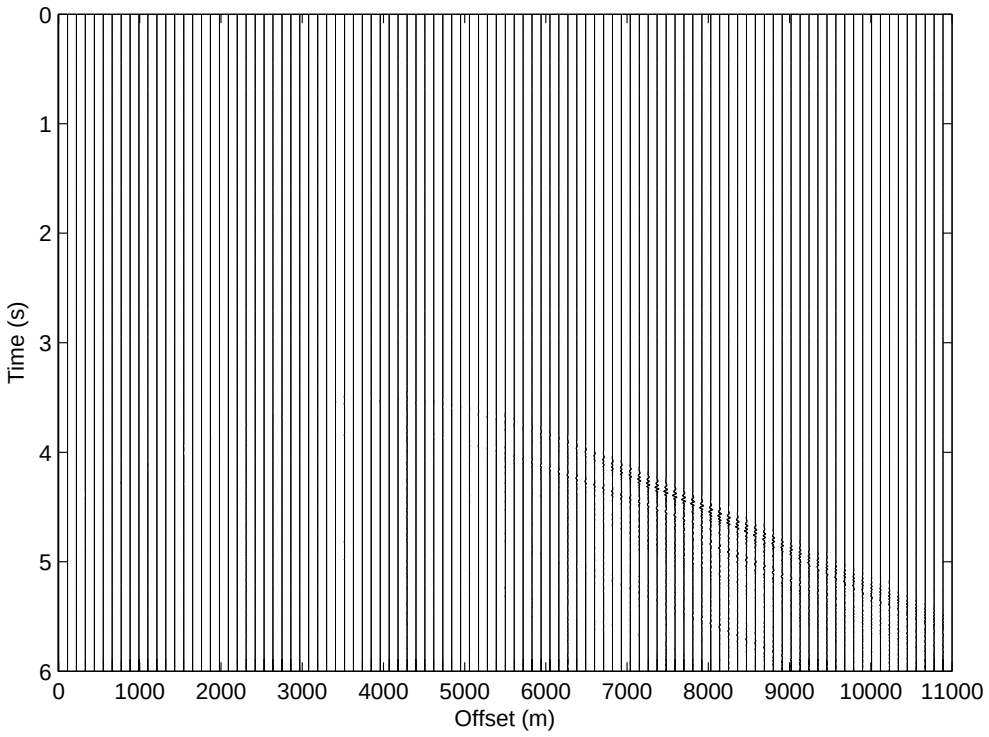

(b)

Figure 6.12: Difference between base and monitor data. Monitor model including a section of the velocity anomaly $l_a = 300$ (maximun section of the anomaly at $\varphi = 0°$).

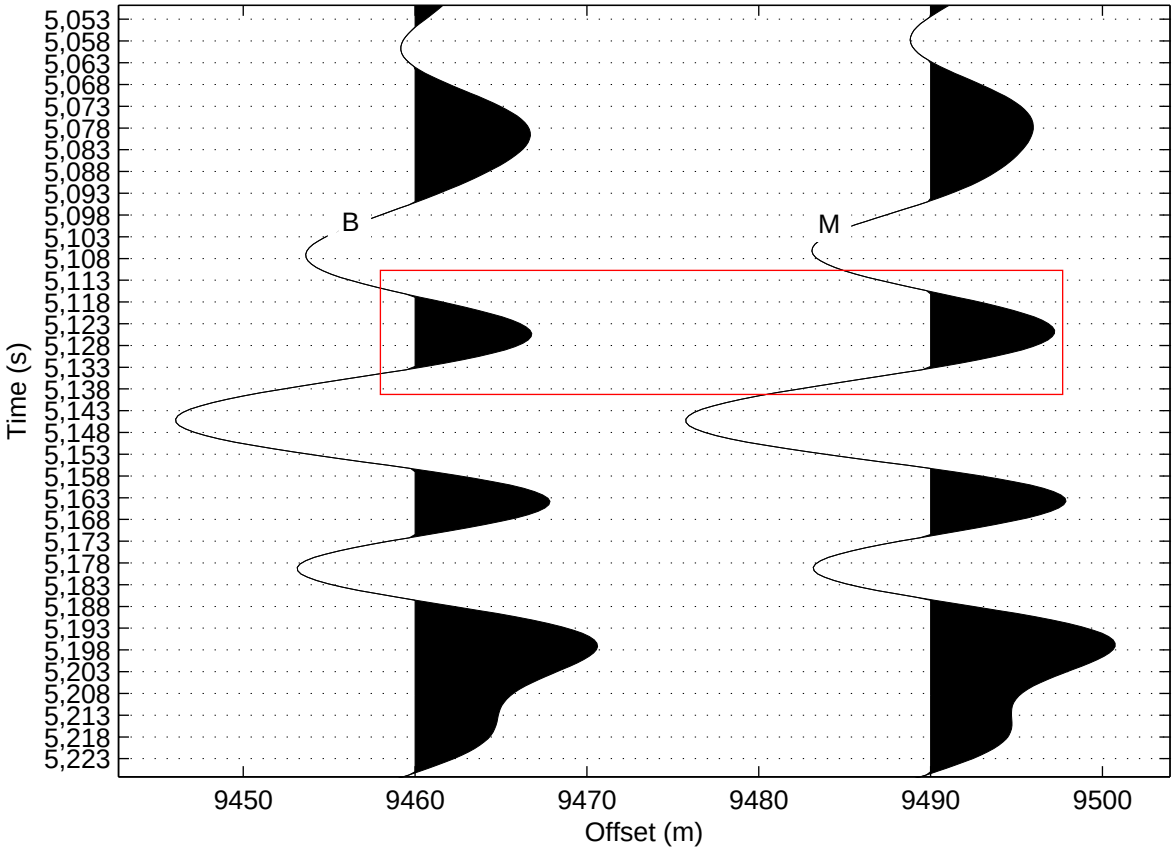

Figure 6.13: Detail comparison between base and monitor data. Monitor model including a section of the velocity anomaly $l_a = 300$ (maximun section of the anomaly at $\varphi = 0°$). A timeshift around $1.5ms$ can be observed.

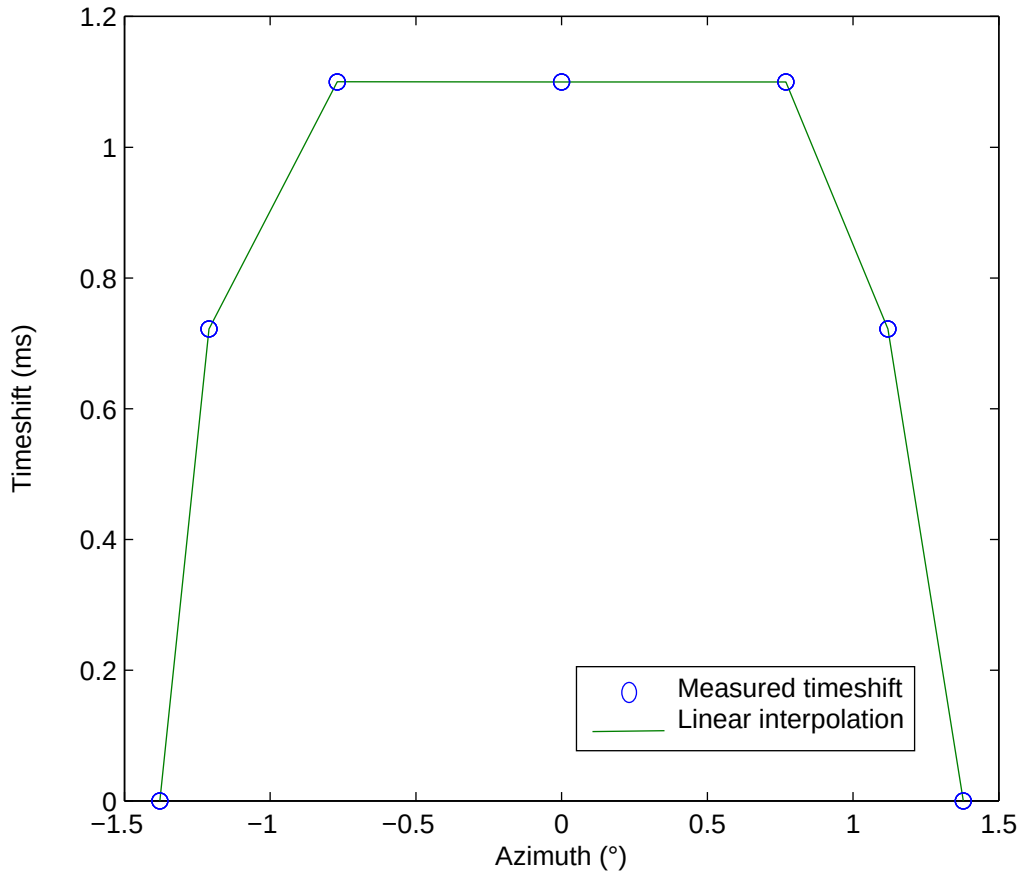

Figure 6.14: Timeshift between base and monitor data versus azimuth. The maximum timeshift is reached from $\varphi = -0.77°$ to $\varphi = 0.77°$.

Chapter 7

Conclusions

From the results, it is possible to conclude that the refraction timeshift method is a good tool to monitor velocity changes due to gas leackage in shallow layers, even when the lateral extension of the anomaly reaches less than hundred meters. It has been proved that a small velocity change will lead to signifficant 4D refraction timeshift. This timeshift allows to estimate P-wave velocity changes with an error of 1 to 2%.

Even under subtle velocity changes, the technique allows to map velocity anomalies, giving its location (l_1) and its extension (l_a). This information can be obtained when 2D lines with a wide range of azimuth values are acquired.

On the other hand, the results for the simplified acquisition design are encouraging. This method was proposed as alternative method in order to decrease either the acquisition time or the costs. According to the results, for low acquisition costs, it is possible to monitor the shallow subsurface layers in a producing hydrocarbon reservoir, although no absolute values for the location and extension can be estimated. For this monitoring system, relative values for the extension and location of the anomaly can be detected in a given area, by analyzing the graph presented in Figure (5.20).

In the monitoring of velocity changes due to gas leackage in deeper layers, as in the case of Snorre Field, the amplitude values for the difference data due to velocity changes becomes smaller when the velocity anomaly is smaller and is located at deeper layers. However, the variations between the two sections (base and monitor) are still detectable. Despite the fact that the resolution of the data for Snorre Field is clearly affected, it is still possible to define where the velocity anomaly is relatively greater and where it is likely located by analyzing the graph presented in Figure (6.14).

Limitations of this method are related with the existence of positive velocity contrast in

the reservoir layer and existence of long-offset data. For real data case, noise, location accuracy, source strength etc. will affect the repeatability of the seismic data. Therefore, the signal variation can be masked, making the velocity changes in the reservoir undetectable. Further investigation is needed, a finite-difference modelling adding noise to the model, is strongly adviced in order to identify crucial bottlenecks that are likely to appear for a real data case.

Bibliography

[1] D. Dubucq, T. Bhakta, and P. Thore, 2010, SAGD Production Monitoring by Seismic Refraction. GeoCanada, pp. 1-4.

[2] D. Forel, T. Benz, and W. Pennington, 2005, Seismic Data Processing with Seismic Unix. Society of Exploration Geophysicits.

[3] D. Lumley, 2001, Time lapse seismic reservoir monitoring. Geophysics, v. 66, pp.50-53.

[4] H. Mehdizadeh, R Srivastava, N. Vedanti, and M. Landrø, 2007b, Seismic monitoring of in-situ combustion in the Balol heavy oil field. 77th Annual Meeting SEG, pp. 2878- 2882.

[5] H. Mehdizadeh and M. Landrø, 2011, Monitoring shallow gas migration by refraction timeshift. Annual Meeting SEG, pp. 4124- 4127

[6] J. Stockwell and J. Cohen, 2007, The New SU Users Manual. Center of Wave Phenomena, Colorado School of Mines.

[7] J. Scales, 1977, Theory of Seismic Imaging. Colorado School of Mines, pp. 173-184.

[8] M. Thompson and M. Andersen, 2008, Focused seismic monitoring. The Leading Edge, pp. 1626-1631.

[9] M. Landrø, O. Solheim, E. Hilde, B. Ekren. and L. Strønen, 1999, The Gullfaks 4D Seismic Study. Petroleum Geoscience, v. 5, pp. 213-226.

[10] M. Landrø, 1999a, Discrimination between pressure and fluid saturation changes from time lapse seismic data. 69th Ann. Internat. Mtg., Soc. Expl. Geophys., Expanded Abstracts, pp. 1651–1654.

[11] M. Landrø, 1999b Repeatability issues of 3-D VSP data. Geophysics, v. 64, pp.1673-1679.

[12] M. Landrø, L. Strønen and P. Digranes, 2001, Mapping reservoir pressure and saturation changes using seismic methods – possibilities and limitations. First Break, v. 19, pp. 671-677.

[13] M. Landrø, A. Nguyen and H. Mehdizadeh, 2004, Time lapse refraction seismic – a tool for monitoring carbonate fields?. 74th Annual Meeting SEG, pp. 2295-2298.

[14] M. Landrø, and J. Stammeijer, 2004, Quantitative estimation of compaction and velocity changes using 4D impedance and traveltime changes. Geophysics, v.69, pp.949-957.

[15] M. Taner and F. Koehler, 1969, Velocity spectra digital computer derivation and applications. Geophysics, 39, pp. 859-881.

[16] N. Vedanti, A. Pathak, R. Srivastava and V. Dimri, 2009, Time Lapse (4D) Seismic: Some Case Studies. e-Journal Earth Science India, pp. 230 – 248, ISSN: 0974 - 8350.

[17] P. Smith, J. Berg, S. Eidsvig, I. Magnus, F. Verhelst and J. Helgesen,2001 4-D seismic in a complex fluvial reservoir: The Snorre feasibility study. The Leading Edge, pp. 270-276.

[18] Petroleum Safety Authority Norway, *Maps*, http://www.ptil.no/main-page/category9.html.

[19] R. Alford, K. Kelly, and D. Boore, 1974, Accuracy of finite-difference modeling of the acoustic wave equation. Geophyics, pp. 39-834.

[20] Y. Liu, and M K. Sen, 2009, Advanced finite-difference methods for seismic modeling. SEG Beijing 2009 International Geophysical Conference, Expanded abstract, ID54.

Appendix A

Seismic Unix routines

```
#! /bin/sh

#/////////////////////////////////////////////////////////////#
#                  SUBSURFACE MATHEMATICAL MODELS             #
#       UNIFORMLY SPACED VELOCITY AND DENSITY PROFILES        #
#                          COMMAND UNIF2                      #
#/////////////////////////////////////////////////////////////#

#-------------------------------------#
#-------------------------------------#
#   Parameters introduced by the user  #
#-------------------------------------#
#-------------------------------------#


#### GRAPHICAL PARAMETERS ####

legend=1                    # Display color scale
lnice=1                     # Nice lenged arragement
units=                      # Unit label for legend
label1=                     # Label on axis 1
label2=                     # Label on axis 2
hbox=400                    # Height in pixels of the window
wbox=600                    # Width in pixels of the window
n2=                         # Number of samples in 2nd (slow) dimension
n1=                         # Number of samples in 1st (fast) dimension
f2=                         # first sample in the 2nd (slow) dimension
f1=                         # first sample in the 1st (fast) dimension
```

```
29
#### SUBSURFACE PARAMETERS ####
31
model=Test1                     # Input file
33 Length=3000                  # Length of the model(meters)
Depth=3000                      # Depth of the model(meters)
35 IR=10                        # Distance between receivers
v00=1904,2900,2970              # Velocity in each layer
37 den=1.750,1.8,1.8            # Density in each layer
fx=0                            # First x sample
39 fz=0                         # First z sample
dx=$IR                          # Sampling interval in x direction
41 dz=$IR                       # Sampling interval in z direction
nx=$(((length+dx)/dx))          # Number of samples in x
43 nz=$(((Depth+dz)/dz))        # Number of samples in z
dvdx=0,0,0                      # Derivate of velocity with distance x (dv/dx)
45 dvdz=0,0,0                   # Derivate of velocity with depth z (dv/dz)
method=linear                   # Interpolation method
47


49 #-------------------------------------#
#-------------------------------------#
51 #              Output files           #
#-------------------------------------#
53 #-------------------------------------#

55 datafile1= Velocity_test1.out # Output file
datafile2= Density_test1.out  # Output file
57 psfile1= Velocity_test1.eps   # Post-Script file
psfile2= Density_test1.eps    # Post-Script file
59

#*********************************#
61 #       Velocity Profile          #
#*********************************#
63

# UNIF2 generates a 2-D uniformly sampled velocity or density profile from a
    layered model. #
65 unif2 <$model \
nz=$nz dz=$dz nx=$nx dx=$dx fx=$fx fz=$fz \
67 v00=$v00 dvdx=$dvdx dvdz=$dvdz method=linear > $datafile1 &
```

```
#### Ximage produces an X-image plot of an uniformly-sample model ####

ximage < $datafile \
n2=$nx d2=$dx n1=$nz d1=$dz  f2=$fz f1=$fx \
legend=1 units="Velocity (m/s)"\
label1="Depth (m)" label2="Distance (m)" \
hbox=$hbox wbox=$wbox &


#### Psimage creates a Post-Script image plot of an uniformly-sample model ####

psimage < $datafile  lnice=1 \
n1=$nz d1=$dz n2=$nx d2=$dx f2=$fz f1=$fx \
legend=1 units="Velocity (m/s)" \
label1="Depth (m)" label2="Distance (m)" \
hbox=$hbox wbox=$wbox > $psfile1 &

#*******************************#
#         Density Profile       #
#*******************************#

# UNIF2 generates a 2-D uniformly sampled velocity or density profile from a
    layered model.
unif2 <$model \
nz=$nz dz=$dz nx=$nx dx=$dx fx=$fx fz=$fz \
v00=$den dvdx=$dvdx dvdz=$dvdz method=linear > $datafile2 &

#### Ximage produces an X-image plot of an uniformly-sample model ####

ximage < $datafile \
n2=$nxx d2=$dx n1=$nzz d1=$dz  f2=$fz f1=$fx \
legend=1 units="Density (g/m3)" \
label1="Depth (m)" label2="Distance (m)" \
hbox=$hbox wbox=$wbox &


#### Psimage creates a Post-Script image plot of an uniformly-sample model ####

psimage < $datafile lnice=1 \
```

```
n1=$nzz d1=$dz n2=$nxx d2=$dx f2=$fz f1=$fx \
legend=1 units="Density (g/m3)" \
label1="Depth (m)" label2="Distance (m)" \
hbox=$hbox wbox=$wbox > $psfile2

exit 0
```

Script A.1: Uniformly sampled velecity and density profiles

```
#! /bin/sh

#////////////////////////////////////////////////////////////#
#                SUBSURFACE MATHEMATICAL MODELS              #
#          TRIANGULATED VELOCITY AND DENSITY PROFILES        #
#                          COMMAND TRIMODEL                  #
#////////////////////////////////////////////////////////////#

#-------------------------------------#
#-------------------------------------#
#  Parameters introduced by the user  #
#-------------------------------------#
#-------------------------------------#


#### SUBSURFACE PARAMETERS ####

xmin=0                          # Minimum horizontal coordinate (x)
zmin=0                          # Minimum vertical coordinate (z)
xmax=5000                       # Maximum horizontal coordinate (x)
zmax=1300                       # Maximum vertical coordinate (z)
xedge=                          # x coordinates of an edge
zedfe=                          # z coordinates of an edge
segde=                          # Velocity along an edge
kedge=                          # Array of indices used to identify edges
sfill=                          # x,z,x0,z0,v00,dvdx,dvdz to fill a region closed
    by the borders, where:
#       * (x,y)= is any point where the velocity is known
#       * (x0,y0)= is a any point, where the velocity variation (dvdx or dvdz)
    is know.
#       *  v00=  is the velocity in (x,y)
#       *  dvdx= is the derivate of velocity with distance x in (x0,y0)
```

```
#       *  dvdz= is the derivate of velocity with distance z in (x0,y0)

#### GRAPHICAL PARAMETERS ####

labelz= "Depth [m]"             # Label on x axis
labelx= "Distance [m]"          # Label on z axis
gedge=1.0                       # Gray to draw fixed edges
gtri=2.0                        # Gray to draw non-fixed edges of triangles
gmin=0.2                        # Min gray to shade triangles
gmax=0.8                        # Max gray to shade triangles
wbox=6.0                        # Width in pixels of the window
hbox=2.0                        # Height in pixels of the window


#-----------------------------------------#
#-----------------------------------------#
#               Output files              #
#-----------------------------------------#
#-----------------------------------------#

datafile= TrimodelVelocity_test1.out # Output file
psfile= TrimodelVelocity_test1.eps   # Post-Script file


#*************************#
#    Velocity Profile     #
#*************************#

# TRIMODEL makes a triangulated velocity model
trimodel xmin=$xmin zmin=$zmin xmax=$xmax zmax=$zmax \
          1 xedge=0,5000 \
            zedge=0,0 \
            sedge=0,0 \
          2 xedge=0,5000 \
            zedge=476,476 \
            sedge=0,0 \
          3 xedge=0,5000 \
            zedge=1201,1201   \
            sedge=0,0 \
```

```
        4 xedge=1500,1500 \
72          zedge=476,1201 \
            sedge=0,0 \
74        5 xedge=2000,2000 \
            zedge=476,1201\
76          sedge=0,0 \
        6 xedge=1500,5000 \
78          zedge=1300,1300 \
            sedge=0,0 \
80          sfill=2000,200,0,0,1904,0,0 \
            sfill=500,1000,0,0,2900,0,0 \
82          sfill=1970,1000,0,0,2960,0,0 \
            sfill=2500,1000,0,0,2900,0,0 \
84          sfill=2500,1290,0,0,2970,0,0 \
            kedge=1,2,3,4,5,6 \
86          >$datafile

88 # SPSPOLT plots a triangulated velocity model via Postscript
   spsplot <$datafile \
90         labelz=$labelz labelx=$labelx \
           gedge=$gedge gtri=$gtri \
92         gmin=$gmin \
           gmax=$gmax \
94         wbox=$wbox hbox=$hbox \
   >$psfile
96 ps2pdf $psfile


98



100 exit 0
```

Script A.2: Triangulated velecity and density profiles

```
   #! /bin/sh
2
   #####################################
4  #        TRIANDULATED MODEL TO      #
   #       UNIFORMLY SAMPLED MODEL     #
6  #           COMMAND TRI2UNI         #
   #####################################
8
```

```
#-------------------------------------#
#-------------------------------------#
#  Parameters introduced by the user  #
#-------------------------------------#
#-------------------------------------#


#### SUBSURFACE PARAMETERS ####

datafile= TrimodelVelocity_test1.out  # input file (Velocity profile nxnz)
Length=3000                           # Length of the model(meters)
Depth=1300                            # Depth of the model(meters)
IR=5                                  # Distance between receivers
fx=0                                  # First x sample
fz=0                                     # First z sample
dx=$IR                                # Sampling interval in x direction
dz=$IR                                # Sampling interval in z direction
nx=$(((length+dx)/dx))                # Number of samples in x
nz=$(((Depth+dz)/dz))                 # Number of samples in z

#### GRAPHICAL PARAMETERS ####

legend=1                          # Display color scale
lnice=1                           # Nice lenged arragement
units=                            # Unit label for legend
label1=                           # Label on axis 1
label2=                           # Label on axis 2
hbox=400                          # Height in pixels of the window
wbox=600                          # Width in pixels of the window
n2=                               # Number of samples in 2nd (slow) dimension
n1=                               # Number of samples in 1st (fast) dimension
f2=                               # first sample in the 2nd (slow) dimension
f1=                               # first sample in the 1st (fast) dimension

#-------------------------------------#
#-------------------------------------#
#              Output files           #
#-------------------------------------#
#-------------------------------------#
```

```
modelfile= UniformVelocity_test1.out # Output file
psfile= UniformVelocity_test1.eps    # Post-Script file


#**************************#
#     Velocity Profile     #
#**************************#

# TRI2UNI converts a triangulated model to uniformly sampled model
tri2uni < $datafile f2=$a n2=$nx d2=$dx n1=$nz d1=$dz > $modelfile


#### Ximage produces an X-image plot of an uniformly-sample model ####

ximage < $datafile \
n2=$nxx d2=$dx n1=$nzz d1=$dz  f2=$fz f1=$fx \
legend=1 units="Density (g/m3)"\
label1="Depth (m)" label2="Distance (m)" \
hbox=$hbox wbox=$wbox &


#### Psimage creates a Post-Script image plot of an uniformly-sample model ####

psimage < $datafile lnice=1 \
n1=$nzz d1=$dz n2=$nxx d2=$dx f2=$fz f1=$fx \
legend=1 units="Density (g/m3)" \
label1="Depth (m)" label2="Distance (m)" \
hbox=$hbox wbox=$wbox > $psfile

exit 0
```

Script A.3: Triangulated model to uniformly sampled model

```
#! /bin/sh
#/////////////////////////////////////////////////////#
#         ACOUSTIC WAVE PROPAGATION USING FINITE      #
#          DIFERENCE MODELLING.COMMAND SUFDMOD2       #
#               UNIFORMLY SAMPELED MODELS             #
#           STADDLE SPREAD ARRAY.SINGLE SHOT          #
#/////////////////////////////////////////////////////#
```

```
#-----------------------------------#
#-----------------------------------#
#  Parameters introduced by the user  #
#-----------------------------------#
#-----------------------------------#


#### GRAPHICAL PARAMETERS ####

legend=1                        # Display color scale
lnice=1                         # Nice lenged arragement
units=                          # Unit label for legend
label1=                         # Label on axis 1
label2=                         # Label on axis 2
hbox=400                        # Height in pixels of the window
wbox=600                        # Width in pixels of the window
clip=                           # Maximun amplitude value of the trace
n2=                             # Number of samples in 2nd (slow) dimension
n1=                             # Number of samples in 1st (fast) dimension
f2=                             # first sample in the 2nd (slow) dimension
f1=                             # first sample in the 1st (fast) dimension


#### SUBSURFACE PARAMETERS ####

datafile1= Velocity_test1.out # input file (Velocity profile nxnz)
datafile2= Density_test1.out  # input file (Density profile)
Length=3000                     # Length of the model(meters)
Depth=1300                      # Depth of the model(meters)
IR=5                            # Distance between receivers
fx=0                            # First x sample
fz=0                            # First z sample
dx=$IR                          # Sampling interval in x direction
dz=$IR                          # Sampling interval in z direction
nx=$(((length+dx)/dx))          # Number of samples in x
nz=$(((Depth+dz)/dz))           # Number of samples in z


#### MODELLING PARAMETERS ####
```

```
fx=0                        #Coordinate x of the first sample
fz=0                        #Coordinate z of the first sample
nxx=$nx                     # Number of samples in x
nzz=$nz                     # Number of samples in z
xs=0                        # x coordinate of the source
zs=30                       # z coordinate of the source
hsz=15                      # z coordinate of horizontal line of seismograms
                            # (Receiver depth)

fmax=60                     # Maximun frequency in source wavelet (Hz)
fpeak=$((fmax/2))           # Peak frequency in ricker wavelet (Hz)
sstrength=1.0               # Strength of the source
abs=0,1,1,1                 # Absorbing boundary conditions on top,left,bottom
    ,right
                            # sides of the model. Free surface condition on
                                the top

mt=5                        # Number of time steps (dt) per output time step
tmax=2                      # Maximun recording time



#-------------------------------------#
#-------------------------------------#
#              Output files           #
#-------------------------------------#
#-------------------------------------#

hsfile= ShotgatherTest1{$xs}.su         # Output file for horizontal line of
                                        # seismograms [nx][nt]

datafile3= ONDASTest1.out               # Output file containing the acustic
    wave
                                        # propagation data

psfile1= ONDASTest1.eps                 # Post-Script file
psfile2= ShotgatherTest1_wigle{$xs}.eps # Post-Script file
psfile3= ShotgatherTest1_gray{$xs}.eps  # Post-Script file
```

```
85 #*******************************#
   #   Waves Propagation Modelling   #
87 #*******************************#

89 # Finite-Difference Modeling (2nd order) for acoustic wave equation. #
   sufdmod2< $datafile1 dfile=$datafile2 \
91 nz=$nz dz=$dz nx=$nx dx=$dx fx=$fx fz=$fz \
   zs=$zs xs=$xs fpeak=$fpeak fmax=$fmax \
93 hsz=$hsz tmax=$tmax abs=$abs mt=$mt \
   hsfile=$hsfile > $datafile3
95

   #---------------------------------------#
97 #---------------------------------------#
   #                movie                  #
99 #---------------------------------------#
   #---------------------------------------#
101

   #### SUXMOVIE produces an X-Windows movie of a SEG-Y or SU data ####
103 suxmovie < $datafile3 \
   n1=$nz d1=$dz n2=$nx d2=$dx f2=$fx f1=$fz clip=$clip \
105 label1="Depth (m)" label2="Distance (m)" \
   loop=1
107

   #### SUPSMOVIE creates a Postscript movie plot of a SEG-Y or SU data ####
109 supsmovie < $datafile3 \
   n1=$nz d1=$dz n2=$nx d2=$dx f2=$fx f1=$fz clip=$clip \
111 title="seismic acoustic waves propagation" \
   label1="Depth (m)" label2="Distance (m)" \
113 hbox=400 wbox=600 > $psfile1

115 #---------------------------------------#
   #---------------------------------------#
117 #              Shotgather               #
   #---------------------------------------#
119 #---------------------------------------#

121 #### SUPSWIGB creates a Postscript bit-mapped wiggle plot of a SEG-Y or SU data
       set ####
   supswigb < $hsfile  clip=$clip f2=$fx f1=$fz \
123 label1="Time (s)" label2="Distance (m)" \
```

```
hbox=$hbox wbox=$hbox > $psfile2

#### SUPSIMAGE creates a Postscript image plot of a SEG-Y or SU data set ####
supsimage <  $hsfile  clip=$clip f2=$fx f1=$fz \
label1="Time (s)" label2="Distance (m)" \
hbox=$hbox wbox=$wbox > $psfile3

#### SUXWIGB produces a X-Windows bit-mapped wiggle plot of a SEG-Y data set
    ####
suxwigb < $hsfile clip=$clip f2=$fx f1=$fz \
label1="Time (s)" label2="Distance (m)" \

#### SUXIMAGE produces a X-Windows image plot of a segy data set ####

suximage < $hsfile  clip=$clip f2=$fx f1=$fz \
label1="Time (s)" label2="Distance (m)" \

exit 0
```

Script A.4: Acoustic wave Propagation. Single shot

```
#! /bin/sh

#////////////////////////////////////////////////////////#
#            ACOUSTIC WAVE PROPAGATION USING FINITE      #
#             DIFERENCE MODELLING.COMMAND SUFDMOD2       #
#                   UNIFORMLY SAMPELED MODELS            #
#             STADDLE SPREAD ARRAY. MULTIPLE SHOTS       #
#////////////////////////////////////////////////////////#


#----------------------------------------#
#----------------------------------------#
#  Parameters introduced by the user     #
#----------------------------------------#
#----------------------------------------#

#### GRAPHICAL PARAMETERS ####

legend=1                    # Display color scale
lnice=1                     # Nice lenged arragement
```

```
units=                          # Unit label for legend
label1=                         # Label on axis 1
label2=                         # Label on axis 2
hbox=400                        # Height in pixels of the window
wbox=600                        # Width in pixels of the window
n2=                             # Number of samples in 2nd (slow) dimension
n1=                             # Number of samples in 1st (fast) dimension
f2=                             # first sample in the 2nd (slow) dimension
f1=                             # first sample in the 1st (fast) dimension

#### SUBSURFACE PARAMETERS ####

model=Test1                     # Input file
Length=5000                     # Length of the subsurface to model(meters)
Lengthmodel=3000                # Length of the model(meters)
Depth=1300                      # Depth of the model(meters)
v00=1904,2900,2970              # Velocity in each layer (m/s)
den=1.750,1.8,1.8               # Density in each layer (g/m3)

#### ADQUISITION PARAMETERS ####

LT=3000                         # Length of the array(meters)
offset_max=$LT                  # Maximum offset(meters)
IR=10                           # Distance between receivers(meters)
IS=50                           # Distance between shots(meters)
NR=$(((Length+IR)/IR))          # Number of receivers
NS=$(((Length-LT)/IS))          # Number of shots
xs=                             # x coordinate of the source(meters)
zs=100                          # z coordinate of the source(meters)
hsz=10                          # z coordinate of horizontal(meters)
                                # line of seismograms (Receiver depth)
tmax=2                          # Maximun recording time(s)

#### MODELLING PARAMETERS ####

fmax=60                         # Maximun frequency in source wavelet(Hz)
fpeak=$((fmax/2))               # Peak frequency in ricker wavelet(Hz)
sstrength=1                     # Strength of the source
abs=0,1,1,1                     # Absorbing boundary conditions on top,left,
                                # bottom,right sides of the model. Free surface
```

```
61                                  # condition on the top
mt=5                                # Number of time steps (dt) per output time step
63 dx=$IR                           # Sampling interval in x direction
dz=$IR                              # Sampling interval in z direction
65 nx=$NR                           # Number of samples in x
nz=$NR                              # Number of samples in z
67 fz=0                             # Coordinate z of the first sample


69
# fx coordinate x of the first sample #
71
LIMIT=$((NS*IS-IS))
73
for ((fx=0 ; fx<=LIMIT ; fx=$((fx+ID))  ))
75 do

77 #--------------------------------------#
#--------------------------------------#
79 #              Output files            #
#--------------------------------------#
81 #--------------------------------------#

83 datafile1=Test1Velocity_profile.out{$fx}
datafile2=Test1Density_profile{$fx}.out
85 datafile3=Test1Shotgather{$fx}.su
datafile4=Test1ONDAS{$fx}.su
87 psfile1=Test1Velocity_profile{$fx}.eps
psfile2=Test1Density_profile{$fx}.eps
89 psfile3=Test1SHOTgather_wiggle{$fx}.eps
psfile4=Test1SHOTgather_color{$fx}.eps
91


93 #*****************************#
#       Velocity Profile      #
95 #*****************************#

97 # UNIF2 generates a 2-D uniformly sampled velocity or density profile from a
    layered model.
unif2 <$model
99 nz=$nz dz=$dz nx=$nx dx=$dx fx=$fx fz=$fz \
```

```
v00=$v00 dvdx=$dvdx dvdz=$dvdz method=linear > $datafile1 &

#### Ximage produces an X-image plot of an uniformly-sample model ####

ximage < $datafile \
n2=$nx d2=$dx n1=$nz d1=$dz  f2=$fz f1=$fx \
legend=1 units="Velocity (m/s)"\
label1="Depth (m)" label2="Distance (m)" \
hbox=$hbox wbox=$wbox &


#### Psimage creates a Post-Script image plot of an uniformly-sample model ####

psimage < $datafile  lnice=1 \
n1=$nz d1=$dz n2=$nx d2=$dx f2=$fz f1=$fx \
legend=1 units="Velocity (m/s)" \
label1="Depth (m)" label2="Distance (m)" \
hbox=$hbox wbox=$wbox > $psfile1 &


#***************************#
#       Density Profile       #
#***************************#

# UNIF2 generates a 2-D uniformly sampled velocity or density profile from a
    layered model.
unif2 <$model \
nz=$nz dz=$dz nx=$nx dx=$dx fx=$fx fz=$fz \
v00=$den dvdx=$dvdx dvdz=$dvdz method=linear > $datafile2 &

#### Ximage produces an X-image plot of an uniformly-sample model ####

ximage < $datafile \
n2=$nxx d2=$dx n1=$nzz d1=$dz  f2=$fz f1=$fx \
legend=1 units="Density (g/m3)"\
label1="Depth (m)" label2="Distance (m)" \
hbox=$hbox wbox=$wbox &


#### Psimage creates a Post-Script image plot of an uniformly-sample model ####
```

```
139
psimage < $datafile lnice=1 \
141 n1=$nzz d1=$dz n2=$nxx d2=$dx f2=$fz f1=$fx \
legend=1 units="Density (g/m3)" \
143 label1="Depth (m)" label2="Distance (m)" \
hbox=$hbox wbox=$wbox > $psfile2
145
#*********************************#
147 # Waves Propagation Modelling     #
#*********************************#
149
# Finite-Difference Modeling (2nd order) for acoustic wave equation. #
151 # xs=fx, coordinate of the source=coordinate x of the first sample #
sufdmod2< $datafile1 dfile=$datafile2 \
153 nz=$nz dz=$dz nx=$nx dx=$dx fx=$fx fz=$fz \
zs=$zs xs=$((fx)) fpeak=$fpeak fmax=$fmax \
155 hsz=$hsz tmax=$tmax abs=$abs mt=$mt \
hsfile=$hsfile > $datafile3
157


159 #-----------------------------------------#
#-----------------------------------------#
161 #                movie                    #
#-----------------------------------------#
163 #-----------------------------------------#

165 #### SUXMOVIE produces an X-Windows movie of a SEG-Y or SU data ####
suxmovie < $datafile3 \
167 n1=$nz d1=$dz n2=$nx d2=$dx f2=$fx f1=$fz clip=$clip \
label1="Depth (m)" label2="Distance (m)" \
169 loop=1

171 #### SUPSMOVIE creates a Postscript movie plot of a SEG-Y or SU data ####
supsmovie < $datafile3 \
173 n1=$nz d1=$dz n2=$nx d2=$dx f2=$fx f1=$fz clip=$clip \
title="seismic acoustic waves propagation" \
175 label1="Depth (m)" label2="Distance (m)" \
hbox=400 wbox=600 > $psfile1
177
```

```
#-------------------------------------#
#-------------------------------------#
#              Shotgather             #
#-------------------------------------#
#-------------------------------------#

#### SUPSWIGB creates a Postscript bit-mapped wiggle plot of a SEG-Y or SU data set ####
supswigb < $hsfile  clip=$clip f2=$fx f1=$fz \
label1="Time (s)" label2="Distance (m)" \
hbox=$hbox wbox=$hbox > $psfile2

#### SUPSIMAGE creates a Postscript image plot of a SEG-Y or SU data set ####
supsimage <  $hsfile  clip=$clip f2=$fx f1=$fz \
label1="Time (s)" label2="Distance (m)" \
hbox=$hbox wbox=$wbox > $psfile3

#### SUXWIGB produces a X-Windows bit-mapped wiggle plot of a SEG-Y data set ####
suxwigb < $hsfile clip=$clip f2=$fx f1=$fz \
label1="Time (s)" label2="Distance (m)" \

#### SUXIMAGE produces a X-Windows image plot of a segy data set ####

suximage < $hsfile  clip=$clip f2=$fx f1=$fz \
label1="Time (s)" label2="Distance (m)" \

exit 0
```

Script A.5: Acoustic wave Propagation. Multiple shots

```
#! /bin/sh

#//////////////////////////////////////#
#              CMP SORTING             #
#//////////////////////////////////////#


#-------------------------------------#
#-------------------------------------#
#  Parameters introduced by the user  #
```

```
#-----------------------------------------#
#-----------------------------------------#


LT=3000                 # Length of the array
offset_max=3000         # Maximum offset
NR=301                  # Number of receivers
NS=50                   # Number of shots
IR=10                   # Distance between receivers
IS=50                   # Distance between shots
min_shot=0              # Minimum key value (Source value for the Shotgather)
max_shot=0              # Maximum key value (Source value for the Shotgather)
min_cmp=1800            # Minimum key value (CMP value for the CMPgather)
max_cmp=1800            # Minimum key value (CMP value for the CMPgather)
LIMIT=3450
clip=                   # Maximun amplitude value of the trace

#-----------------------------------------#
#-----------------------------------------#
#                Output files             #
#-----------------------------------------#
#-----------------------------------------#

datafile=SHOTS
datafile1=SHOTShea
datafile2=SHOTSheader
datafile3=SHOTGATHER_CONCATENATE.su   # Output file containing Shotgathers
                                      # from min= value to max= value.
datafile4=CMPTXT
datafile5=CDPGATHER_CONCATENATE.su    # Output file containing CMPgathers
                                      # from min= value to max= value.
datafile6=CDPgather{$min}.su          # Output file containing a single CMPgather
                                      # from min=min value to max=min value.
psfile1=ConcatenateShotgathers.eps
psfile2=ConcatenateCMPgathers.eps


for ((min=0 ; min<=LIMIT ; min=$((min+ID)) ))
do

```

```
#*******************************#
# Concatenation of Shotgathers    #
#*******************************#

# CAT concatenates a set of files #
cat Shotgathershots* > $datafile

# SUSHW adjust the parameters in the header of a file with SU format #
# parameters:
#         *gx= group coordinate - x
#         *tracl= trace sequence number within line
#         *tracr= trace sequence number within reel
#         *sx= source coordinate - x
#         *flrd= Original field record number
#         *offset= distance between source and receiver
#         *cdp= ensemble number of COMMON MID POINT (CMP)
#         *a= values on the first trace
#         *b= increments within group
#         *c= group increments
#         *j= number of elements in the group

sushw < $datafile key=gx a=0 b=$IR c=$ID j=$NR > $datafile1


sushw < $datafile1 key=tracl,tracr,tracf,sx,fldr,offset a=1,1,1,0,1,0 b
    =1,1,1,0,0,$IR c=0,0,0,$ID,1,0 j=$(($NR*$ND)),$(($NR*$ND)),$NR,$NR,$NR,$NR >
    $datafile2

suchw < $datafile2 key1=cdp key2=gx key3=sx b=1 c=1 d=2 > $datafile3

# SUGETHW writes the values of the selected key words #
#    * outout=geom ASCII output file for geometry setting #
sugethw < $datafile3 key=tracl,tracr,tracf,sx,gx,fldr,offset,cdp output=geom >
    $datafile4


### SUWIND rearrange the data by key word ###
### SUPSWIGB creates a Postscript bit-mapped wiggle plot ####
suwind < $datafile3 key=sx min=$min_shot max=$max_shot | suwind j=4 | supswigb
    clip=0.01 \
```

```
title="Shot Gathers" label1="time (s)" label2="offset (m)" \
wbox=5 hbox=8 \
> $psfile1
ps2pdf $psfile1

### SUWIND rearrange the data by key word ###
#### SUXWIGB produces a X-Windows bit-mapped wiggle plot ####
suwind < $datafile3 key=sx min=$min_shot max=$max_shot | suwind j=4 | suxwigb
    clip=0.01 \
title="Shot Gathers" label1="time (s)" label2="offset (m)" \ &

#*******************************#
#          CMP sorting          #
#*******************************#

# SUSORT sorts on any SEG-Y or SU header keywords #
susort < $datafile3 cdp offset > $datafile5

### SUWIND rearrange the data by key word ###
suwind key=cdp min=$min max=$min clip=0.005 < $datafile5 > $datafile6

### SUWIND rearrange the data by key word ###
### SUPSWIGB creates a Postscript bit-mapped wiggle plot ####
suwind < $datafile5 key=cdp min=$min_cmp max=$max_cmp | supswigb clip=0.01 \
title="CMP Gathers" label1="time (s)" label2="Distance  (m)" \
wbox=5 hbox=8 \
> $psfile2
ps2pdf $psfile2

### SUWIND rearrange the data by key word ###
#### SUXWIGB produces a X-Windows bit-mapped wiggle plot ####
suwind < $datafile5 key=cdp min=$min_cmp max=$max_cmp | suxwigb clip=0.005 \
title="CMP Gathers" label1="time (s)" label2="Distance  (m)" \


done
```

Script A.6: CMP sorting

Appendix B

SegyMAT

SegyMAT is a set of m-files that allow the ease importing and exporting of SEG-Y and SU files from MATLAB. As it is a free software library can be modify to make more complicated subroutines. The latest version of segyMAT is always available from sourceforge: http://segymat.sourceforge.net/. SegyMAT may be run on Linux and Windows XP. Any other Matlab supported platform should work. An advantage of this library is that no Matlab toolboxes are required.

To compute the thimeshift between base and monitor surveys, the routines `ReadSegy.m` and `Wiggle.m`of SegyMAT library have been implemented. Using `ReadSegy.m`it is possible to import files from *Seismic Unix* and `Wiggle.m`allows to plot those files `ReadSegy.m`routine allow the fast reading of specific traces. The corresponding traces parameters are first located in the header files, and then tha data are read using the traces options.

The following Script will read "ShotgatherTest1(xs).su" file, which was generated by Script (A.4). This Script uses the data sample format specified in the binary header, and plot the data.

```
clc
clear

%%%% ReadfileSU: Use the ReadSegy routine from SegyMAT library to Read .SU file
    from SEISMIC UNIX
% Call:
% [Data,SegyTraceHeaders,SegyHeader]=ReadSegy(filename);
% Data is a 2D variable containing the seismic data. [Nsamples*Ntraces];
% SegyTraceHeadersis a structure of size [1,Ntraces] structure containing all
    the header values from the traces.
% SegyHeader is a structure containing all the header values.
```

```
%%%% wiggle : plot wiggle/VA/image plot
%
% Call
%    wiggle(Data); % wiggle plot
%    wiggle(x,t,Data,'VA') % variable Area (pos->black;neg->transp)
%    wiggle(x,t,Data,'VA2') % variable Area (pos->black;neg->red)
%    wiggle(x,t,Data,'VA',scale); % Scaled wiggle
% Data : [nt,ntraces]
% x : [1:ntraces] X axis (ex [SegyTraceheaders.offset])
% t : [1:nt] Y axis
% style : ['VA'] : Variable Area
%         ['wiggle'] : Wiggle plot
% scale : scaling factor, can be left empty as [] (Clip)

[trace1,SuTraceHeaders,SuHeader]=ReadSu('Shotgatheranom{2000}');
[trace2,SuTraceHeaders,SuHeader]=ReadSu('Shotgatheranom{50}');

% Difference;
trace=trace2-trace1;

% Temporal Sampling dt=dx/(vmax*2, dx= Spatial sampling
dt=1/(2*2970);

% [1:dt:tmax] Y axis, tmax= Maximun recording time
t=[0:dt:2];

% [1:ntraces] X axis, ntrace= (length of the model)/dx
x=[0:1:size(trace1,2)];

t2=t;

x2=x + 6;

% figure (1) ;
%
% wiggle(x,t,trace1,'VA',0.1)
%
% hold on
%
```

```
% wiggle(x2,t2,trace2,'VA',0.1)

figure (2)

wiggle(x,t,trace,'VA',0.01)

figure (3)

imagesc(x,t,trace)
```

Script B.1: Importing and exporting SU files from MATLAB

```
% This function computes the timeshift between two Gathers for the refrated
% event.
function out = Dt(Nmin,Nmax,trace1,trace2,dt)

% Nmin : first trace that has to be considered
% Nmax : last trace that has to be considered
% Trace1: 2D variable containing the seismic data. [Nsamples*Ntraces]
% Trace2: 2D variable containing the seismic data. [Nsamples*Ntraces]
% dt: Sampling Interval

[Nx,Ny]=size(trace1)
out = zeros(3,Nmax-Nmin+1);

for j=Nmin:Nmax

    i=2;

    while(trace1(i,j)<= 0)
            i = i+1;
    end

    k=2;
     while(trace2(k,j)<=0)
             k=k+1;
     end

   out(1,j-Nmin+1)=k ;
   out(2,j-Nmin+1)=i;
```

```
    out(3,j-Nmin+1)= abs((i-k)*dt);
end

% Reservoir Depth
h=476
% Overburden Velocity
v1=1904
% Reservoir Velocity
v2=2900
% Velocity variation
dv2=-60
% Timeshift Formula coefficients
b = -(h*v1/(v2^2-v1^2)^0.5)*dv2/v2^2
a = - dv2/v2^2
% Anomaly extension
la=150
% Fist position of the anomaly
l1=1707
% Offset critico / 2
xcri2=415
% minimum offset to display
min=1600;
% maximum offset to diplay
max=2500;
% Sampling interval
ID=1;

figure(1)
hold on

size([min:ID:max])
size(out(3,:))
plot([min:ID:max],out(3,:),'x')
% plot([min:ID:l1+xcri2],0,'g')
% plot([l1+xcri2:ID:l1+xcri2+la],(a*[l1+xcri2:ID:l1+xcri2+la]-b-l1*a),'g')
% plot([l1+xcri2+la:ID:max],la*a,'g')
% plot([3180:1:3181],-0.00001,'black')

out
```

Script B.2: Refraction timeshift calcuation